Characterizing the spatial and temporal dynamics of phytoplankton phenology in the British Columbia and Southeast Alaska coastal oceans using satellite ocean colour data

By

Sejal Pramlall

B.Sc. Honours University of Cape Town, 2019

A Thesis Submitted in Partial Fulfilment of the Requirements for the

Degree of

MASTER OF SCIENCE

in the Department of Geography

We acknowledge and respect the lək^{w}əŋən peoples on whose traditional territory the university stands and the Songhees, Esquimalt and W̱SÁNEĆ peoples whose historical relationships with the land continue to this day.

Characterizing the spatial and temporal dynamics of phytoplankton phenology in the British Columbia and Southeast Alaska coastal oceans using satellite ocean colour data

By

Sejal Pramlall

B.Sc. Honours University of Cape Town, 2019

Supervisory Committee:

Dr. M. Costa, Co-Supervisor (Department of Geography)

Dr. J.M. Jackson, Co-supervisor (Department of Geography)

Dr. David Atkinson, Committee Member (Department of Geography)

Abstract

The coastal waters of British Columbia (B.C.) support diverse food webs and provide habitats for various species of Pacific salmon, which are of vital importance to the regional economy and for First Nations culture and subsistence. To effectively monitor marine environmental health of these regions and any changes thereof, it is necessary to employ ecological indicators to provide objective and quantitative metrics upon which to evaluate the state of the ecosystem and their response to environmental and climatic perturbation. Phytoplankton phenology is an important ecological indicator that characterises the timing of annually occurring phytoplankton growing periods and has been typically synthesized into a set of indices encompassing the timing, duration, and magnitude of bloom events. Observing changes in phytoplankton phenology in this region requires vast spatial coverage and short temporal frequencies, which is achieved through ocean colour satellite imagery. Here, we evaluate the performance of the merged multi-sensor ocean colour chlorophyll-a products, GlobColour and OC-CCI, in the British Columbia coastal waters via a statistical match-up analysis and a qualitative analysis to determine whether the data reflects the region's large-scale seasonal trends and latitudinal dynamics. Using the chlorophyll-a product that is best suited to our purpose, we then derive a suite of phenological indices on a pixel-by-pixel basis, which is used to partition the study area into phenological bioregions using an objective, unsupervised partition strategy (Hierarchical Agglomerative Clustering method). The delineated bioregions are then used to describe region-specific phytoplankton phenological patterns associated with bloom magnitude, frequency, duration, and timing. The interannual variability of spring bloom initiation was evaluated considering interactions with environmental variables, sea surface temperature anomaly and the El Nino Southern Oscillation index. The GlobColour interpolated chlorophyll-a product revealed sound statistical results ($r^2 = 0.63$, slope

= 0.88, bias = 0.81, MdAD = 1.69, RMSE = 0.37, n = 797) and demonstrated the expected seasonal and local dynamics for this region, and average concentrations within ranges reported for satellite-derived observations. The derived phenology indices showed longitudinal gradients. From east to west, bloom initiation along the coast was observed in spring, gradually progressing to fall dominated blooms further offshore, with peak chlorophyll concentrations of 38.5mg.m^{-3} and 3mg.m^{-3}, respectively. The spatial patterns of number of blooms per pixel has shown to be inversely correlated to average bloom duration, with lower number of blooms having longer durations and vice versa. Four coherent bioregions were identified over the study region with distinctive phytoplankton phenological properties: two coastal regions, one shelf region and an offshore region. We found that early spring blooms were associated with a positive SST anomaly and El Nino conditions. Conversely, average or late spring blooms occurred in years where there was a negative SST anomaly and La Nina conditions. Furthermore, the relationship between spring bloom initiation and principal bloom initiation was evaluated, and we found that when there is a later spring bloom initiation we can expect a later principal bloom initiation, and vice versa. The findings of this study can help better inform fisheries management and conservation programs, by being able to infer the timing of spring bloom initiation in relation to SST anomalies and ENSO index.

Table of Contents

List of Tables

List of Figures

Acknowledgements

For their assistance and support throughout the duration of this project, my acknowledgement and thanks are given to:

My supervisors, Maycira Costa and Jennifer Jackson, for your guidance, support, and availability for the duration of this project. Thank you for the opportunities to travel and learn. These lessons and experiences are invaluable and will last a lifetime. You have provided a platform for me to improve my capabilities, and enabled me to reach a higher potential, and for that I am truly grateful.

My colleagues and co-authors, Karyn Suchy, Christian Marchese, and Marta Konik, for your expertise, mentorship, and support.

The NSERC DG to Costa, MEOPAR – Marine Environmental Observation, Predication and Response Network, and the Canadian Space Agency for funding my MSc. research. Without their financial support, my studies would have not been possible.

The Spectral Lab members for the moral support and camaraderie. A special thank you to Lianna Gendall for the help and guidance and you gave me, and for helping me retain a good sense of (in)sanity in the final months.

And finally, I would like to thank my family, without whom, undertaking this degree would have been impossible. And a particular thank you to my brother, Minal Pramlall, for your technical support. To both my parents, your support in my pursuit of my passion is paramount. Thank you.

1.0 Introduction

1.1 Overview

The environment is experiencing a period of rapid global change, at a pace that is unprecedented in Earth's geologic time (Beardall et al., 2009). Such changes can have severe implications on the pivotal autotrophic organism, phytoplankton, which are particularly sensitive to changing environmental conditions (Ferreira et al., 2014). The health of the marine ecosystem is dependent on the phytoplankton, which in turn is responsible for manifesting the energy from the sun into a usable form upon which all aquatic life depends (Platt et al., 2010). Phytoplankton account for less than 1% of the photosynthetic biomass on the planet, and are nevertheless responsible for approximately half of the global net primary production (Friedland et al., 2018; Krug et al., 2018; Winder & Sommer, 2012). Phytoplankton thus forms the base of the aquatic food web, fuelling the growth and reproduction of living marine resources (Friedland et al., 2018), and they also play an integral role in global climate regulation and biogeochemical cycling (Winder & Sommer, 2012).

Changes at the base of the aquatic food web can have severe repercussions for the entire ecosystem; of particular concern is the timing and magnitude of phytoplankton blooms (Henson et al., 2009; Winder & Sommer, 2012). Cushing's match-mismatch hypothesis states that "the timing of food availability may be as important, or even more so, than the abundance of food" (Cushing, 1959; Henson et al., 2009). When the timing of phytoplankton blooms fluctuates, it can cause a mismatch with the timing of the primary consumer, herbivorous zooplankton, which would result in a decreased biomass peak and change in the zooplankton community

composition (Suchy et al., 2019; Tommasi et al., 2013; Wolfe et al., 2016). Since zooplankton are the main food source of various juvenile Pacific salmon species, this match-mismatch scenario could result in a decreased recruitment success and is thus a concern to the stocks in British Columbia waters, which are of vital importance for the regional economy and for First Nations culture and subsistence (Ajmani, 2011; Chebanova et al., 2018; Craddock et al., 1976). The repercussions of bloom timing mismatch on the survival of higher trophic levels emphasize the importance of understanding the spatio-temporal variability in primary producers (Brody et al., 2013; Racault, Sathyendranath, et al., 2014a).

Phytoplankton blooms are triggered by the life history and physiological responses of individual species to abiotic conditions that best support their growth (Winder & Sommer, 2012). It is useful to acknowledge that the term 'bloom' is relative, because it is used to describe a variety of phytoplankton growth events with contrastingly different biomass concentrations. Therefore, in this context we will consider an algal bloom to be defined as 'the rapid growth of one or more species which leads to an increase in the biomass of the species' (Blondeau-Patissier et al., 2014; Richardson, 1997). The spatial and temporal bloom dynamics are driven by a wide diversity of underlying processes, including local and large scale oceanographic and atmospheric circulation patterns, topographic irregularities, coastal upwelling and continental freshwater outflows, which may vary with latitude and regional oceanographic conditions (Krug et al., 2018; Salgado-Hernanz et al., 2019). Phytoplankton distribution and timing therefore coccurs in regions where the conditions support their growth, and when conditions are optimal (Winder & Sommer, 2012).

Regionally, optimal conditions for phytoplankton productivity is primarily controlled by light and nutrients, and it is the interplay between the availability of these key resources that determine the distribution and seasonality of phytoplankton (Allen & Wolfe, 2013b; Ji et al., 2010). High latitude regions, poleward of 60°N and S, are subjected to light limitation due to the low sun angle, which is suboptimal for phytoplankton growth (Henson et al., 2009). The increase in incident light and stratification of surface waters during spring results in the shallowing of the mixed layer depth to below a 'critical depth', the depth at which the average light intensity allows for the phytoplankton growth to exceed its losses, and for the spring bloom to commence (Henson et al., 2009). Transition zones, which are the regions between subtropical (23.5-35°N and S) and subpolar regimes (50-70°N and S), may experience blooms when either nutrients or light, or both, become available at a level that supports phytoplankton growth (Brody et al., 2013; Henson et al., 2009). The conditions in these transition zones may favour a secondary, smaller bloom during the year in addition to the 'primary' bloom event, which is the high magnitude bloom resulting from the cessation of the principle limiting factor to phytoplankton growth (Brody et al., 2013).

In the coastal northeast Pacific Ocean (Figure 1), phytoplankton productivity is characterised by a dominant spring bloom that is driven by large-scale climate patterns combined with regional and local-scale physical environmental conditions (Malick et al., 2015). Coastal waters contain an abundance of iron and silicic acid that supports a high productivity, that is only seasonally limited by nitrogen availability (Ribalet et al., 2010). These nutrients are fed into the coastal waters by upwelling of nutrient rich waters and/or coastal runoff from major rivers, which also provides stability and shoaling of the upper ocean layer (Ware & Thomson, 2005). Having both

of these nutrient sources, the coastal waters off Washington and southern British Columbia have been found to have the highest productivity in the northeast Pacific (Ware & Thomson, 2005). Alternatively, the offshore waters are characterized by a gyre system that is a high-nitrate, low chlorophyll (HNLC) region, where productivity is limited by iron availability (Ribalet et al., 2010). The large-scale current systems in the northeast Pacific Ocean in combination with the along-shore estuarine circulation creates a consistent supply of relatively fresh coastal waters into more saline oceanic waters (Ribalet et al., 2010). Therefore, phytoplankton productivity in the northeast Pacific Ocean follows global trends of phytoplankton growth being tightly coupled with ocean surface mixed layer dynamics, and regulated by atmospheric forcing and large scale climate variability (Krug et al., 2018; Sasaoka et al., 2011).

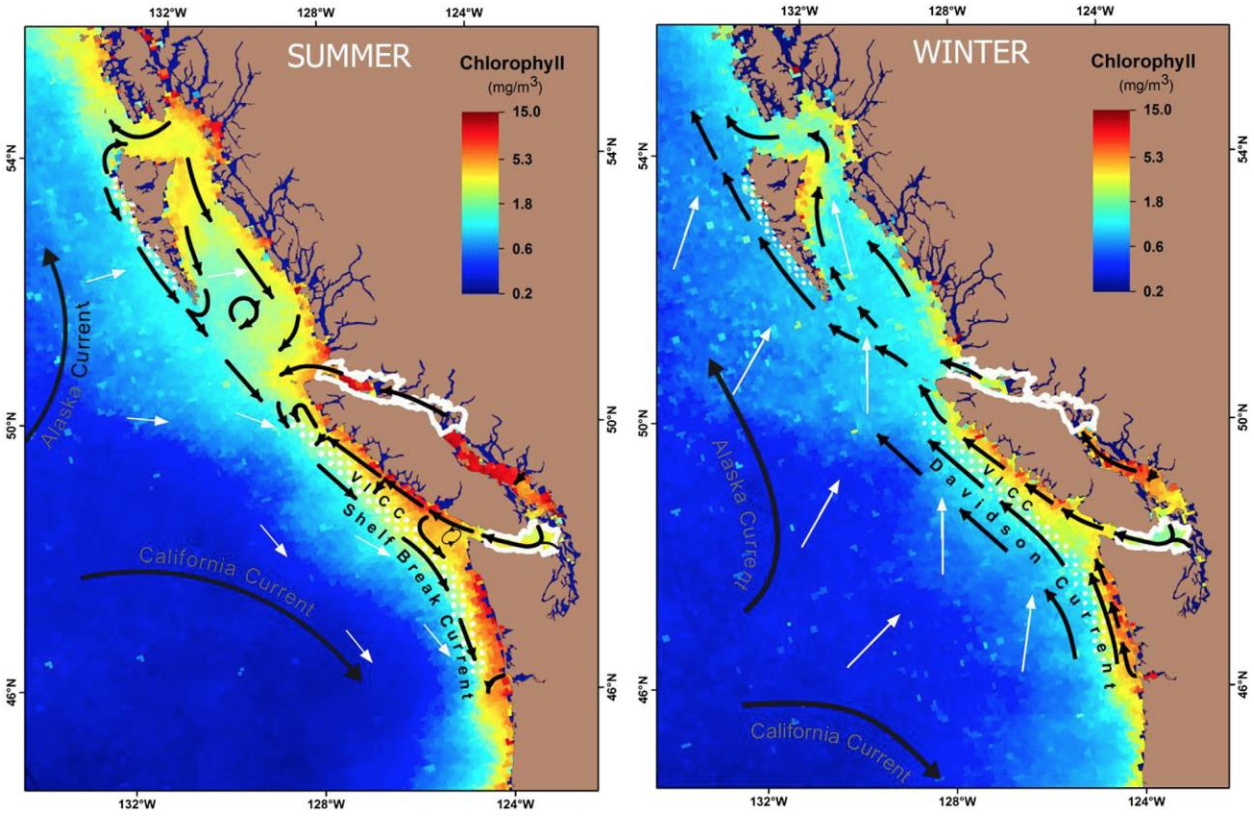

Figure 1: Schematic of the prevailing surface currents of the northeast Pacific superimposed on the long-term average (1997–2010) surface chlorophyll concentration. The surface chlorophyll concentration is presented in log-transformed units for (left) summer (April–September) and (right) winter (October–March). VICC denotes the Vancouver Island Coastal Current. Areas

outlined in white represent regions with strong tidal mixing, and areas with white dots near the coast represent regions with downwelling in winter and upwelling in summer. The predominant wind direction (computed from the seasonal average NCEP-NCAR reanalysis winds from 1997 to 2010) is displayed as white arrows.(Image and caption: from (Jackson et al., 2015)

Large scale climatic forcing such as El Nino Southern Oscillation (ENSO), Pacific Decadal Oscillation (PDO), North Pacific Gyre Oscillation (NPGO) and Aleutian Low-Pressure variations have shown to have significant consequences on the oceanic ecosystem, particularly with regards to phytoplankton phenology dynamics (Sasaoka et al., 2011). The ENSO is a well-known source of hemisphere wide interannual climate variations for the Pacific and global tropics, which dominates the interannual variability of phytoplankton productivity (Jackson et al., 2015; Mantua & Hare, 2002). A strong El Niño year causes warm equatorial waters to be transported northwards along the coast of North America, resulting in low phytoplankton productivity (Philander, 1983; Zebiak & Cane, 1987). PDO can be thought of as a long-lived El Niño-like pattern of Pacific climate variability, having a roughly decadal pattern linked to the Aleutian low-pressure system over the mid-latitude North Pacific basin (Mantua & Hare, 2002). Positive PDOs are characterized by anomalously warm sea surface temperatures (SST) along the west coast of North America, westerly winter winds and lower primary productivity (Di Lorenzo et al., 2008; Mantua & Hare, 2002). Another long-term climatic pattern that is driven by sea level pressure changes in the North Pacific Ocean is the NPGO. The NPGO is controlled by regional and basin-scale variations in wind-driven upwelling and horizontal advection, where negative NPGO causes escalated SST and decreased phytoplankton productivity (Di Lorenzo et al., 2008). The coupling of negative NPGO and positive PDO events can result in a multiyear persistence of warm SST anomalies, as exhibited by the 2014-2015 marine heat wave in the Northeast Pacific Ocean (Joh & Di Lorenzo, 2017).

In addition to the effects of natural variability due to large scale climatic forcing, anthropogenically induced climate change has been shown to impact the timing and magnitude of seasonal phytoplankton blooms globally (Edwards & Richardson, 2004; Straile, 2002; Winder & Sommer, 2012). However, not all regions of the ocean are going to experience the extent of the changing climate to the same degree, with significant differences being felt in the Atlantic, Indian and Pacific Oceans due to the particular underlying mechanisms dominating each of these domains (Beardall et al., 2009). The repercussions of a warming ocean can either have direct impacts, such as the alteration of rates of biological processes, or indirect impacts through changes in water mixing and stratification that alter the nutrient supply and light availability for phytoplankton in the mixed layers (Beardall et al., 2009). Such changes may have far-reaching impacts on phytoplankton productivity.

Among the first consequences of climate warming and global change are seen in an alteration of phytoplankton phenology (Ji et al., 2010). Phytoplankton phenology is therefore a commonly used indicator that systematically monitors the state of marine ecosystems due to its particular sensitivity to changing environmental conditions (Ferreira et al., 2014). Phenology indices characterize the timing and magnitude of periodic phytoplankton blooms, and can be calculated either per pixel or per region using satellite data (Land et al., 2014). According to Ferreira et al. (2014), the ideal phenology metric 'should be accurate, precise, and simultaneously sensitive to the underlying environmental processes.' In compliance with this criterion, the most commonly used indices applied to phytoplankton phenology patterns are the timing of bloom initiation, termination, peak amplitude, duration and magnitude. Multiple methods have been developed to

derive these specific metrics (Krug et al., 2018). The choice of most suitable phenological metric, and the nature of its derivation, depends upon the research question at hand as well as implications of geographic location and dominant forcing mechanisms that are at play (Ferreira et al., 2014; Ji et al., 2010). Observing changes in phytoplankton phenology at large spatial scales requires vast spatial coverage and temporal frequencies on the order of a week or less for at least 20 years (Groom et al., 2019; Henson et al., 2009), in order to effectively differentiate between short-term variability and longer-term changes (Allen & Wolfe, 2013b). The sole means of achieving this is through the use of ocean colour remote sensing, which provides continuous global estimates of surface chlorophyll concentration, interpreted as a proxy for phytoplankton biomass since the late 1990's (Kahru et al., 2011; Kostadinov et al., 2017).

Remote sensing ocean colour imagery provides extensive global coverage of chlorophyll concentration at high spatial resolutions (<=1km) and regular sampling frequencies (1 day; Platt & Sathyendranath, 2008; Racault et al., 2014a). Up to the present, satellite-based ocean colour observations have established a detailed record of data from several sensors spanning more than three decades (Racault et al., 2014a). These long term ocean colour records play a critical role in assessing the effects of natural and anthropogenic changes on the oceans (Muller-Karger et al., 2018). In order to distinguish between the natural variability of phytoplankton biomass and climate change driven trends, a contiguous record of 20-40 years is required (Groom et al., 2019; Henson et al., 2009). Since the contiguous record began in 1997 with the launch of SeaWiFS, our chlorophyll data record currently spans 24 years. Considering that no single sensor encompasses this entire duration due to sensor calibration degradation with age and limited lifespans, merging data from individual sensors is needed to generate a continuous time series (Groom et al., 2019).

Despite revolutionizing the extent and availability of earth observation data, remote sensing cannot be considered as a universal panacea for all observational needs (Platt & Sathyendranath, 2008). The spatiotemporal coverage of satellite imagery is limited by gaps in the data which can be discrete, due to sun-glint, persistent cloud cover, atmospheric aerosols and sensor saturation over ice, sand or snow, or it could be continuous over a period of time due to low sun angle in winter, particularly in the high latitudes (Land et al., 2014; Racault et al., 2014b). Gaps may also occur when satellite missions are delayed, lost or cancelled (Blondeau-Patissier et al., 2014). Additionally, satellite derived Chl-a data only represents surface Chl-a, and therefore does not account for all the phytoplankton production in the ocean. To best utilize this wealth of data, it is desirable to combine satellite data with in situ observations, as in situ data can help calibrate satellite algorithms for regional applications, as well as enable the validation of satellite data.

While several studies using ocean colour data have investigated phytoplankton phenology patterns in the North Atlantic (Henson et al., 2009; Platt & Sathyendranath, 2008; Siegel et al., 2002; Vargas et al., 2009), only a few studies have been conducted on phytoplankton phenology in the subarctic North Pacific using remote sensing (Jackson et al., 2015; Marchese et al., 2022; Sasaoka et al., 2011; Ware & Thomson, 2005). The investigation of phytoplankton phenology at a more regional scale over the British Columbia coastal waters have primarily been restricted to the Salish Sea (Suchy et al., 2019; Suchy et al., 2022). Thus, information on the phytoplankton phenology patterns over the entire British Columbia and South-East Alaska coastal oceans, its interannual variability and underlying environmental drivers, is still limited. This lack of coherent spatial information severely limits our ability to map conditions experienced by juvenile

salmon along their entire migration route. This research aims to bridge that gap, by investigating phytoplankton phenology patterns, and the underlying environmental drivers, over the British Columbia and South-East Alaska coastal and open ocean waters using 23-years (1998-2020) of merged satellite ocean colour data.

1.2 Research Objectives

To achieve our goal, two specific objectives must be met:

(1) Evaluate the performance of the merged multi-sensor ocean colour chlorophyll-a products, GlobColour and OC-CCI, in the British Columbia coastal waters via a statistical match-up analysis and a qualitative analysis to determine whether the data reflects the region's large-scale seasonal trends and latitudinal dynamics.

(2) Partition the study area into phenological bioregions using an objective unsupervised partition strategy based on a suite of phenological indices computed on a pixel-by-pixel basis, to evaluate the climatological region-specific phytoplankton phenology indices and describe the interannual variability of the spring bloom initiation in relation to sea-surface temperature (SST) anomaly and large-scale climate index, the El Nino Southern Oscillation (ENSO) index.

1.3 Thesis Structure

This thesis is separated into two papers to address the research objectives. The first paper (Chapter 2) evaluates the performance of OC-CCI and GlobColour merged Chl-a products in B.C. waters using in situ data to determine which product is the most suitable for use in this

region. The second paper (Chapter 3) uses the most suitable merged Chl-a product determined by the first paper to partition the study area into phenological bioregions in order to characterize the spatial and temporal variability of phytoplankton phenology indices in relation to SST anomaly and large-scale climate index, ENSO. Each of these papers was developed as independent publications, and as such, some information may overlap between the two. Lastly, the conclusion (Chapter 4) united these two papers and summarized the broad implications of this work.

2.0 Merged multi-sensor ocean colour chlorophyll product evaluation for the British Columbia coast

2.1 Abstract

The GlobColour project and the Ocean-Colour Climate Change Initiative (OC-CCI) produce merged chlorophyll-a products from 1997 to present on a global scale by integrating chlorophyll-a estimates from multiple sensors to minimise temporal discontinuities and spatial biases among single satellite sensors. Despite being validated on a global scale, a regional comparison to in situ Chl-a concentrations should be done to enable product application in optically complex waters. This study aims to evaluate the performance of the merged multi-sensor ocean colour chlorophyll-a products, GlobColour and OC-CCI, in the British Columbia coastal waters via a statistical match-up analysis and a qualitative analysis to determine whether the data reflects the region's large-scale seasonal trends and latitudinal dynamics. GlobColour CHL1 emerged as the best performer across most metrics (RMSE = 0.23, r = 0.91, MdAD = 1.35, BIAS = 0.99), followed closely by OC-CCI (RMSE = 0.27, r = 0.91, MdAD = 1.45, BIAS = 0.87). The statistics for all products had degraded in Case 2 waters, thus highlighting the dilemma of applying algorithms designed for Case 1 waters in Case 2 waters. Our results indicate how the quality of products can vary in different environmental conditions. To aid product selection, we recommend a comparison between products and in situ water samples in Case 2 water bodies.

2.2 Introduction

Ocean colour-derived chlorophyll-a concentration (Chl-a), interpreted as a proxy for phytoplankton biomass, is one of 54 essential climate variables (ECV) that critically contribute to the characterization of Earth's climate (Bojinski et al., 2014). In order to provide empirical evidence needed to understand and predict the evolution of climate change, ECV's need detailed historical records spanning decades at a global scale to be able to discern natural changes from anthropogenically induced change (Henson et al., 2009). Ocean colour satellites meet these requirements by providing global coverage of Chl-a products at relatively high spatial resolutions (<1km) and regular sampling frequencies since 1978 (Platt & Sathyendranath, 2008). Unfortunately no single ocean colour satellite encompasses this entire 40-plus year duration, thus merging data from different satellites is needed to generate a continuous time series (Groom et al., 2019). The merging process is complex because each sensor possesses distinct features such as orbits (different timing of overpasses), swaths and revisit times, spatial resolution (ranging from 300m-4km), and spectral resolution (number and position of spectral wavebands; Groom et al., 2019). This merging process must therefore be carefully thought out, to prevent biases, artifacts or discontinuities from being introduced (Groom et al., 2019; Hammond et al., 2017).

The GlobColour project and the Ocean-Colour Climate Change Initiative (OC-CCI) produce merged Chl-a products on a global scale by integrating Chl-a estimates from multiple sensors to minimise temporal discontinuities and spatial biases among single satellite sensors (ACRI-ST GlobColour Team, 2020; Belo Couto et al., 2016; Garnesson et al., 2019; Welch et al., 2020). The GlobColour project was developed in 2005 by the European Space Agency (ESA) as a Data User Element program to provide a continuous data set of merged level 3 ocean colour products

that accommodate global carbon cycle research (ACRI-ST GlobColour Team, 2020). Subsequently, in 2010 ESA launched the OC-CCI to produce a coherent, long-term and error-characterized chlorophyll product to meet the needs and quality standards required for ECV's (Belo Couto et al., 2016; Welch et al., 2020). While both products share the common goal of producing high-quality merged Chl-a datasets on global and regional scales, the primary difference in product performance is thought to be due to their merging strategies and flagging schemes (Garnesson et al., 2019; Moradi, 2021). Additionally, GlobColour processing architecture focuses on providing near-real-time data products, which risks inconsistencies in the time series until undergoing an annual full reprocessing. Alternatively, OC-CCI prioritizes 'climate quality' consistency with minimal inter-sensor bias without providing near-real-time data (CMEMS, 2021b). Despite merged products improving the data coverage in both time and space, missing data due to sun-glint, persistent cloud cover, atmospheric aerosols or sensor saturation over ice, sand or snow is still prevalent. Missing data are particularly challenging for studies concerning phytoplankton phenology, as it has been shown to affect the accuracy of seasonality metrics (Cole et al., 2012). GlobColour therefore provides an additional daily 'cloud free' Chl-a interpolated product that minimizes missing data (CMEMS, 2021a). Both GlobColour and OC-CCI have been validated and assessed for quality standards on a global scale (ACRI-ST, 2007; ESA OC-CCI, 2021). However, Chl-a products have shown regional accuracy biases when compared to observed data (Bailey & Werdell, 2006), and it is therefore recommended that a comparison between products and in situ water samples should be implemented to aid product selection (Welch et al., 2020).

Regional accuracy biases are particularly pronounced in Case 2 water bodies, where the contribution of colour dissolved organic matter (CDOM) and inorganic mineral particles in addition to phytoplankton affect the optical signal (Matsushita et al., 2012), making the application of ocean colour remote sensing challenging (Carswell et al., 2017; Gbagir & Colpaert, 2020; Giannini et al., 2021; Gordon & Morel, 1983; Hilborn & Costa, 2018; Komick et al., 2009; Moradi, 2021; Phillips & Costa, 2017a). This highlights the need for product validation where Case 1 algorithms are applied to complex Case 2 waters. Specifically on the west coast of Canada, the evaluation of Chl-a product performance is necessary due to the optically complex nature of the B.C. coastal waters (Carswell et al., 2017; Giannini et al., 2021; Hilborn & Costa, 2018; Komick et al., 2009; Loos & Costa, 2010; Phillips & Costa, 2017). This study area is complex, having a 27300 km long coastline comprised of a network of inlets, straits, passes, sounds and narrows (O'Neel et al., 2015; Richard E Thomson, 1981). This coastal region is under the influence of many riverine systems discharging terrigenous materials, including inorganic sediments and dissolved organic matter, which impact the water bio-optical properties (Giannini et al., 2021; Loos et al., 2017; McNicol et al., 2019; Oliver et al., 2017; Phillips & Costa, 2017; St. Pierre et al., 2020; Thomson, 1981). The off-shelf B.C. waters are optically simpler because particles are primarily composed of phytoplankton (Bishop et al., 1999). The ocean productivity is spatially and temporally dynamic in the B.C. coast, as it responds to regional and global forcings such as seasonal riverine outflows and large-scale climate oscillations (i.e. El Niño Southern Oscillation, Pacific Decadal Oscillation (PDO), the North Pacific Gyre Oscillation (NPGO) and the Southern Oscillation Index (SOI)), respectively (Giannini et al., 2021; Marchese et al., n.d.; Peña et al., 2019; Sasaoka et al., 2011; Suchy et al., 2019). To unravel the complexity of ocean productivity dynamics on an interannual and decadal

time scales, a long and continuous time series of remote sensing data is needed. As a first step to acquiring a suitable long term time series of Chl-a for the B.C. coast, this study evaluates OC-CCI and GlobColour merged Chl-a products. An additional qualitative analysis is done to determine whether the data reflects the region's large-scale seasonal trends and latitudinal dynamics. The most consistent product in this region can then be used for monitoring applications such as phytoplankton phenology and bioregionalization studies that will allow for data incorporation into marine management strategies along the B.C. coast.

2.3 Methods

2.3.1 Study Area

The study area, extending from 47-60° N and 122-140° W (**Figure 2a**), includes the coastal waters off northern Washington state, British Columbia, southeast Alaska and the adjacent open ocean waters of the subarctic northeast Pacific Ocean. The continental shelf off B.C. is generally narrower than 45 km, reaching 95 km in the shallow basins of the Hecate Strait and Queen Charlotte Sound (Thomson, 1981). In this region (**Figure 2a**), phytoplankton productivity varies spatially and interannually. The highest phytoplankton biomass and earliest blooms have been observed in the Strait of Georgia on the southern B.C. coast, with surface concentrations ranging from < 1 mg m^{-3} in winter to > 15 mg m^{-3} during bloom conditions, and the second-highest biomass along the southwest coast of Vancouver Island (Giannini et al., 2021; Jackson et al., 2015; Suchy et al., 2019). This high productivity can be attributed to upwelling favourable winds in summer (April-September) which brings nutrient-rich water toward the surface (Allen & Wolfe, 2013; Jackson et al., 2015; Masson & Peña, 2009; Peña et al., 2019; Ware & Thomson, 2005). Similarly, freshwater discharge increases both the stability and the supply of land-derived

silicate, which keeps both nutrients and phytoplankton in the euphotic zone (Jackson et al., 2015; Masson & Peña, 2009; Ware & Thomson, 2005). The northern B.C. coast to western Alaska regions are dominated by downwelling favourable winds most of the year, though nutrients supplied by river discharge, current-induced upwelling, coastal eddies, and winter upwelling winds increase phytoplankton production (Ware & Thomson, 2005).

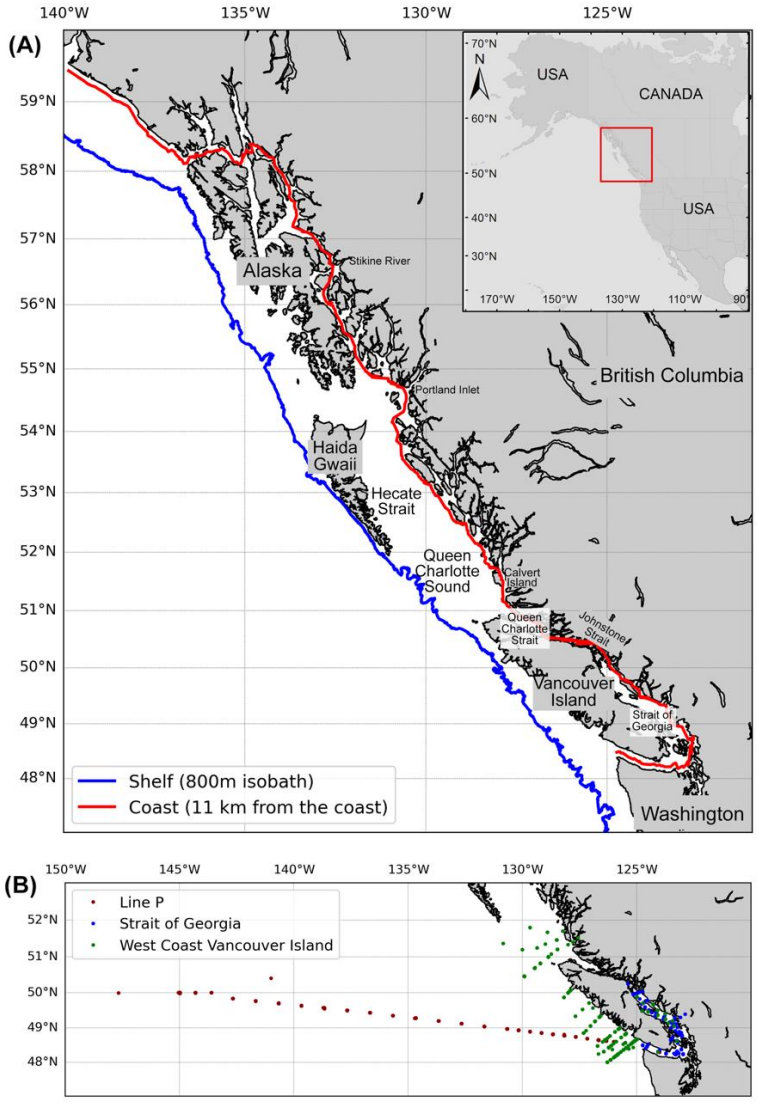

Figure 2: **(a)** Study area map with names of the main rivers and locations cited in the text and transect lines used to extract satellite product data from the coast (red line) and continental shelf over the 800m isobath (blue line). **(b)** Locations of in situ Chl-a data collected by DFO.

2.3.2 Datasets

The performance of three merged multi-sensor satellite Chl-a datasets, namely GlobColour CHL1 (Chla-GC), GlobColour interpolated (Chla-GCint) and OC-CCI (Chla-OC), were evaluated in the coastal and open ocean waters of B.C. using in situ Chl-a data provided by Fisheries and Oceans Canada (DFO), via a one-to-one match up analysis.

2.3.2.1 In situ Chl-a data

Chl-a data using High-Performance Liquid Chromatography (HPLC) methods were collected by DFO as part of their monitoring of the marine ecosystem. The validation data set (total = 1914) consisted of the Northeast Pacific measurements along Line P, conducted three times a year in winter, spring, and summer (2006-2017), off the west coast of Vancouver Island twice a year in spring and summer (2004-2017) and the Strait of Georgia three times a year in spring, summer, and fall (2011-2017), where physical, chemical and biological data were collected (**Figure 2b**). Briefly, water samples were filtered onto 47mm GF/F filters and stored at -80°C prior to analysis. In the lab, samples were extracted in 95% methanol at -20°C for 24 hours and analyzed on a WATERS 2695 HPLC separations system as detailed in Nemcek & Pena, (2014). Only surface samples less than 6.1 m were considered, and values flagged by DFO as poor measurements were removed prior to analysis. Additional information and the datasets can be accessed at https://open.canada.ca/data/en/dataset/871b0b32-3135-40c8-868e-c5d87800ca76. Other data sources were not used in an attempt to be consistent with the HPLC analytical methods implemented by DFO.

2.3.2.2 Merged multi-sensor satellite data

GlobColour and OC-CCI data products used in this study are open-access daily global data at a 4 km × 4 km spatial resolution downloaded for the period 1998-2021. Due to low solar elevation conditions in this region during the winter months, the analysis was computed using nine months, from mid-February to mid-November (Carswell et al., 2017; Jackson et al., 2015; Suchy et al., 2019).

GlobColour daily Chl-a product

GlobColour products correspond to continuous 23-year time series (1997-present) created by merging data from the following sensors: SeaWiFS (1997-2010), MERIS (2002-2012), MODIS-Aqua (2002-present), VIIRS-NPP (2012-present), OLCI-S3A (2016-present), VIIRS-SNPP (2017-present) and OLCI-S3B (2019-present). GlobColour provides merged products using three merging techniques: (i) simple averaging method (AV) of Level-2 Chl-a estimates, (ii) weighted average (AVW) of Level-2 Chl-a estimates adjusted to MERIS using the OC4Me algorithm, and (iii) using the Garver-Siegel-Maritorena (GSM) model to merge Level 3 normalized water-leaving radiances across sensors prior to producing Chl-a retrievals (ACRI-ST GlobColour Team, 2020; Welch et al., 2020). The algorithms used to determine chlorophyll concentration also vary. The CHL1 product is computed using classic blue to green band ratios (OC4 ocean colour algorithm) applicable for Case 1 waters (available in AVW and GSM merging), CHL-OC5 is based on the blended OC5/CIA-Hu algorithm (AVW merging) and to obtain CHL2, neural networks trained for Case 2 waters are used (with AV merging; ACRI-ST GlobColour Team, 2020). Due to limited temporal availability of CHL2 (2002-2012), it was not considered

in this analysis. Initial validation of the CHL-OC5 resulted in poor statistics (not shown), therefore, only the CHL1 algorithm with GSM merging is further considered for this analysis.

The CHL1 product that has been merged using the GSM model has been shown to provide more accurate chlorophyll concentration estimates in the Northeast Pacific (Komick et al., 2009) and the best fit to in situ Chl-a compared to alternative GlobColour products (ACRI-ST GlobColour Team, 2020; Clay et al., 2019). Although the CHL1 algorithm provides the best performance over Case 1 waters and has not been recommended for use over optically complex coastal waters (ACRI-ST GlobColour Team, 2020; Moradi, 2021), the application of Case 1 algorithms to coastal waters can occur provided that a verification of the Chl-a concentration using in situ measurements confirms the reliability of the product (Jackson et al., 2015). GlobColour data was obtained in April 2021 from http://hermes.acri.fr.

GlobColour interpolated Chl-a product

Since 2016, the Copernicus Marine Environment Monitoring Service (CMEMS) has provided a 'cloud free' interpolated daily product, significantly improving quality and coverage of daily data upstream (CMEMS, 2021a). This interpolated product is produced by first merging Chl-a fields estimated using different algorithms (OC3 and OC5 for Case 1 and 2 waters, respectively) generated from Level 2 reflectance (Saulquin et al., 2019). This Level 3 multi-algorithm product is then used as input for the spatio-temporal interpolation, an advanced version of the standard optimal interpolation technique that includes anisotropic covariance models at the coastline for a better reconstruction of coastal gradients (Saulquin et al., 2019). Interpolated GlobColour data

was obtained in October 2021 from https://resources.marine.copernicus.eu/product-detail/OCEANCOLOUR_GLO_CHL_L4_REP_OBSERVATIONS_009_082/DATA-ACCESS.

OC-CCI Chl-a product

The OC-CCI Chl-a dataset (v5.0) is generated by shifting the wavelengths of SeaWiFS, MODIS, VIIRS and OLCI data to match MERIS bands, applying bias-correction, merging the datasets and computing per-pixel uncertainty estimates (Jackson, 2020). POLYMER (v.4.12) atmospheric processing is applied, and Chl-a is estimated using a blended algorithm including OCI, OCI2, OC2, OC3, OCx and OC5 algorithms, which attempts to weight the outputs of the best-performing algorithm based on the water types present (Jackson, 2020). The OC-CCI dataset, Version [v5.0], ESA, was obtained in September 2021 from http://www.esa-oceancolour-cci.org/. Additional information can be accessed at: https://climate.esa.int/en/projects/ocean-colour/key-documents/https://climate.esa.int/en/projects/ocean-colour/data/)

2.3.3 Satellite data analysis

To ensure that the Chl-a concentrations derived from the merged satellite products are accurate in B.C. waters, the Chl-a retrievals were compared to the in situ measurements. Match-up product Chl-a data was obtained from a 3 × 3 pixel window (144 km^2) centered in the in situ sampling location, with a time window of ± 3 hours from 12:00 in the Strait of Georgia, ± 5 hours for the west coast of Vancouver Island and ± 12 hours for Line P (**Figure 2b**). This time window was defined to be short enough to reduce the effects of temporal variability of the in situ data, particularly in more dynamic regions, yet large enough to allow for the greatest possibility

of a match (Bailey & Werdell, 2006). The mean, median, standard deviation, filtered mean, filtered standard deviation and coefficient of variation (CV) were computed, and match-ups were retained if a minimum of 5 out of the 9 pixels were available and the CV < 25% (Bailey & Werdell, 2006; Giannini et al., 2021). To minimize the impact of low quality match-ups, the area of the Fraser River plume was excluded since high turbidity has been shown to result in inaccurate chlorophyll estimates (Carswell et al., 2017; Giannini et al., 2021; Komick et al., 2009), and the high spatial variability of plume-ocean transitional waters can compromise the results of satellite validation, satellite retrievals and downstream products and results (Hussain et al., 2022). To quantitatively evaluate the performance of the merged satellite products, metrics for accuracy (Root Mean Square Error (RMSE) and Median Absolute Difference (MdAD)), bias and goodness of fit (r^2 and slope) were calculated (Seegers et al., 2018):

$$\text{Filtered mean} = \frac{\Sigma_i(\bar{X}-1.5*\sigma)<X_i<(\bar{X}+1.5*\sigma)}{N} \quad (1)$$

$$\text{RMSE} = \sqrt{\frac{\sum_{i=1}^{n}(log_{10}(Sat_i)-log_{10}(InSitu_i))^2}{n}} \quad (2)$$

$$\text{MdAD} = 10^{Median|log_{10}(Sat_i)-log_{10}(InSitu_i)|} \quad (3)$$

$$\text{BIAS} = 10\text{^}\left(\frac{\sum_{i=1}^{n} log_{10}(Sat_i)-log_{10}(InSitu_i)}{n}\right) \quad (4)$$

where Sat_i is the filtered mean of the 3 × 3 pixel window of the satellite-derived data, $InSitu_i$ is the in situ measurement, and n is the number of samples. For equation 1, $\overline{X}$ is the unfiltered mean value, σ is the standard deviation of the unfiltered data, and N is the number of values within $1.5 * \sigma$ (standard deviation). Note that chlorophyll was log-transformed prior to calculating error metrics (Seegers et al., 2018).

Additional analysis was done to evaluate the data quality for large-scale dynamics of the study region. Seasonal trends were derived from the 23-year (1998-2021) climatology of Chl-a data produced with the product with the best statistical match up results, which was separated into averages and standard deviations for Spring (February-May; **Figure 4a**), Summer (June-August; **Figure 4b**) and Fall (September-November; **Figure 4c**; Giannini et al., 2021). Latitudinal transects were extracted from the seasonal composites of chlorophyll concentration along the coastline (11km from the coast) and over the outer margin of the continental shelf (following the 800 m isobath, which is ~65 km from the coastline; **Figure 2a**). The transect data was averaged from a 3 × 3 pixel window of the data, representing a 12 km wide band which was averaged along each latitude. The resulting latitudinal trends (**Figure 5a-c**) were verified according to known Chl-a seasonal and latitudinal dynamics over the study region.

2.4 Results

2.4.1 Statistical analysis

The performance of three different merged satellite products were evaluated by comparing satellite-derived Chl-a to in situ Chl-a concentrations via a one-to-one match up analysis described in Section 2.3. The in situ Chl-a for the match-ups ranged from 0.04 to 40.4 mg m^{-3}, reflecting the expected annual conditions experienced in the British Columbia waters (Jackson et al., 2015). From the total 1914 in situ measurements, 124 were match-ups for Chla-GC, 201 were match-ups for Chla-OC and 797 were match-ups for Chla-GCint. The number of match-ups differs for products due to differing valid pixels for the same in situ data points. **Figure 3a-f** and **Table 1** show the results for all the match-ups for each Chl-a product. Generally, Chla-GC outperformed the other products in all statistics apart from slope and r-value, where Chla-GCint had a slope (slope = 0.88) closer to unity than Chla-GC (slope = 0.77) and Chla-OC (r = 0.91) had the same r-value as Chla-GC (r = 0.91; **Table 1**). The Chla-GC match-up analysis resulted in data that are closely concentrated around the best fit line with very few values exceeding two standard deviations (RMSE = 0.23, r = 0.91; **Figure 3e**), a slope relatively close to unity (slope = 0.77), a relative measurement error of 35% (MdAD = 1.35), and a model underestimation of 1% (BIAS = 0.99; **Table 1**). Additionally, 84% of the variance in the Chla-GC concentration is predictable from the in situ Chl-a concentration (r^2 = 0.84). The distribution of Chla-GC follows the in situ Chl-a data distribution very closely up to about 0.6 mg m^{-3}, and slightly overestimates the higher range of Chl-a; it begins to diverge thereafter (**Figure 3b**). The regression line crosses the 1:1 line at -0.2 $\log_{10}$ meaning that Chla-GC underestimate (overestimate) values greater (less) than 0.6 mg m^{-3} (**Figure 3e**).

The statistics resulting from the Chla-OC match-up analysis were only slightly inferior to those of Chla-GC, having data also closely concentrated around the best fit line (RMSE = 0.27, r = 0.91), a more gradual slope (slope = 0.68), a relative measurement error of 45% (MdAD = 1.45), a model underestimation of 13% (BIAS = 0.87), and 82% of explained variance (r^2 = 0.82). Similarly, the Chla-OC distribution follows the in situ curve, although not as closely as Chla-GC, and diverges at a lower Chl-a of 0.3 mg m^{-3} (**Figure 3c**). Identical to Chla-GC, Chla-OC underestimate (overestimate) values greater (less) than 0.6 mg m^{-3}, however, Chla-OC over/underestimates at a slightly greater degree with a slope of 0.68 (**Figure 3f**). Chla-OC has a larger number of match ups (n = 201) than Chla-GC (n = 124), which indicates that it has better spatial coverage (**Figure 3f**) and fewer missing data.

Lastly, the distribution of the Chla-GCint shows a similar shape to the in situ Chl-a distribution, with a slight underestimation compared with the in situ values (**Figure 3a**). The Chla-GCint also has the fewest missing data out of all products evaluated (**Figure 3d**), which is reflected in the slightly lower performance in all statistics apart from slope (0.88), having data dispersed around the best fit line with numerous outliers beyond two standard deviations (RMSE = 0.37, r-value = 0.79, **Figure 3d**), a relative measurement error of 69% (MdAD = 1.69), a model underestimation of 19% (BIAS = 0.81) and 63% of explained variance (r^2 = 0.63).

When considering solely Case 1 waters (Line P match-ups), Chla-GC outperforms the other two products for all the metrics, including slope, with Chla-OC following closely. The statistics for Chla-GC Case 1 have even improved from the combined Chla-GC statistics for all the parameters except intercept and BIAS, having a value of 1.06 indicates a model overestimation

of 6%, compared to a model underestimation of 1% for all water types combined (**Table 1**). The Chla-GCint product, however, showed a degradation of statistics, specifically a slightly lower r-value (0.77 from 0.79) and slope (0.71 from 0.88; **Figure 3d**). Further, the Chla-GCint data points show a clear pattern based on the sampling region. The data points for Case 1 waters are very concentrated at lower Chl-a concentration values compared to the data points for Case 2 waters (west coast of Vancouver Island and Strait of Georgia match-ups), which yield higher concentrations and a greater spread, meaning that the match-ups in coastal waters are more variable (**Figure 3d**). For these waters, although very small differences occurred, Chla-GC has the best statistics for slope (0.60), intercept (0.05), BIAS (0.93), MdAD (1.43) and RMSE (0.28), and Chla-OC has the best statistics for r (0.81), r^2 (0.65) and intercept (0.04; **Table 1**).

Table 1. Statistical output comparing product performance for the OC-CCI, GlobColour CHL1 and GlobColour interpolated match-up analysis. The shaded cells indicate which product performed best for each water type, and the bold numbers show which product had the best performing statistic overall.

	All			**Case 1**			**Case 2**		
	OC-CCI	**GC**	**GC int**	**OC-CCI**	**GC**	**GC int**	**OC-CCI**	**GC**	**GC int**
n	201	124	797	73	60	514	128	64	283
r	0.91	0.91	0.79	0.96	**0.97**	0.77	0.81	0.73	0.51
r²	0.82	0.84	0.63	0.91	**0.94**	0.59	0.65	0.54	0.26
slope	0.68	0.77	**0.88**	0.70	0.81	0.71	0.51	0.60	0.50
intercept	-0.05	**-0.02**	-0.12	-0.13	-0.04	-0.30	0.04	0.05	0.15
P value	<.001	<.001	<.001	<.001	<.001	<.001	<.001	<.001	<.001
BIAS	0.87	**0.99**	0.81	0.91	1.06	0.68	0.84	0.93	1.10
MdAD	1.45	1.35	1.69	1.34	**1.30**	1.61	1.51	1.43	1.79
RMSE	0.27	0.23	0.37	0.22	**0.17**	0.29	0.29	0.28	0.48

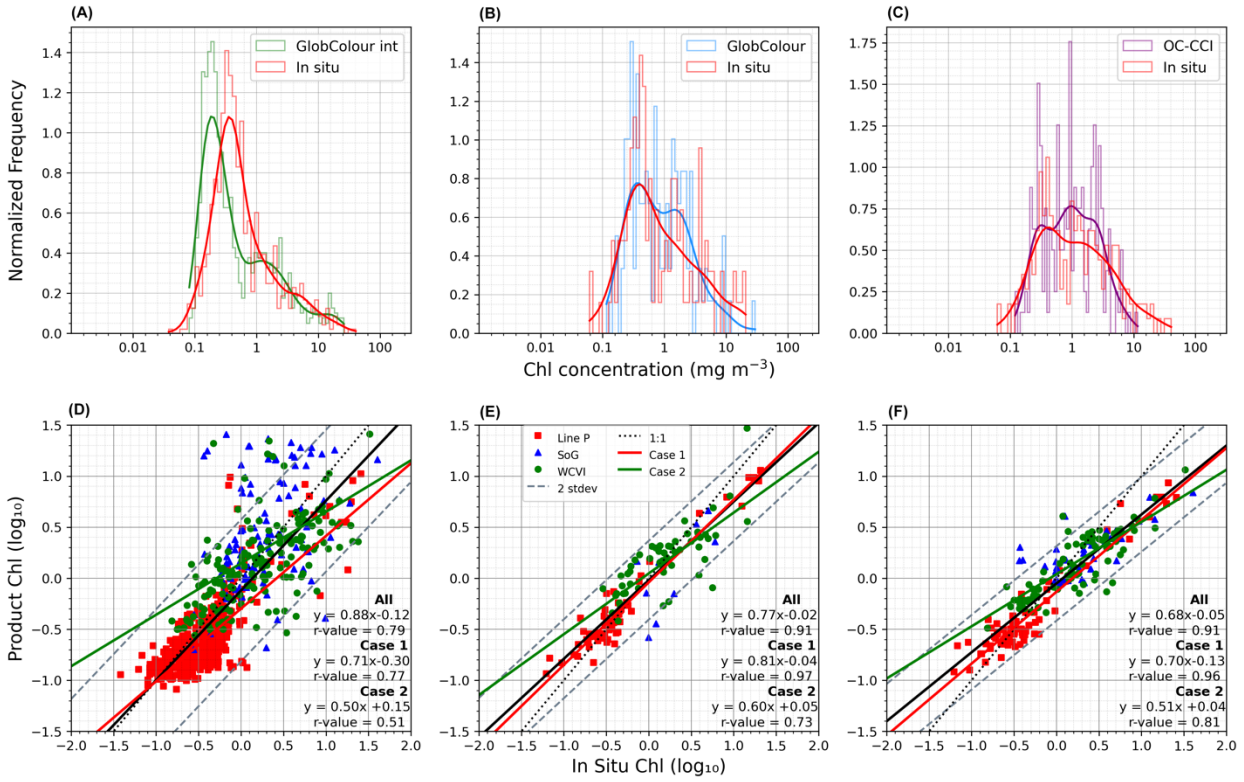

Figure 3: The top row shows the normalized frequency distribution of the Chl-a match-up measurements for **(a)** GlobColour interpolated (green), **(b)** GlobColour CHL1 (blue) and **(c)** OC-CCI (purple) with coincident in situ measurements (red). The lines show a stepped histogram with 50 bins, while the curve represents a kernel-density estimate using Gaussian kernels. The bottom row shows the **(d)** GlobColour interpolated, **(e)** GlobColour CHL1 and **(f)** OC-CCI derived Chl-a to in situ Chl-a match-up scatterplot comparisons. The red, green and blue markers represent data from Line P, west coast of Vancouver island (WCVI) and Strait of Geogria (SoG) locations, respectively. The black line represents the best fit line, the black dotted line is the 1:1 line, and the grey dotted lines represent 2 standard deviations of the best fit line. The green and red lines represent Case 1 waters (Line P) and Case 2 waters (SoG and WCVI) respectively. Data were $\log_{10}$ transformed for display.

2.4.2 Seasonal and latitudinal trends

Based on the statistical analysis, GlobColour was found to be the best performing product and has therefore undergone a further analysis to evaluate the quality of this product to capture known spatial and temporal patterns of bloom dynamics for this region. Seasonal trends corresponding to spring, summer and fall were derived from the 23-year (1998-2021) Chla-GC data series. The retrieved temporal trends showed that, in the B.C. coast, the maximum bloom concentrations are observed in the Strait of Georgia in spring and on both the west coast of Vancouver Island and Queen Charlotte Strait in summer (**Figure 4a,b**). In fall, a secondary

phytoplankton bloom is observed, with the highest concentrations occurring on the west coast of Vancouver Island and Washington coast (**Figure 4c**). The central and northern B.C. coastal waters had lower concentrations on average, with the lowest surface chlorophyll concentrations observed off the west coast of Haida Gwaii (**Figure 4a-c**).

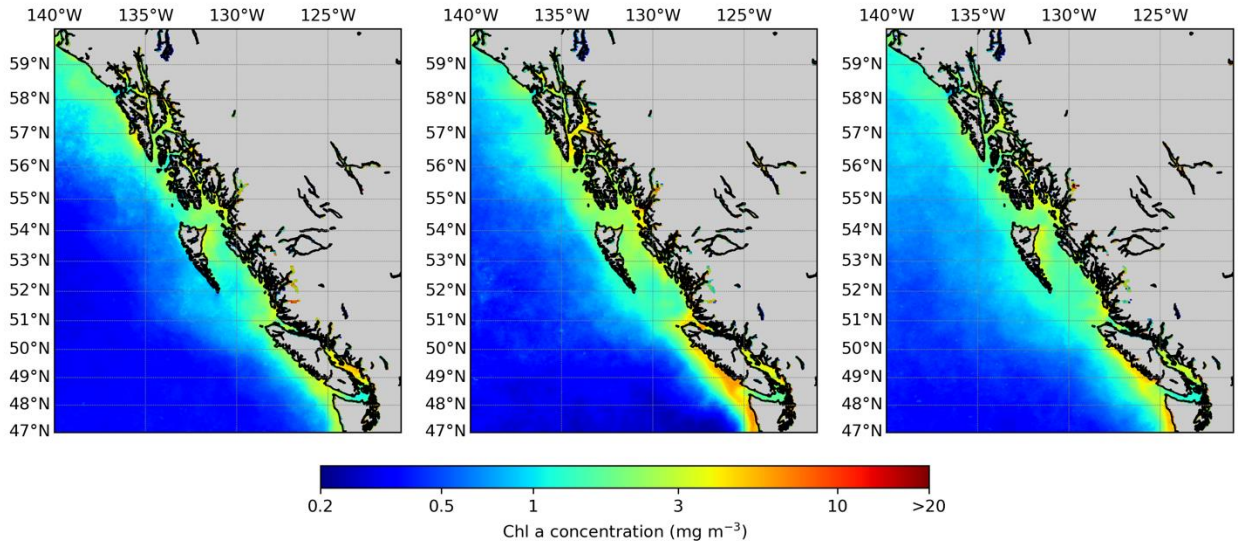

Figure 4: Seasonal climatology derived from GlobColour Chl-a data for **(a)** Spring (February-May), **(b)** Summer (June-August), **(c)** Fall (September-November).

Spatially, transects of Chl-a seasonal averages along the continental shelf and coastline reveal that in the B.C. coastal region, Chl-a values ranged from 0.7 ± 0.2 to 8.1± 5.1 mg m^{-3} (**Figure 5a-c**). The maximum coastal Chl-a values were found in the Central SoG in spring (7.0 ± 6.2 mg m^{-3} at ~49.3°N; **Figure 5a, coast**), near Portland Inlet in summer (8.1 ± 5.1 mg m^{-3} at ~54.8°N; **Figure 5b, coast**), and near Calvert Island in fall (5.3 ± 3.7 mg m^{-3} at ~51.5°N; **Figure 5c, coast**). Additionally, a Chl-a peak can be observed in the vicinity of the Stikine River mouth at ~57.1°N in summer (**Figure 5b**), and a secondary bloom in the Strait of Georgia at ~48.9°N in fall (**Figure 5c, coast**). In contrast, the lowest Chl-a coastal values were found along Johnstone

Strait (50.2-50.5°N, **Figure 5c, coast**), and generally low Chl-a values in the northern southeast Alaska waters (north of 58.4°N, **Figure 5a-c, coast**).

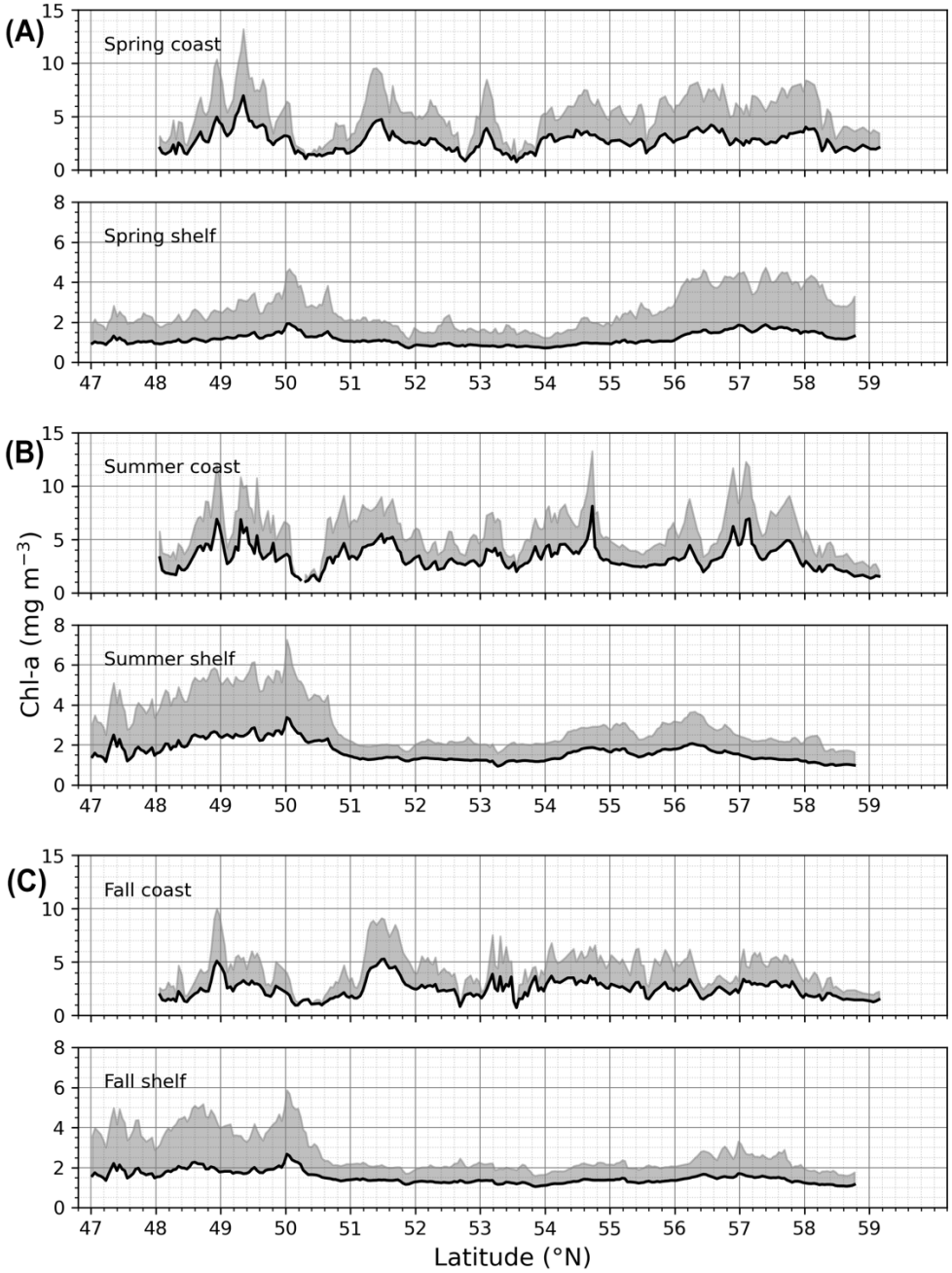

Figure 5: Chl-a latitudinal distribution for GlobColour seasonal averages for **(a)** Spring, **(b)** Summer and **(c)** Fall along the coast and continental shelf transects in British Columbia and Southeast Alaska. Gray shaded area represents positive standard deviations. Note the different y-axis scales between the coast and shelf plots.

2.5 Discussion

This study provides an evaluation of merged multi-sensor Chl-a products from OC-CCI, GlobColour CHL1 and interpolated GlobColour in the coastal and open ocean waters off southern B.C. This is an important step prior to using these products for monitoring applications such as phytoplankton phenology and bioregionalization studies, since regional optical complexity makes the application of ocean colour remote sensing challenging and can introduce accuracy biases (Bailey & Werdell, 2006; Carswell et al., 2017; Giannini et al., 2021; Phillips & Costa, 2017b; Welch et al., 2020). The comparison of satellite-derived Chl-a with in situ measurements suggests that the GlobColour CHL1 products are generally more consistent in this region compared to OC-CCI and interpolated GlobColour products. The other data products have their advantages - OC-CCI has fewer missing data than any other global time series for ocean color due to the implementation of the POLYMER atmospheric correction algorithm (Sathyendranath et al., 2019) while the GlobColour interpolated product is free from missing data. However, for interpolated products, there are caveats of having degraded statistics due to the estimations of interpolated values being based on assumptions (Stock et al., 2020; Hilborn and Costa, 2018), causing Chl-a values to diverge from in situ Chl-a. Despite having different absolute Chl-a concentrations (r^2=0.63, **Table 1**), the GlobColour interpolated product shares the same distribution as the in situ data (**Figure 3a**), which makes it suitable for use in studies concerning phytoplankton phenology where Chl-a trends and seasonality are prioritized over absolute concentrations.

Generally, the differences between the Chl-a retrievals for the different products can be attributed to the characteristics of the products themselves, such as the choice and performance

of the atmospheric correction scheme, the ocean color inversion algorithm and merging techniques applied, or due to the spatial and temporal quality of the match-ups, including uncertainties associated with in situ Chl-a data, and the chosen statistics. The differences in the performance between OC-CCI and GlobColour can be attributed to the algorithms, atmospheric correction, merging strategies and flagging schemes (Garnesson et al., 2019). OC-CCI uses the CIA and OC5 algorithms, whereas GlobColour CHL1 employs the OC4 ocean colour algorithm. The merging strategy used by OC-CCI is based on a preliminary merging of remote sensing reflectance of a set of sensors which is then used to derive Chl-a. OC-CCI derives Chl-a using a blended Chl-a algorithm that attempts to weight the outputs of the best performing algorithms based on the water types present (Garnesson et al., 2019). Alternatively, GlobColour first computes Chl-a for each sensor using their specific resolutions and spectral bands, and subsequently resamples and merges the single sensor Chl-a products (Garnesson et al., 2019). Further, the continuity for GlobColour algorithms used for mesotrophic and complex waters are determined by the OC5 lookup table, and when Chl-a concentrations range from 0.15 to 0.2 mg m^{-3} a linear interpolation of OC5 and CIA is used (Garnesson et al., 2019). Beyond the different approaches to generate a merged Chl-a product, different quality flagging strategies are used: GlobColour uses the OC5 flagging strategy, which employs an algorithm that uses the official flags and empirical thresholds that have been adjusted for each sensor; OC-CCI uses a more constrained flagging strategy that depends on the sensor – for instance, a pixel-classification algorithm (Idepix) was implemented for MERIS and SeaWiFs data processing in v2, with NASA's Level 2 Generator being used for the other sensors (Sathyendranath et al., 2019).

Beyond the different atmospheric correction, merging strategies and flagging schemes applied to these products, differences in the spatio-temporal scale of sampling between the satellite and in situ measurements need to be considered in the analysis of the Chl-a accuracy of each product. The GlobColour and OC-CCI products footprint (16 km^2) covers an area orders of magnitude larger than that captured by the in situ measurement (<1m; Sá et al., 2015; Holm-Hansen et al., 2004), and this disparity is exacerbated due to the 3 × 3 pixel box (144 km^2) used in the match up analysis. This 3 × 3 pixel box is widely applied to account for the spatial variability of biogeochemical information and as a rationale for satellite sensor navigation not being accurate to the pixel (Bailey & Werdell, 2006; Barnes et al., 2019; Pahlevan et al., 2016; Patt, 2002). The spatial variability of coastal waters also affects the quality of the in situ data to be used in a match up, where data acquired from interface or transition waters are generally of a lower quality (Hussain et al., 2022; Pahlevan et al., 2016). Additionally, the temporal aspect of the match-up time difference between the in situ data and the satellite overpass poses considerable uncertainties on the validation of satellite-derived products especially for coastal waters. Coastal waters are highly dynamic and have a greater optical complexity due to the influences of river discharge containing terrestrial suspended particulates, re-suspended sediments and CDOM that vary independently of the phytoplankton assemblage (Blondeau-Patissier et al., 2014; Hussain et al., 2022; IOCCG, 2000; Loos et al., 2017; Loos & Costa, 2010; Phillips & Costa, 2017). To account for this, the area of the Fraser River plume was excluded since it is very temporally dynamic due to tide, current and river discharge conditions, which can result in inaccurate chlorophyll estimates (Carswell et al., 2017; Giannini et al., 2021; Hussain et al., 2022; Komick et al., 2009). GlobColour and OC-CCI products do not contain a timestamp, however products are obtained from sun-synchronous satellites having a Crossing Nodal Time at the equator

between 9:50 to 13:30 (PDT) depending on the satellite, which is why an approximate time of 12:00 is used in this analysis and by GlobColour global validation (ACRI-ST, 2007). Temporal match-up windows of ±3, ±5 and ±12 h intervals around midday were applied to the Strait of Georgia (estuarine), the west coast of Vancouver Island (coastal) and Line P (open ocean; **Figure 2b**) respectively, in order to reduce the effects of temporal variability of the in situ data, particularly in more dynamic regions (Bailey & Werdell, 2006). The longer time window of 12 hours is acceptable for open ocean waters since the subarctic North Pacific is a high nitrate low chlorophyll region (HNLC), controlled by large-scale currents with minimal seasonal variability of primary productivity, and is relatively more homogenous than coastal waters (Brickley & Thomas, 2004; Childers et al., 2005). While these specific conditions were taken into consideration to minimize the match-up time in more dynamic regions (Section 2.4), inconsistencies can still occur because the in situ collection and satellite overpass did not occur simultaneously.

Other sources of uncertainty that can impact the validation results includes error associated with analytical quality of the in situ measurements; despite being used as 'ground truth' measurements, they are seldom 'absolute truth' and their uncertainties should be recognized (Bailey & Werdell, 2006). The quality of in situ data is dependent on measurement protocols involving sampling, filtration, storage, extraction, HPLC analysis, instrument calibration and deployment, to name a few (Sá et al., 2015). In an attempt to reduce systematic uncertainties pertaining to data processing, it is advised that data be consistently processed using a single-source processor (Bailey & Werdell, 2006), which is why HPLC data processed solely by DFO was used here.

Lastly, the metrics used for the statistical analysis needs to be carefully chosen to suit the data type. BIAS and MdAD are metrics based on simple deviations that are well suited for evaluating non-Gaussian distributions and outliers, and therefore take precedence over the interpretation of RMSE, the coefficient of determination (r^2) and regression slopes, which are most appropriate for Gaussian distributions with outliers making them suboptimal metrics to determine ocean colour algorithm assessment (Seegers et al., 2018). Additionally, slope and r^2 are useful metrics for ocean colour validation, however, they must be interpreted in the context of BIAS and MdAD, as these metrics could be misleading when interpreted in isolation (Seegers et al., 2018). Here, we took these precautions into consideration by giving precedence to BIAS and MdAD and interpreting the other metrics in context of them.

Given the many sources of uncertainties associated with these merged data products, many studies perform a regional comparison to in situ Chl-a concentrations to ensure that the products can be applied to optically complex waters, despite these merged multi-sensor products having been already validated on a global scale. Particularly, the analysis undertaken by Swart et al. (2012) over the Good Hope line south of Africa, showed similar r^2 of 0.84 as our results (**Table 2)**, but a slightly higher RMSE of 0.50. Pitarch et al. (2016) also performed a comparison between GlobColour and OC-CCI in the Baltic Sea, however in contrast to our findings, OC-CCI OC5 emerged as the best performing product and GlobColour performed worst in that region. Nonetheless, the OC-CCI OC5 statistics defined by Pitarch et al. (2016) are comparable to the OC-CCI Case 2 statistics defined here. The validation of Case 1 waters generally have better statistics than those derived in Case 2 waters (**Table 2**). Many studies do not perform a regional

validation prior to utilizing data products in their research (**Table 2** – not validated), and of other studies that did perform a validation, the statistics obtained were generally inferior to the validation statistics derived here. Compared to regional studies that utilize different satellites and implement different methodologies, the statistics obtained here are comparable to, and in some cases outperform, the statistics obtained in other local studies. For instance, the GlobColour statistics obtained here generated a lower BIAS and RMSE, and a larger r-value than Carswell et al. (2017), and a greater r-value, slope and lower BIAS and MdAD than Giannini et al., (2021), therefore attesting to the quality of the GlobColour derived product.

Considering the match-up statistics for Case 1 and Case 2 waters individually, our results indicate how the quality of products can vary in different environmental conditions, highlighting the need for continuous assessment of satellite derived Chl-a products, particularly in optically complex waters (Bailey & Werdell, 2006; Giannini et al., 2021; Hilborn & Costa, 2018; Komick et al., 2009; Swart et al., 2012; Welch et al., 2020). The results for Case 1 waters showed the improved statistics for Chla-GC and Chla-OC since the Chl-a algorithms were modeled for these water types (ACRI-ST GlobColour Team, 2020; Sathyendranath et al., 2019), and the statistics degraded for Chla-GCint (**Table 1**). The statistics obtained for Case 2 waters for OC-CCI (**Table 1**) were similar to those obtained by OC-CCI OC5 algorithm from Pitarch et al., 2016 (**Table 2**). The statistics for all products had degraded in Case 2 waters, thus highlighting the challenges of ocean colour remote sensing, and particularly the application of algorithms designed for Case 1 waters in these Case 2 waters.

Despite the statistics obtained here, considering all the possible challenges mentioned hitherto and the caution taken to minimize these issues, it remains complicated to truly evaluate the uncertainties associated with global products. As such, a general comparison with the Chl-a trends published in the literature also provides a tool for product evaluations. Therefore, to further evaluate the application of the GlobColour Chl-a product for British Columbia and southeast Alaska, the seasonal and latitudinal ranges of variability in Chl-a were compared with those previously reported for different parts of the coast (**Figure 5a-c**), particularly since our in situ match-up dataset was mostly constrained to the southern B.C. coast due to data availability. The GlobColour Chl-a product demonstrated the expected seasonal and local dynamics for this region, and average concentrations within ranges reported for satellite-derived observations (Carswell et al., 2017; Giannini et al., 2021; Gower et al., 2013; Jackson et al., 2015; Marchese et al., 2022; Suchy et al., 2019), and in situ measurements (Masson & Peña, 2009). For instance, this region typically experiences maximum Chl-a concentrations in the spring and summer (Carswell et al., 2017; Del Bel Belluz et al., 2021; Giannini et al., 2021; Jackson et al., 2015; Masson & Peña, 2009; Noakes et al., 2000; Suchy et al., 2019), with a secondary fall bloom being observed in the BC coastal waters (Chandler et al., 2015; Giannini et al., 2021; Suchy et al., 2019), particularly evident in the vicinity of Calvert Island (51.5°N; Fig 1g, coast). Along the continental shelf, the west coast of Vancouver Island experienced relatively higher Chl-a concentrations (maximum of 3.4 ± 3.9 mg m^{-3}; 50°N, Fig.1e-g, shelf), consistent with reported concentration ranges and bloom timing (Chandler et al., 2015; Giannini et al., 2021). The B.C. central shelf region between Haida Gwaii and Vancouver Island show lower Chl-a concentrations overall, compared to the southeast Alaska shelf region that is shown to be relatively more productive in summer.

Table 2. Non-exhaustive list of research using GlobColour/OC-CCI merged Chl-a data in different regions, study periods and water types. Table is separated into research that has validated the Chl-a data prior to use, and the reported statistics, followed by those that did not validate the products with in situ Chl-a data.

Author	Product	Time	Location	Case 1/2	N	R^2	RMSE	BIAS
Validated								
(Swart et al., 2012)	GC-OC4	2010-2011	the GoodHope line south of Africa	1	121	0.84	0.50	
(Laiolo et al., 2021)	GC-GSM	2016	offshore eastern Australia ocean region	1	9			0.63
(Johnson et al., 2013)	GC-AVW	2001-2008	Southern Ocean	1		0.25		
(Gbagir & Colpaert, 2020)	GC CHL-OC5	1997-2019	Lake Ladoga	2	Not reported			
(Pitarch et al., 2016)	GC-GSM	1997-2012	Baltic Sea	2	1873	0.3	0.42	0.77
	OC-CCI OC5				1873	0.44	0.28	0.86
	OC-CCI OC4v6				1873	0.43	0.33	1.44
(Moradi, 2021)	GC-CHL2	2008-2018	Persian Gulf	2	275	0.41	0.53	4.15
	OC-CCI				487	0.44	0.49	0.38
(Cherkasheva et al., 2014)	GC-GSM	1998-2009	Fram Strait/ Greenland Sea	1 & 2	108	0.34	0.58	
(El Hourany et al., 2019)	GC CHL-OC5	1997-2014	Global	1 & 2		0.49		
Not validated								
(Navarro et al., 2012)	GC-GSM	1997-2010	center of the Gulf of Cádiz, eastern North Atlantic	1				
(Martinez et al., 2018)	GC	1997-2014	Marquesas Islands (Central South Pacific)	1				
(Welch et al., 2020)	GC-AVW, GC-GSM, OC-CCI	2015-2018	California Current Ecosystem	1 & 2				
(Ford et al., 2012)	GC-GSM	1997-2011	Global	1 & 2				
(Cole et al., 2012)	GC-AVW	2002-2006	Global	1 & 2				

(Garnesson et al., 2019)	GlobColour and OC-CCI	1997-2019	Global	1 & 2				

2.6 Conclusion

The performance of OC-CCI and GlobColour merged Chl-a products were evaluated in B.C. waters using in situ data to determine which product is the most suitable for use in this region. An additional qualitative analysis was done to determine whether the data reflects the region's large-scale seasonal trends and latitudinal dynamics. The satellite to in situ match-up analysis in this region revealed that GlobColour CHL1 emerged as the best performer across most metrics, followed closely by OC-CCI. The GlobColour CHL1 dataset also reflects the expected general seasonal and latitudinal averages over the entire study region. Compared to other studies, the GlobColour statistics obtained here were comparable to, and in some cases outperformed other validation statistics. OC-CCI has better spatial coverage in this region compared to GlobColour, having a higher number of match-ups. Lastly, the GlobColour interpolated product has the highest spatial coverage since it has been 'gap-filled,' and would be appropriate for use in studies requiring a spatially and temporally complete dataset with a slight disregard for absolute Chl-a concentration, such as phytoplankton phenology studies. Although several studies have shown that the OC-CCI and GlobColour Chl-a datasets can be implemented in coastal turbid waters to monitor Chl-a concentrations (Johnson et al., 2013; Mélin et al., 2017; Moradi, 2021; Sá et al., 2015), the application of these products in primarily Case 2 waters needs to be done with caution, considering the reduction in statistical performance shown in this study. It is therefore recommended that a comparison between products and in situ water samples should be implemented in study areas that are solely Case 2 to aid product selection.

3.0 Characterizing phytoplankton phenology patterns in the Northeast Pacific coastal waters from 1998 to 2020 based on GlobColour satellite data

3.1 Abstract

Phytoplankton phenology is an important ecological indicator that characterises the timing of annually occurring phytoplankton growing periods and has been typically synthesized into a set of indices encompassing the timing, duration, and magnitude of bloom events. Phytoplankton phenology and its underlying drivers are spatially variable, and the study of its patterns over heterogenous regions benefits from a delineation of regions with specific phenological properties. This study aims to characterize phytoplankton phenology patterns over the B.C. and SE Alaska coast over a 23-year period (1998-2020), using the Hierarchical Agglomerative Clustering method based on phenological indices derived from the interpolated GlobColour product. The delineated bioregions are then used to describe region-specific phytoplankton phenological patterns associated with bloom magnitude, frequency, duration, and timing. The interannual variability of spring bloom initiation was evaluated considering interactions with environmental variables, sea surface temperature anomaly and the El Nino Southern Oscillation index. Four coherent bioregions were identified over the study region with distinctive phytoplankton phenological properties: two coastal regions, one shelf region and an offshore region. We found that early spring blooms were associated with a positive SST anomaly and El Nino conditions. Conversely, average or late spring blooms occurred in years where there was a negative SST anomaly and La Nina conditions. Furthermore, the relationship between spring bloom initiation and principal bloom initiation was evaluated, and we found that when there is a later spring bloom initiation we can expect a later principal bloom initiation, and vice versa.

3.2 Introduction

Phytoplankton are single-celled photosynthetic bacteria and microalgae that occupy the photic zone of the ocean (Kirby, 2011), where they play a vital role in regulating the structure and health of marine ecosystems (Brody et al., 2013). Forming the base of the marine food web, phytoplankton are the dominant primary producers of the marine ecosystem contributing to approximately half of the global primary production (Field et al., 1998), and are key drivers of the biological carbon pump and the transfer of energy to higher trophic levels (Henson et al., 2009). Increase in phytoplankton cell numbers, often referred to as a phytoplankton 'bloom,' can result from favourable environmental conditions, such as water column stratification, increase in light availability, water temperature and nutrient levels (Blondeau-Patissier et al., 2014; Gohin et al., 2003; Kogeler & Rey, 1999; Santoleri et al., 2003; Siegel et al., 1999; Thomas et al., 2003). These environmental conditions are tightly linked to the dynamics of the ocean surface mixed layer and are therefore controlled by atmospheric forcing and large scale climate variability patterns (Boyce et al., 2010; Cloern, 2005; Longhurst, 2010; Racault et al., 2012; Zhai et al., 2013), as well as regional coastal dynamics such as river input and topographic irregularities (Carstensen et al., 2015; Cloern et al., 2016; Krug et al., 2018). The variable nature of these driving forces in addition to complex biological factors relating to the dynamics between the rates of cell reproduction and mortality associated with death and grazing, are responsible for oceanic photosynthetic production not being constant in time and space (Behrenfeld & Boss, 2014; Cherkasheva et al., 2014; Friedland et al., 2018). The study of the interannual variability in the timing of important biological life cycle events in response to changes in biotic and abiotic factors is known as phenology (Lieth, 1974).

Phytoplankton phenology characterises the timing of annually occurring phytoplankton growing periods and has been typically synthesized into a set of ecologically relevant indices encompassing the timing, duration, and magnitude of bloom events (Friedland et al., 2018; Krug et al., 2018; Platt et al., 2009; Platt & Sathyendranath, 2008; Racault, Sathyendranath, et al., 2014; Suchy et al., 2022). Phytoplankton phenology can provide important insight into the dynamics of marine ecosystems (Ferreira et al., 2014). Variability in phytoplankton phenology occurs because the amplitude and phasing of environmental conditions and phytoplankton responses are not perfectly repetitive between years (Ji et al., 2010). When there is strong interannual variability of environmental cycles (e.g. light, temperature and density stratification) and biotic responses (e.g. population densities, dormancy, reproduction and migration) but their variability is asynchronous, changes in timing can potentially propagate through to the bloom dynamics, causing alterations in the phenology indices such as the bloom initiation, peak, duration and termination (Ferreira et al., 2014; Ji et al., 2010; Platt & Sathyendranath, 2008). This demonstrated sensitivity to external processes results in phytoplankton phenology being a commonly used indicator of both climate variability and climate change, since some of the first repercussions of climate warming and global change are often seen in altered species phenology and geographical distribution limits (Edwards & Richardson, 2004; Ferreira et al., 2014; Ji et al., 2010; Thackeray et al., 2010).

Phytoplankton bloom phenology is also linked to the survival of numerous fish species during their larval and juvenile stages (Cushing, 1990; Ferreira et al., 2014). A theory to explain the relationship between juvenile fish survival and phytoplankton phenology is Cushing's match-mismatch hypothesis, which states that the timing of food availability may be as important, or

even more so, than the abundance of food (Cushing, 1959; Henson et al., 2009). The reason for this lies in the degree of overlap between the timing of peak abundance of phytoplankton and the peak in their zooplankton prey, which in turn provides food for juvenile fish (Cushing, 1990; Kahru et al., 2011; Platt et al., 2003; Suchy et al., 2022). When there is a timing mismatch, where phytoplankton blooms occur earlier or later than expected, there is a small degree of temporal overlap between the phytoplankton bloom and zooplankton growth, resulting in insufficient food being available for larval fish, and therefore an increase in larval mortality (Cushing 1990). Conversely, a successful recruitment of juvenile fish occurs in years when there is a match in the timing and sufficient food as a result. It is therefore necessary to evaluate phytoplankton phenology, since any changes can have a cascading effect throughout the entire food web, leading to trophic mismatches which alters the functioning of the marine ecosystem (Edwards & Richardson, 2004; Racault et al., 2015). In this context, phytoplankton therefore presents a critical connection between environmental conditions, ecosystem dynamics, and productivity (Krug et al., 2018).

Changes in environmental conditions can occur naturally at a broad range of temporal and spatial scales and include changes in physical forcings such as sea surface temperature, winds, cloud cover and precipitation, which in turn originate from climatic patterns (Racault et al., 2012). In the northeast Pacific, large scale climate patterns are generally represented by indices of climatic modes such as El Niño Southern Oscillation (ENSO), Pacific Decadal Oscillation (PDO), and Aleutian Low Pressure variations (Sasaoka et al., 2011), and have been shown to cause large-scale shifts in the relative dominance of diatoms within less than a decade of observations (Alvain et al., 2013; Racault, et al., 2014). The oceanic ecosystem is affected by

the variability of such climatic modes, and it has been recognized as an important factor influencing the ecosystem dynamics of phytoplankton, zooplankton and higher trophic levels (Sasaoka et al., 2011). However, the impact of large-scale forcing on regional phytoplankton timing can often be masked by local effects such as wind driven upwelling, shallow bathymetry, tidal mixing and freshwater runoff which modify the seasonality of stratification and light/nutrient availability, thus underscoring the complexity of coastal ecosystems that are driven by nonlinear interactions of multiple physical and biological processes (Ji et al., 2010). Additionally, interannual changes in these underlying drivers are spatially variable, and considering the region-specific properties and drivers of bloom dynamics indicates that a geographical partitioning of the marine ecosystem should be implemented for the characterization of phytoplankton phenology (Krug et al., 2018; Zhao et al., 2013).

The geographic partitioning of the ocean into biogeographic provinces presents an appropriate strategy to simplify ocean complexity and discern the interactions between phytoplankton and multiple environmental determinants (Dowell et al., 2009; Krug et al., 2017, 2018). The classification of biogeographic provinces, which can also be referred to as ecological regions, bioregions or 'phenoregions', establishes consistent and relatively homogenous biogeochemical regions with distinct boundaries (Marchese et al., 2022). This strategy is particularly relevant for heterogenous marine domains, and it provides a framework for spatially constraining biological processes, testing ecological hypotheses, contextualizing observations, and applying functional and spatially relevant management and conservation schemes (Krug et al., 2017, 2018; Marchese et al., 2022; Reygondeau & Dunn, 2019). Partitioning the ocean surface into bioregions has been achieved objectively using the shape of phytoplankton climatological seasonal cycles derived

from Chl-a time series at global (d'Ortenzio et al., 2012) or regional scales (Ardyna et al., 2017; D'Ortenzio & Ribera d'Alcalà, 2009; Krug et al., 2018; Marchese et al., 2022; Sasaoka et al., 2011). In other instances, the ocean surface had been delineated into "phenological provinces" using the phytoplankton phenology indices directly as input variables (Krug et al., 2018; Land et al., 2014; Sasaoka et al., 2011; Xu et al., 2013). In this study, we investigate the phytoplankton phenology patterns over the British Columbia and Southeast Alaska coast over a 23-year period (1998-2020) using GlobColour satellite data. The specific objectives of this study are: (i) to adapt an algorithm from Krug et al. (2018) to compute a suite of phenological indices on a pixel-by-pixel basis; (ii) to use the suite of phenological indices to partition the study area into phenological bioregions using an objective, unsupervised partition strategy; (iii) to evaluate the climatological region-specific phytoplankton phenology indices and (iv) evaluate the interannual trends of spring bloom initiation and interactions with environmental variables such as SST anomaly and the ENSO index. This study enables the heterogenous marine domain of the B.C. and SE Alaska coast to be simplified into coherent spatial regions from which the complex interactions with environmental drivers can be unraveled. The findings of this study can help better inform fisheries management and conservation programs, by being able to infer the timing of spring bloom initiation in relation to SST anomalies and ENSO index.

3.3. Materials & Methods

3.3.1 Study Area

The study area, extending from 47-60° N and 122-140° W (**Figure 6**), includes the coastal waters off northern Washington state, British Columbia, southeast Alaska, and the adjacent open ocean waters of the subarctic northeast Pacific Ocean. The continental shelf off B.C. is generally

narrower than 45 km, reaching 95 km in the shallow basins of the Hecate Strait and Queen Charlotte Sound (Thomson, 1981). In this region (**Figure 6**), phytoplankton productivity varies spatially and interannually. The highest phytoplankton biomass and earliest blooms have been observed in the Strait of Georgia on the southern B.C. coast, with surface concentrations ranging from < 1 $mg.m^{-3}$ in winter to > 15 $mg.m^{-3}$ during bloom conditions, and the second-highest biomass along the southwest coast of Vancouver Island (Giannini et al., 2021; Jackson et al., 2015; Suchy et al., 2019). This high productivity can be attributed to upwelling favourable winds in summer (April-September) which brings nutrient-rich water toward the surface (Allen & Wolfe, 2013; Jackson et al., 2015; Masson & Peña, 2009; Peña et al., 2019; Ware & Thomson, 2005). Similarly, freshwater discharge increases stability, which keeps both nutrients and phytoplankton in the euphotic zone (Jackson et al., 2015; Masson & Peña, 2009; Ware & Thomson, 2005). The northern B.C. coast to western Alaska regions are dominated by downwelling favourable winds most of the year, though nutrients supplied by river discharge, current-induced upwelling, coastal eddies, and winter upwelling winds increase phytoplankton production (Ware & Thomson, 2005).

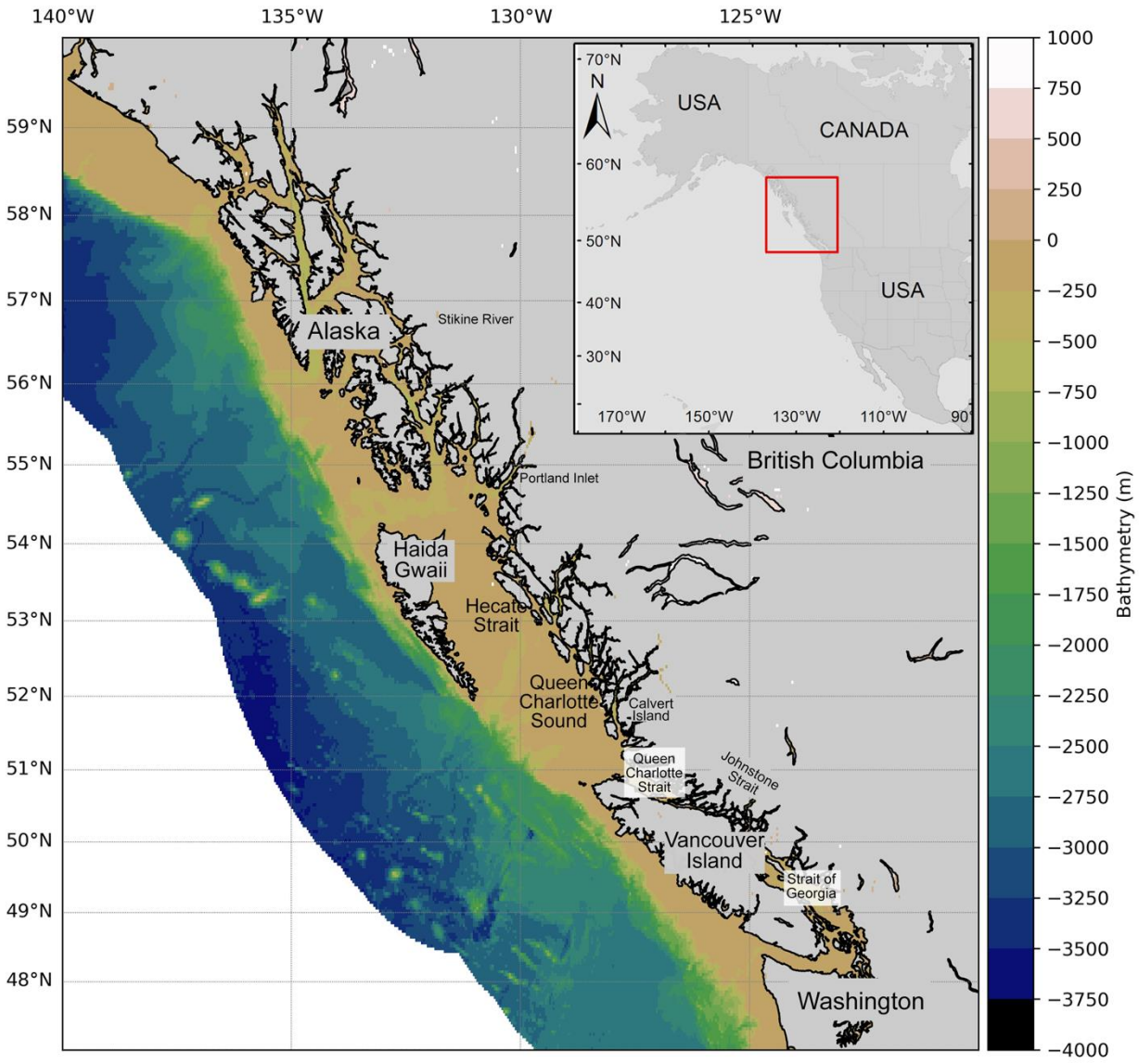

Figure 6: Study area map showing the bathymetry of the region and the locations of interest.

3.2.2 Data

Chl-a concentration

The analysis was based on satellite-derived chlorophyll-a concentration from a 'cloud free' interpolated daily product provided by the Copernicus Marine Environment Monitoring Service (CMEMS) at a 4 km spatial resolution from 1998-2020. Using an interpolated product

significantly improves the coverage of daily data, which is essential for increasing the accuracy and precision in the calculation of phenological indices. Details of satellite data processing are described in Pramlall et al. (submitted; Chapter 2). Briefly, Chl-a fields estimated using different algorithms (OC3 and OC5 for Case 1 and 2 waters, respectively) generated from Level 2 reflectance's are first merged and then used as input for the spatio-temporal interpolation. Interpolated Level 4 Chl-a data was obtained in October 2021 from https://resources.marine.copernicus.eu/product-detail/OCEANCOLOUR_GLO_CHL_L4_REP_OBSERVATIONS_009_082/DATA-ACCESS. The daily data were binned into 8-day composites using the pixel-by-pixel median, in order to smooth the data time series. The Chl-a time series covered a 23-year period (n= 805 Chl-a 8-day composites), over the entire study area (n=313x458 pixels). Due to low solar elevation conditions in this region during the winter months, the analysis was computed using nine months, from mid-February to mid-November (Carswell et al., 2017; Jackson et al., 2015; Suchy et al., 2019).

The accuracy of interpolated Chl-a product for the study region was previously assessed in Pramlall et al., (submitted), which found that despite having somewhat different absolute Chl-a concentrations (r^2=0.63), the interpolated product shared the same distribution as the in situ data, meaning that the shape of the seasonal cycles reflected reality, which makes it suitable for use in studies concerning phytoplankton phenology where Chl-a trends and seasonality are prioritized over absolute concentrations (Ardyna et al., 2017; Foukal & Thomas, 2014; Marchese et al., 2022; Mayot et al., 2016).

SST anomaly

The National Oceanic and Atmospheric Administration (NOAA) provides an optimum interpolation (OI) sea surface temperature (SST) dataset that is produced weekly on a one-degree grid using in situ and satellite SSTs. The satellite data is adjusted for biases using the method of Reynolds (1988) and Reynolds & Marsico, (1993). NOAA Optimum Interpolation (OI) SST V2 data is provided by the NOAA PSL, Boulder, Colorado, USA, at https://psl.noaa.gov. The SST anomaly data was averaged from 15th February to 31st May to capture the conditions experienced leading up to bloom initiation. We recognize the oceanographic complexity of Pacific northeast waters (Thomson, 1981) and acknowledge that SST alone does not represent the environmental drivers of the region. However, previous studies (Allen & Wolfe, 2013b; Collins et al., 2009; Suchy et al., 2019) showed that SST anomalies were correlated with the timing of the spring bloom so for this work we will examine only SST anomaly as the environmental driver.

ENSO index

Large scale climatic forcing such as El Nino Southern Oscillation (ENSO) variations have shown to have significant consequences on the oceanic ecosystem, particularly with regards to phytoplankton phenology dynamics (Sasaoka et al., 2011). The ENSO is a well-known source of hemisphere wide interannual climate variations for the Pacific and global tropics, which dominates the interannual variability of phytoplankton productivity (Jackson et al., 2015; Mantua & Hare, 2002). A strong El Niño year causes warm equatorial waters to be transported northwards along the coast of North America, generally resulting in low phytoplankton productivity (Philander, 1983; Zebiak & Cane, 1987). Monthly averages of the Oceanic Niño

Index (ONI) were obtained from https://origin.cpc.ncep.noaa.gov/products/analysis_monitoring/ensostuff/ONI_v5.php. The data were averaged from January to May to capture the conditions experienced leading up to bloom initiation. Other large scale climate indices such as PDO and NPGO were not considered in this study since the decadal dynamics of PDO and NPGO are linked through their relationship to ENSO (Di Lorenzo et al., 2008). ENSO is correlated with PDO such that warm-phase El Nino conditions generally coincide with positive PDO years, and cold phase La Nina conditions coincide with negative PDO years (Mantua et al., 1997).

3.2.3 Data analysis

We applied a phytoplankton phenology based partition strategy developed by Krug et al. (2018), illustrated in **Figure 7**. Eight phytoplankton phenological indices were computed on a pixel-by-pixel basis, both on the climatological average and per year. To select a set of independent phenological indices to be used as partitioning variables, a dissimilarity analysis (Krug et al., 2018) was performed. Subsequently, an unsupervised classification technique, Hierarchical Agglomerative Clustering analysis (Krug et al., 2018), was used to classify the study area into bioregions (or clusters) with similar phenological properties. The phenological based delineation of the study area was then used as a foundation from which to investigate region specific phenological indices and the interannual variability of spring bloom initiation over the past two decades.

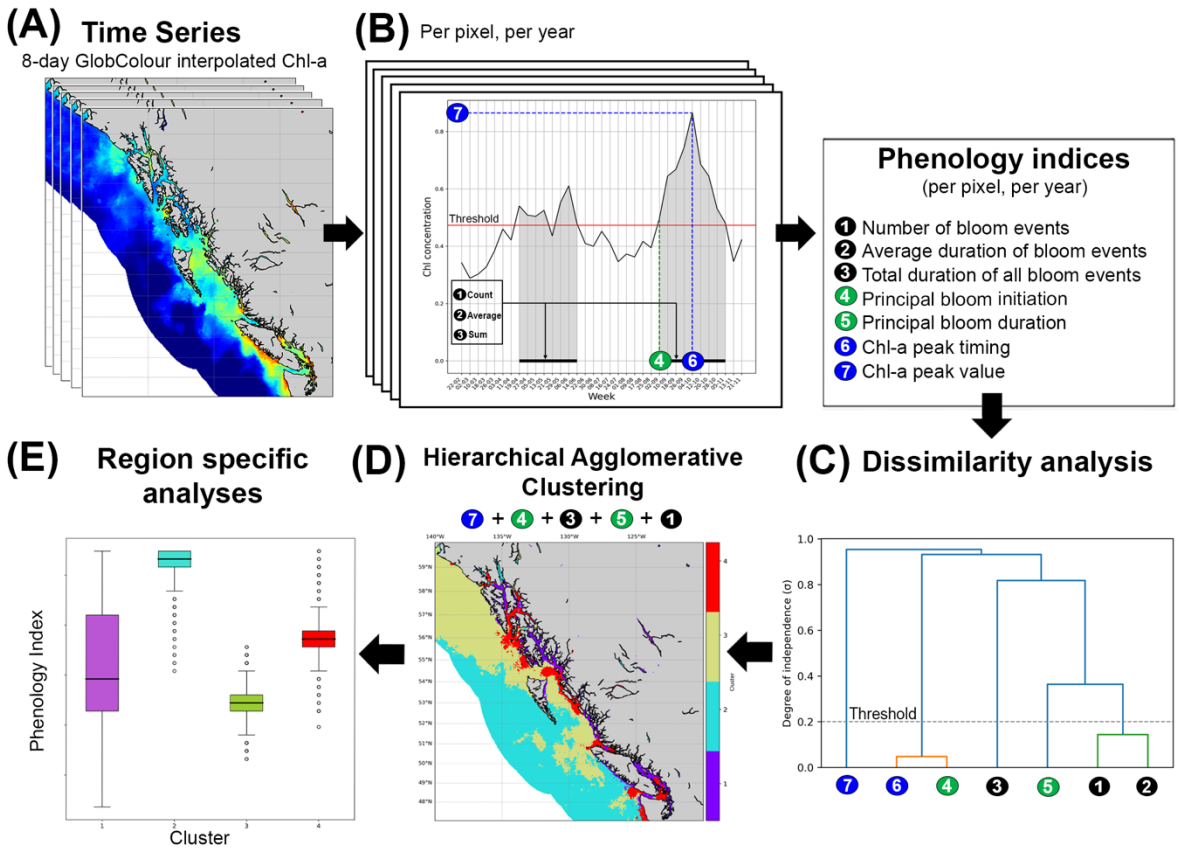

Figure 7: Flow chart depicting the different steps (A-E) taken to partition the B.C. and SE Alaska coast based on phytoplankton phenology over a 23-year period (1998-2020). (A) Extraction of Chl-a time series on a pixel-by-pixel basis; (B) calculation of seven phenological indices, on a pixel-by-pixel basis; (C) selection of independent phenological indices to be used as portioning variables; (D) applying the hierarchical agglomerative clustering method to delineate the region into coherent, phenology-based regions; and (E) analyzing the region-specific phenological indices for different bloom indices. (Figure and caption adapted from Krug et al. (2018).

3.2.3.1 Phytoplankton phenology indices

Different metrics for defining the initiation of blooms in remote sensing studies include the date when Chl-a concentrations reach a predefined absolute concentration (Jackson et al., 2015), the time when the maximum growth rate is reached (Marchese et al., 2019; Mayot et al., 2020), or the date when Chl-a concentrations surpass a certain threshold criterion (Henson et al., 2009; Krug et al., 2018; Siegel et al., 2002; Suchy et al., 2022). In this study, bloom initiation events were defined as instances when the Chl-a concentration rose above the threshold criterion of 5%

above the local annual median value per pixel (Krug et al., 2018; Siegel et al., 2002), for at least two consecutive weeks, in order to avoid prematurely assigning brief bursts of phytoplankton production as the start of the bloom period (Brody et al., 2013; Cole et al., 2012; Schweigert et al., 2013; Suchy et al., 2022). This biomass-based threshold approach is widely used in phytoplankton phenology studies (Henson et al., 2009; Krug et al., 2018; Lavigne et al., 2013; Racault et al., 2012; Sapiano et al., 2012), including in our local waters (Suchy et al., 2022), and is considered a robust and precise strategy (Ferreira et al., 2014; Krug et al., 2018). The following eight phenological indices were calculated for all detected bloom events during the climatological average and for each year on a pixel-by-pixel basis (**Figure 7**): (i) number of bloom events; (ii) total duration of all bloom events per year; (iii) average duration of bloom events; and (iv) Chl-a peak concentration. The bloom event associated with the Chl-a peak concentration for each year is considered the principal annual bloom, and the following phenological indices were calculated for the principal bloom: (v) timing of bloom initiation (the first week when Chl-a concentration rose above the threshold criteria for at least two consecutive weeks); (vi) bloom peak timing (the week that the maximum Chl-a concentration was reached); (vii) timing of bloom termination (the first week of Chl-a below the threshold criteria for at least two consecutive weeks); and (viii) bloom duration (the time elapsed between bloom initiation and termination). A sensitivity test was undertaken to determine to what extent the resulting phenology indices would change with varying threshold percentages. Since a large percentage of pixels remained unchanged when varying from 5-15%, a threshold of a median plus 5% was adopted. Additionally, when comparing the bloom initiation results with literature (Marchese et al., 2022; Suchy et al., 2022), we found that using a threshold of the median plus 5% resulted in bloom initiation that best matched the expected bloom initiation dates in this region.

3.2.3.2 Phenology-based delineation of bioregions

Selection of classification variables

Seven phenological indices (Section 3.2.3.1) derived from the 23-year climatology on a pixel-by-pixel basis were analyzed as potential classification variables. To avoid the dominance of indices with significantly higher variance, the value of each index was normalized by dividing by its standard deviation (Wilks, 2011). A robust classification requires independent input variables, which is generally not the case with environmental data sets (Fendereski et al., 2014). Then, to eliminate strongly correlated, redundant variables the collinearity between the 7 phytoplankton phenological metrics was investigated using Spearman's rank correlation coefficient (r_s). The variables were represented in a dendrogram (**Figure 8**), where the degree of independence (σ) between variables derived from their correlation coefficient ($\sigma = 1 - r_s$) represented the vertical axis. A degree of independence of 0.2 (Fendereski et al., 2014) was used as a threshold to eliminate strongly correlated, redundant phenological indices that fell below this value. From each branch of the dendrogram, each independent variable was used, and for groups of redundant indices ($\sigma < 0.2$) a single index was selected as a classification variable. From this analysis, peak concentration, total duration and principal bloom duration were directly selected, while we chose peak start and number of blooms from the two groups of highly correlated variables.

The decision of a correlation coefficient threshold and a single variable from each branch was a trade-off between retaining as many phenological predictor variables as possible and avoiding high correlations that could potentially confound the interpretation of the results. A sensitivity test was conducted to determine the effect of the choice of phenological predictor variables from the two groups of highly correlated variables on the classification results. Several tests were run where one of the input variables were exchanged with another representative from the same

group (i.e., variable with a high degree of correlation), with all other parameters kept constant. The result of each test, which was different maps of phenological bioregions, was compared to the original classification. The similarity of the two classification outputs were quantified by computing the percentage of unchanged pixels, and the Kappa index of agreement (**Table 3**). The Kappa index provides a chance-adjusted, relative measure of similarity between two classification results, taking into consideration the location and value of corresponding pixels (Fendereski et al., 2014; Gregr & Bodtker, 2007). The range of possible kappa values is from -1 to 1, with 1 representing perfect agreement, 0 indicating agreement no better than expected by chance, and -1 suggesting worse than random agreement (Fendereski et al., 2014; Sim & Wright, 2005). The Kappa score ranged from 0.89 to 0.95 (**Table 3**), indicating a considerable agreement between the reference map and the sensitivity test maps. This suggests that little variation occurred in the classification results when the dependent variables from the same cluster were interchanged, and while the size of individual bioregions depended on the choice of index used, the general pattern of the outcome remained robust (Fendereski et al., 2014; Sim & Wright, 2005).

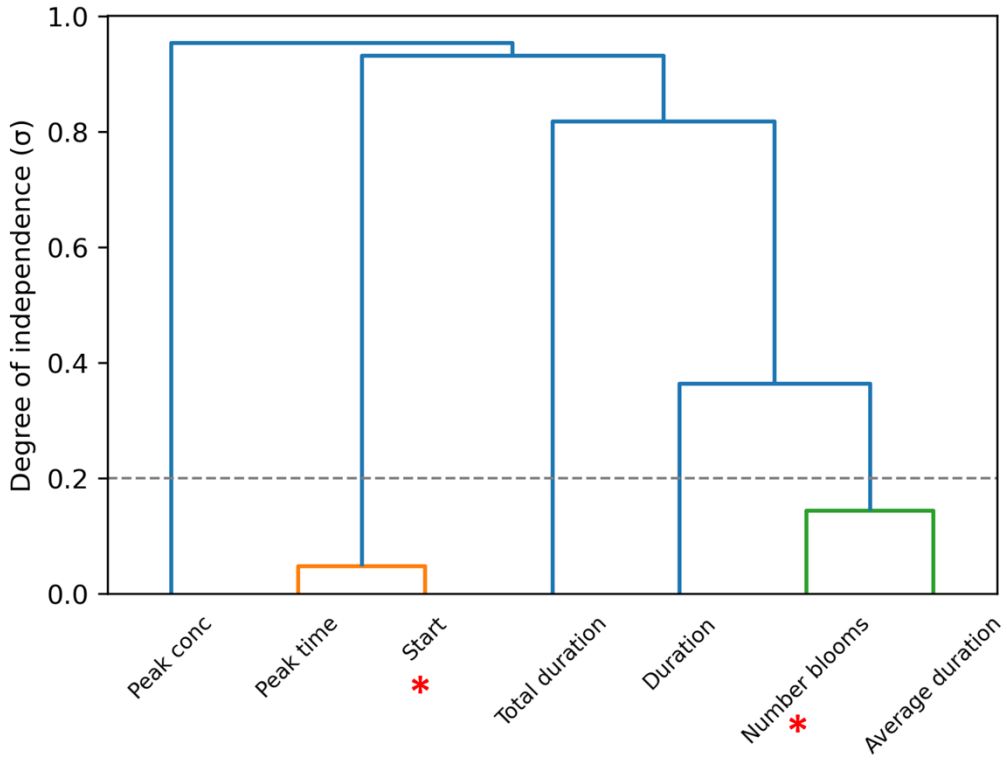

Figure 8: Dissimilarity analysis based on the phenological indices averaged over the B.C. and SE Alaska coast during the 1998-2020 time period. Orange and green nodes indicate groups with dissimilarity values below the defined threshold of 0.2. The red asterisk denotes the index selected to represent the group of highly correlated variables.

Table 3: Kappa index of agreement (0-1) comparing the different combinations of dependent input variables (underlined) with the final classification used in this study as a reference.

Input variables	Kappa index	% unchanged
Peak start, Number of blooms, Peak conc, total duration, peak duration	1	100
Peak start, Average duration, Peak conc, total duration, peak duration	0.89	93
Peak time, Number of blooms, Peak conc, total duration, peak duration	0.95	97.2
Peak time, average duration, Peak conc, total duration, peak duration	0.93	95.7

Classification method

Regions with similar phenological properties were delineated using a Hierarchical Agglomerative Clustering (HAC) analysis, an unsupervised learning technique. Unsupervised learning approaches have been shown to provide a less biased delineation and more accurate representation of phytoplankton variability (Krug et al. 2017). HAC represents the underlying relationship among objects hierarchically through a dendrogram (Karna & Gibert, 2022), which is formed by recursively merging objects that are close to each other in n-dimensional space using a division that simultaneously minimizes differences between objects of a given cluster, based on Euclidean distance, and maximizes differences between objects of different clusters, using Ward's linkage (Krug et al., 2018). Rather than needing the expected number of clusters to be defined a priori, like in clustering methods such as k-means, the number of clusters emerges as a consequence of the hierarchical clustering process itself, which is often determined by visual inspection of the resulting dendrogram by finding the biggest horizontal gap on larger branches (Karna & Gibert, 2022).

Cutting the dendrogram at the appropriate level results in the clustering of objects into discrete groups (Halkidi et al., 2001). The choice of where to cut the dendrogram is what results in the overall quality of clusters, so it is common practice to incorporate the optimization of some goodness of cluster indicator such as the distortion score (7 clusters; **Figure 9B**), silhouette score (2 clusters; **Figure 9C**) or the Calinski harabasz score (3 clusters; **Figure 9D**). After visual inspection of the possible number of clusters (**Figure 9A**), and taking the mean of the goodness of cluster indicators (**Figure 9B-D**), we chose to use four clusters to regionalize the study region. Finally, to test whether the bioregions differed in their phenological characteristics (i.e., number

of blooms, average duration of blooms, etc.), a Kruskal-Wallis H test, which is a non-parametric, one-way analysis of variance by ranks (Krug et al., 2018), was performed. A significant result ($p < 0.05$) of the Kruskal-Wallis H test suggests that at least one bioregion differs from all others. Furthermore, the Dunn's test, which is a multi-step a posteriori pairwise testing procedure, was applied to determine which bioregions differ significantly from the others (Fendereski et al., 2014; Marchese et al., 2022).

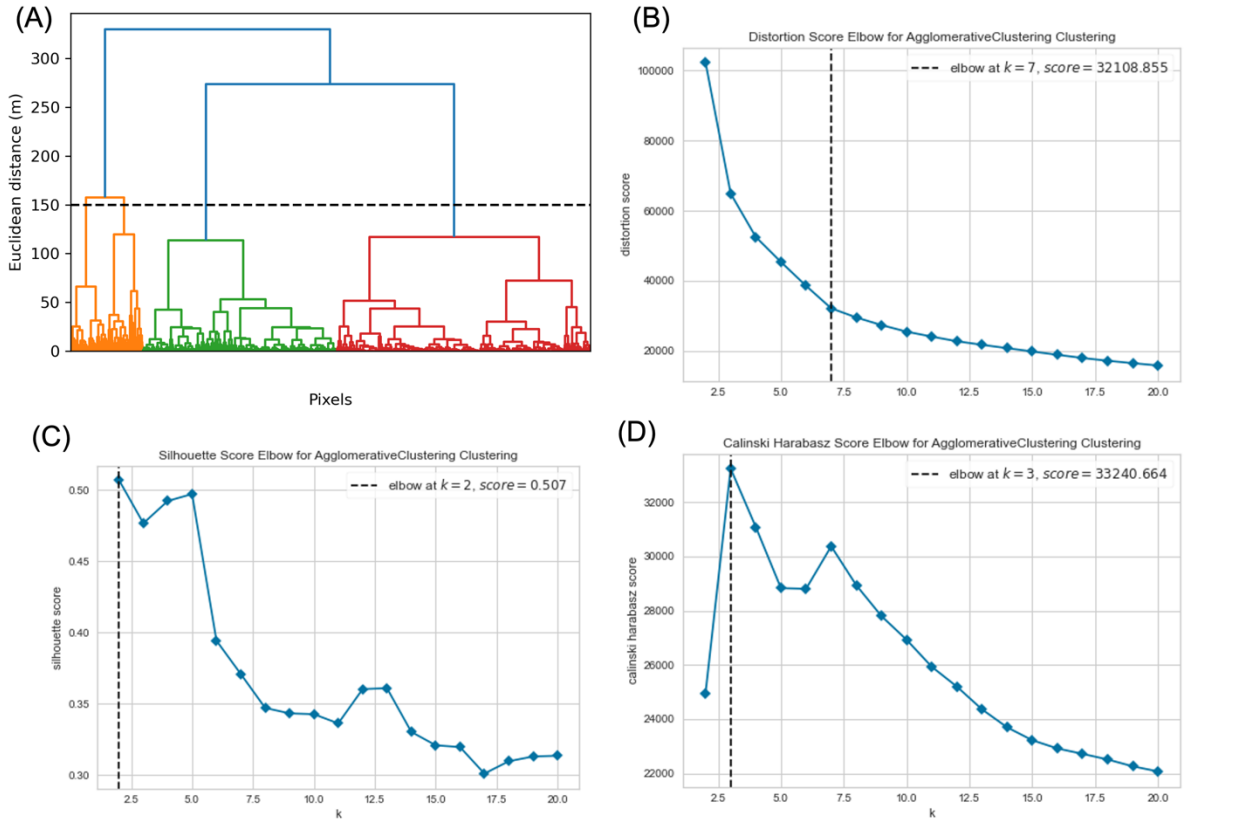

Figure 9: To determine the optimal number of clusters for the Hierarchical Agglomerative Clustering method, we took the mean of (A) the dendrogram, (B) the distortion score, (C) the Silhouette score and (D) the Calinski Harabasz score.

3.2.3.3 Region specific phenological properties

The differences between phenological bioregions were analyzed using the Chl-a climatology time-series averaged over each region. Thereafter, for each delineated phenological bioregion,

the phytoplankton phenological metrics were again evaluated for the 23-year climatological average.

3.2.3.4 Spring bloom interannual variability patterns and environmental drivers

Considering that the spring bloom initiation is of great importance to the rest of the food web, since it dictates the start of the food availability season for zooplankton and therefore juvenile salmon, we investigated the interannual variability of the spring bloom over the 23-year (1998-2020) study period. The spring bloom is generally defined as a time of rapid accumulation of phytoplankton biomass, which occurs after the relatively low biomass observed in winter (Collins et al., 2009). Here we defined the spring bloom initiation as the first bloom of the year and considered the bloom timing in relation to the average of the spring bloom initiation over the 23 years. When the bloom initiation is below the average, it is considered an early year, and when the bloom initiation is above the average, it is considered a later year. Additionally, the regions interannual variability of spring bloom initiation was described in relation to SST anomaly calculated per bioregion and the El Nino Southern Oscillation (ENSO) index. Lastly, we investigated the relationship between early and late spring bloom initiations with the timing of the principal bloom initiation.

3.4 Results

3.4.1 Climatological phytoplankton phenology by pixel

The descriptive statistics of selected phytoplankton phenological indices over the B.C. and SE Alaska coast for the 23-year climatology, over the period February 1998-November 2020,

obtained on a pixel-by-pixel basis is outlined in **Table 4**. Over the entire study area, the number of bloom events ranged from 1-4 blooms with a median and mean of 2 blooms. The total duration of all bloom events ranged from 56-160 days with a median and mean ± the standard deviation of 120 ± 11 days. The average duration of all bloom events ranged from 22-160 days per bloom, with a median of 60 days, a mean of 62 days and a standard deviation of 17 days. Over the entire study area, the Chl-a peak value ranged from 0.23 – 38.57 mg m^{-3} with a median of 0.52 mg m^{-3} and a mean of 1.39 mg m^{-3} and a standard deviation of 2.15 mg m^{-3}. The timing of Chl-a peak concentration ranged from the 22nd February (DOY: 53) to the 13th November (DOY: 317) with the median and mean occurring on the 4th October (DOY: 277) and 12th August (DOY: 224), respectively, and a standard deviation of 80 days. The timing of the principal bloom initiation ranged from the 22nd February (DOY:53) to the 5th November (DOY:309) with the median and mean occurring on the 17th August (DOY: 229) and 12 July (DOY 224) respectively, and a standard deviation of 75 days. The duration of the principal bloom ranged from 16-160 days with a median and mean of 72 and 71 days, respectively, with a standard deviation of 22 days.

Chl-a climatology: peak concentration and timing of peak

The Chl-a peak values revealed a distinct gradient from the coastal to offshore regions, with high Chl-a concentrations (5 to >20 mg.m^{-3}) observed along the coast, particularly in the Strait of Georgia in the proximity of the Fraser River, along the Vancouver Island shelf, in Queen Charlotte Strait, North Vancouver Island, Hecate Strait and the area surrounding the Dixon shelf (**Figure 10D**). Moderate Chl-a concentrations (1 to 3 mg.m^{-3}) were found along the continental slope and low Chl-a concentrations (<1 mg.m^{-3}) were found in offshore waters (**Figure 10D**).

The timing of peak Chl-a concentration (**Figure 10E**) showed a distinct pattern where the coastal and continental shelf regions reach the peak concentrations in the spring (late April to late May), and the offshore region reaching the peak concentrations in the fall (October to November).

Blooms: number, average and total duration

The number of bloom events per year ranged from one to four over the entire study area, with most of the shelf bioregion having one or two blooms, and offshore bioregion having two blooms. Relatively smaller regions show three blooms, including in the coast by the Strait of Juan de Fuca, northern Strait of Georgia (SoG), near Calvert Island, the shelf region off the west coast of Haida Gwaii, and offshore regions (**Figure 10A**), and very few pixels experience four blooms. The opposite pattern was shown by the average duration of phytoplankton blooms where regions containing one bloom period yielded the longest average durations of more than 100 days, regions having 3 bloom periods had shorter average durations of less than 50 days, and areas with 2 blooms had an average duration between 50-70 days (**Figure 10B**).

The total duration of all bloom events showed that 70.4% of the study area had a duration over 120 days, 27.1% had a duration between 90 and 120 days, and 2.5% had a duration of less than 90 days (**Figure 10C**).

Principal bloom: timing, duration and termination

The pattern shown by the timing of peak Chl-a concentration is mimicked by the principal bloom initiation, where the coastal and continental shelf regions experience the start of the bloom from March to April (spring), and this continues to September in offshore region (**Figure 10F**). There

is also a latitudinal gradient present in the offshore waters, where bloom initiation happened later farther south (October), and progressively shifts to an earlier bloom initiation to the north (August; **Figure 10F**). The west coast of Vancouver Island also had a later bloom initiation (around July to August) which is more similar to offshore waters despite being in the continental shelf (**Figure 10F**).

The principal bloom termination generally shares the same patterns as the initiation and peak timing, with the coastal regions terminating earlier (July) and offshore regions terminating later (November; **Figure 10H**). However, there are localized areas along the coast that have a later termination, near the southern Strait of Georgia in the vicinity of Puget Sound, around the Juan de Fuca eddy region, Queen Charlotte Strait, Hecate Strait and the Alexander Archipelago (**Figure 10H**).

The localized areas along the coast that have a later termination (mentioned above) are the same areas where the duration of the principal bloom is greater than 110 days long (**Figure 10G**). These regions of long principal bloom duration are also similar to the regions of long average bloom duration (**Figure 10B**). The west coast of Vancouver Island and the Washington coast, show the next highest duration of principle bloom events, ranging from 85-100 days, and similar durations are found to a lesser degree in the coastal waters off SE Alaska. There are patches of short duration blooms found off the west coast of Haida Gwaii and southern offshore regions ranging from 25-50 days. The most commonly occurring duration is between 55-75 days, making up 50% of the study area.

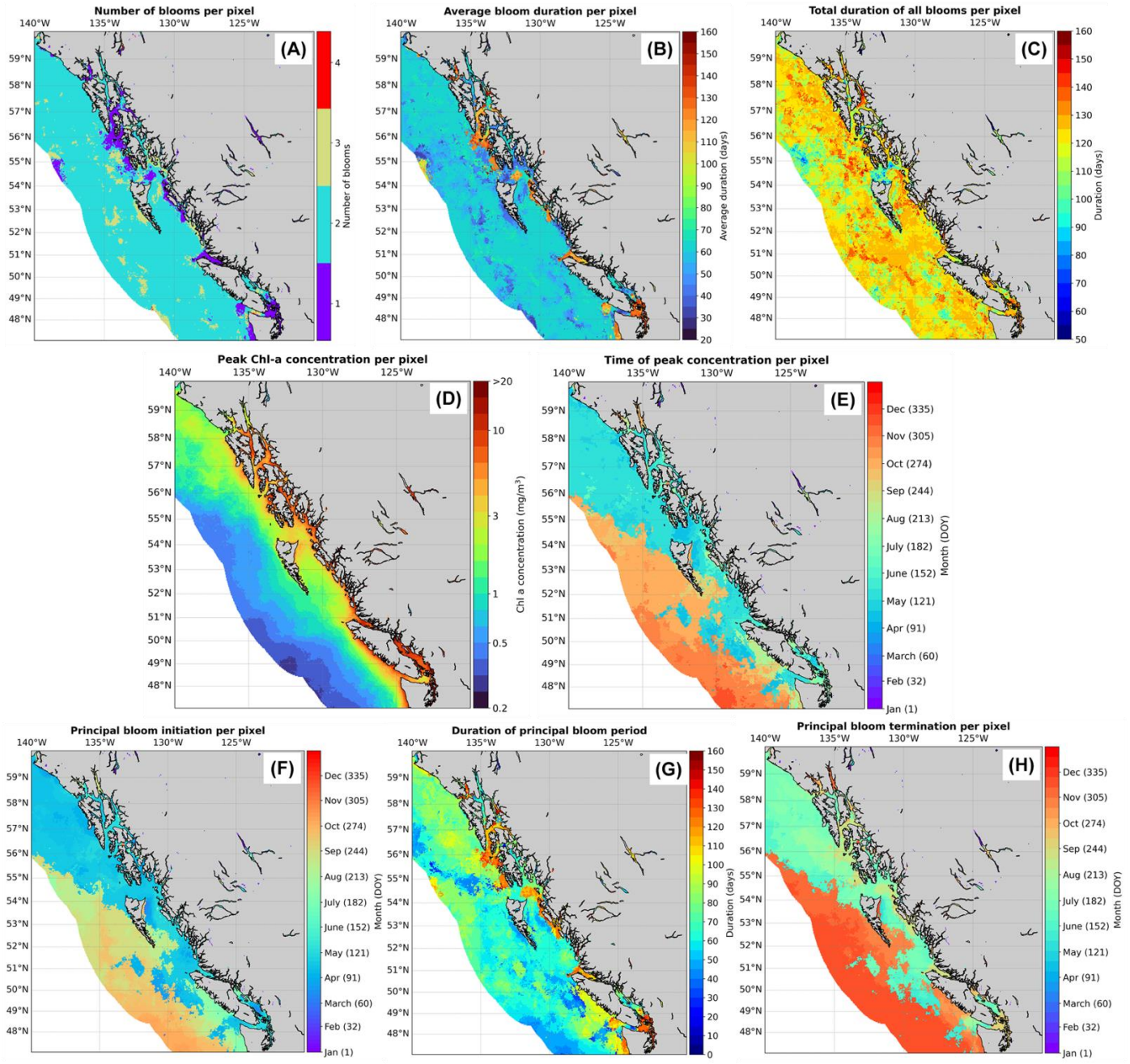

Figure 10: Distribution of selected phytoplankton phenological indices over the British Columbia and Southeast Alaska coast, estimated from the 23-year climatology (mid-February 1998 to mid-November 2020) on a pixel-by-pixel basis. (A) Number of bloom events per year; (B) Average duration of bloom events; (C) Total duration of all bloom events; (D) Chl-a peak value. Considering the principal bloom: (E) Time of Chl-a peak concentration; (F) Timing of initiation of principal bloom; (G) Duration of principal bloom; (H) Termination of principal bloom.

Table 4: Descriptive statistics of phytoplankton phenological indices over the British Columbia and Southeast Alaska coast, estimated from the 23-year climatology (mid-February 1998 to mid-November 2020) on a pixel-by-pixel basis (n = 23 years ×

47449 pixels = 1091327). Details include minimum (Min), maximum (Max), median and mean values, and standard deviation (SD). * refers to the principal bloom period.

Climatology					
Phenological index	Min	Max	Median	Mean	SD
Number of bloom events (bloom events.year^{-1})	1	4	2	2	0.44
Total duration of all bloom events (days.year^{-1})	56	160	120	120	11
Average duration of all bloom events (days.bloom^{-1})	22	160	60	62	17
Chla peak value (mg.m^{-3})	0.23	38.57	0.52	1.39	2.15
Timing of bloom initiation* (day of year)	53	309	229	193	75
Chla peak timing* (day of year)	53	317	277	224	80
Timing of bloom termination* (day of year)	69	325	309	264	71
Bloom duration * (days)	16	160	72	71	22

3.4.2 Phenology-based regionalization

The choice of relevant partition variables to be included in HAC analysis was established from a dissimilarity dendrogram (**Figure 8**), produced by the inversion of the correlation matrix of the seven normalized phenological indices (see Section 3.2.3.2). According to the methods followed in Section 3.2.3.2 under the 'Selection of classification variables', the input dataset was therefore based on five phenological indices: Chl-a peak concentration, total duration of all bloom, the number of bloom events and the duration and start time of the principal bloom. Taking the mean of the goodness of cluster indicators associated with HAC analysis, such as the distortion score, silhouette score and the Calinski harabasz score, estimated using a number of clusters varying between 2 and 20, and by visual inspection of the possible number of clusters, it was evident that phytoplankton phenology over the study region was optimally represented by four distinct clusters sharing similar phytoplankton phenology patterns.

The four phenological bioregions were situated coherently over the B.C and SE Alaska region (**Figure 11A**). The coastal region, which is temporally dynamic due to tide, current and river discharge conditions, was divided into two clusters - one being characterised by multiple bloom periods, with the dominant bloom in spring (Cluster 1; **Figure 11B**), and the other being dominated by a single prolonged bloom, which also peaks in spring and gradually decreases with time (Cluster 4; **Figure 11E**). The shelf bioregion was delineated into a cluster that had two distinct bloom periods, with a dominant spring bloom and a secondary fall bloom (Cluster 3; **Figure 11C**). This region occasionally extends beyond the shelf to the west of SE Alaska, and to the northwest of Vancouver Island. Conversely, the offshore region, also containing two distinct bloom periods, had a dominant fall bloom and a smaller spring bloom period (Cluster 2; **Figure 11D**), which also extends beyond the offshore boundary to the southeast of Haida Gwaii and the west coast of Vancouver Island.

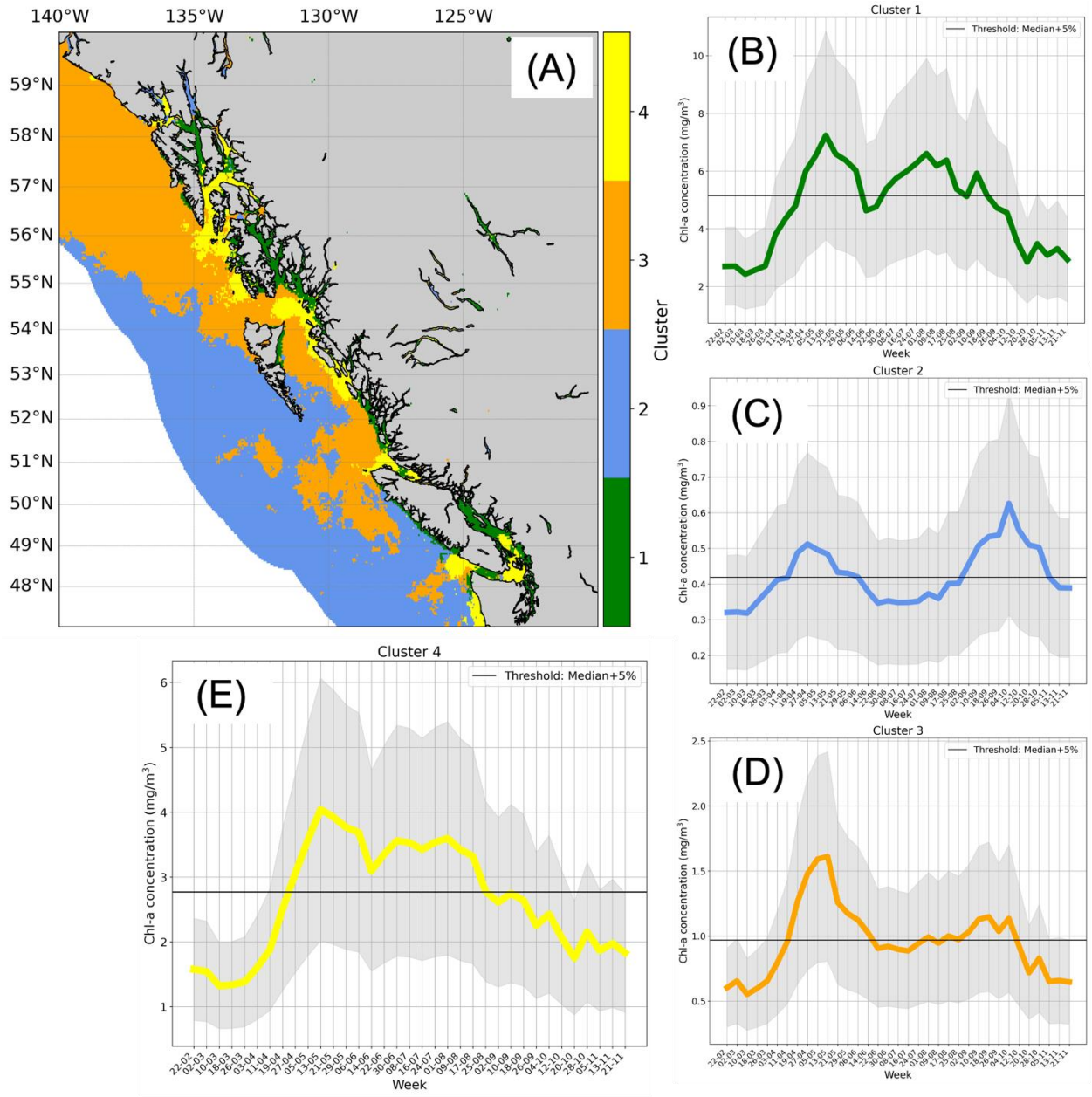

Figure 11: The classification of the British Columbia and Southeast Alaska coast into distinct regions based on phytoplankton phenological indices (Chl-a peak concentration, total duration of all bloom events per annum, the number of bloom events and the duration and start time of the principal bloom), for the Chl-a climatology averaged over a period of 23 years (February 1998 – November 2020). (A) Spatial distribution of the four distinct bioegions. (B) Coastal 1, (C) Offshore, (D) Shelf, (E) Coastal 2 regions. Black horizontal lines (B-E) show the Chl-a threshold criteria of 5% above the median, used delineate bloom from non-bloom periods for each bioregion. Note the different magnitude of the y-axis (B-E).

3.4.3 Phytoplankton phenology by bioregion

Chl-a patterns during the 23-year study period (**Figure 12**) and Chl-a weekly climatological seasonal cycle varied across the four phenological bioregions (**Figure 11B-E**). One of the coastal

bioregions, Cluster 1, experienced multiple blooms per year between April and September, yielding the highest concentrations compared to other clusters (**Figure 12A**) with Chl-a bloom values ranging from 5-7 $mg.m^{-3}$ ± 3 (**Figure 11B**). Distinct from the other bioregions, Cluster 4, is characterised by a single prolonged bloom period starting in late April at ~ 3.2 $mg.m^{-3}$ ± 1.5, peaking in May at ~ 4.2 $mg.m^{-3}$ ± 2, and gradually declining until termination in August (**Figure 11E and Figure 12D**). The shelf bioregion, Cluster 3, has two distinct bloom periods (**Figure 12C**); a dominant spring bloom (April-June) ranging from 0.8-1.5 $mg.m^{-3}$ ± 0.75, and a secondary fall bloom (September-October) ranging from 0.8-1 $mg.m^{-3}$ ± 0.5 (**Figure 11D**). Conversely, the offshore bioregion Cluster 2, also having two distinct bloom periods (**Figure 12B**), is characterised by a dominant fall bloom (August-November) ranging from 0.5-0.7 $mg.m^{-3}$ ± 0.6, and a weaker bloom period in spring (April-May) reaching a maximum of ~0.6 $mg.m^{-3}$ ± 0.28 in late April (**Figure 11C**).

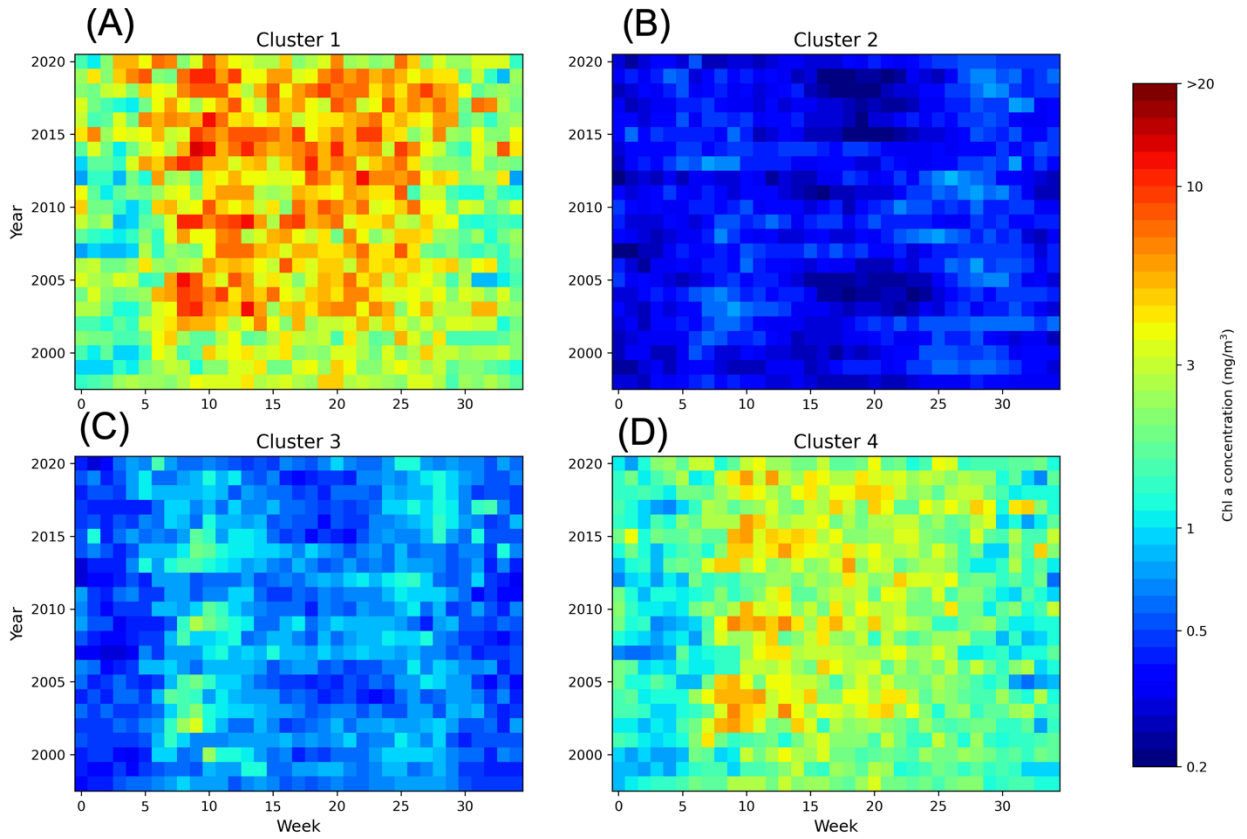

Figure 12: Weekly Chl-a values for each phenological region between 1998 and 2020. Week 0 being the 22nd February and week 35 being the 21st November. Refer to Figure 11 for region location.

The Kruskal-Wallis H test revealed the statistical differences of the eight phenological indices (i.e., number of bloom events per year, total duration of all bloom events per year, average duration of all bloom events per year, Chl-a peak concentration, time of Chl-a peak concentration, and the initiation, duration, and termination of the principal bloom), having a p-value of less than 0.05 indicated that at least one bioregion differed from all others. Additionally, the Dunn's test was applied to determine which bioregions differed significantly from the others. Results showed significant differences in the number of bloom events and average duration of all bloom events among all bioregions, except for the offshore bioregion (Cluster 2) and shelf bioregion (Cluster 3; **Figure 13A and B**). For the total duration of all bloom events per year,

Cluster 2 and 4 were significantly different, but Clusters 1 and 3 were not (**Figure 13C**). The coastal bioregions, Clusters 1 and 4, proved to not be statistically different for the principal bloom initiation (**Figure 13F**). Significant differences among all bioregions were found for the peak Chl-a concentration, time of peak Chl-a concentration, and principal bloom duration and termination (**Figure 13D,E,G,H**).

Bioregion Chl-a climatology: peak concentration and timing of peak

Chl-a peak values increased along the offshore-coastal gradient (**Figure 13D**), with the offshore region (Cluster 2) having the lowest concentrations (0.3-1.4 $mg.m^{-3}$), the shelf region (Cluster 3) having the second lowest concentrations (0.3-3.8 $mg.m^{-3}$), followed by the coastal Cluster 4 (0.8-10.5 $mg.m^{-3}$) and Cluster 1 having the highest concentrations (3.2-16.7 $mg.m^{-3}$). The time of peak Chl-a concentration had the largest variability for the coastal Cluster 1, the interquartile range spanning DOY 132-212 and a median of DOY 140 (**Figure 13E**). Coastal Cluster 4 shared the same median of DOY 140 with Cluster 1 but had less variability (IQR: DOY 124-180). The timing of peak Chl-a concentration in the offshore region, (Cluster 2) occurred in the fall (DOY 252-316), whereas the shelf region (Cluster 3) experienced the Chl-a peak time in spring (DOY 92-156; **Figure 13E**).

Bioregion Blooms: number, average and total duration

For the phenology index, number of blooms per year, Cluster 1 (coastal) yielded the greatest range of observations spanning from 1-4 blooms, having a median of 2 blooms and an interquartile range of 2-3 blooms (**Figure 13A**). For the rest of the clusters, the box and whiskers

diagrams have been compressed into the median line, which represents the full range of non-outlier observations, thus highlighting that almost all the observations have converged at a single value of 2 blooms for Clusters 2 (offshore) and 3 (shelf) and 1 bloom for Cluster 4 (coastal; **Figure 13A**).

Cluster 4, having only a single bloom period, yields a higher average duration ranging from 68-160 days, highlighting its characteristic single prolonged bloom period (**Figure 13B**). The other coastal cluster, Cluster 1, shows a high variability of average duration of all blooms, ranging from 20-96 days (**Figure 13B**). The offshore (Cluster 2) and shelf bioregions (Cluster 3), both having an average of 2 blooms per year, also share an average bloom duration ranging from 44-76 days and a median of 60 days (**Figure 13B**). For the total duration of all bloom events per year, Clusters 1, 2 and 3 share an identical range of 88 – 152 days, and all clusters sharing a median of 120 days, with Cluster 4 having the least variability (range 112-136 days; **Figure 13C**).

Bioregion principal bloom: initiation, duration, termination

Considering the principal bloom initiation, duration, and termination (**Figure 13F-H**), the coastal Cluster 1 had the largest variability for all three indices. Coastal clusters 1 and 4, previously shown to be statistically similar for principal bloom initiation, shared the same median of DOY 116, with Cluster 4 having smaller variability (IQR: DOY 108-124) than Cluster 1 (IQR: DOY 108-180; **Figure 13F**). The principal bloom initiation of the offshore region (Cluster 2) occurred

in fall (IQR: DOY 228-260), and the shelf region (Cluster 3) occurred in spring (IQR: DOY 100-108; **Figure 13F**).

Coastal cluster 4 had the longest bloom duration (88-152 days; **Figure 13G**). The principal bloom duration and variability of Cluster 3 (shelf; median DOY 72) was slightly greater than Cluster 2 (offshore; median DOY 64; **Figure 13G**). Cluster 4 had a median termination on DOY 236 (**Figure 13H**), which is later than the median termination of Cluster 1 (DOY 196), despite these clusters sharing the same median initiation (DOY 116). The shelf region (Cluster 3) terminated between DOY 140-204, and the offshore region (Cluster 2) terminated between DOY 284-324 (**Figure 13H**).

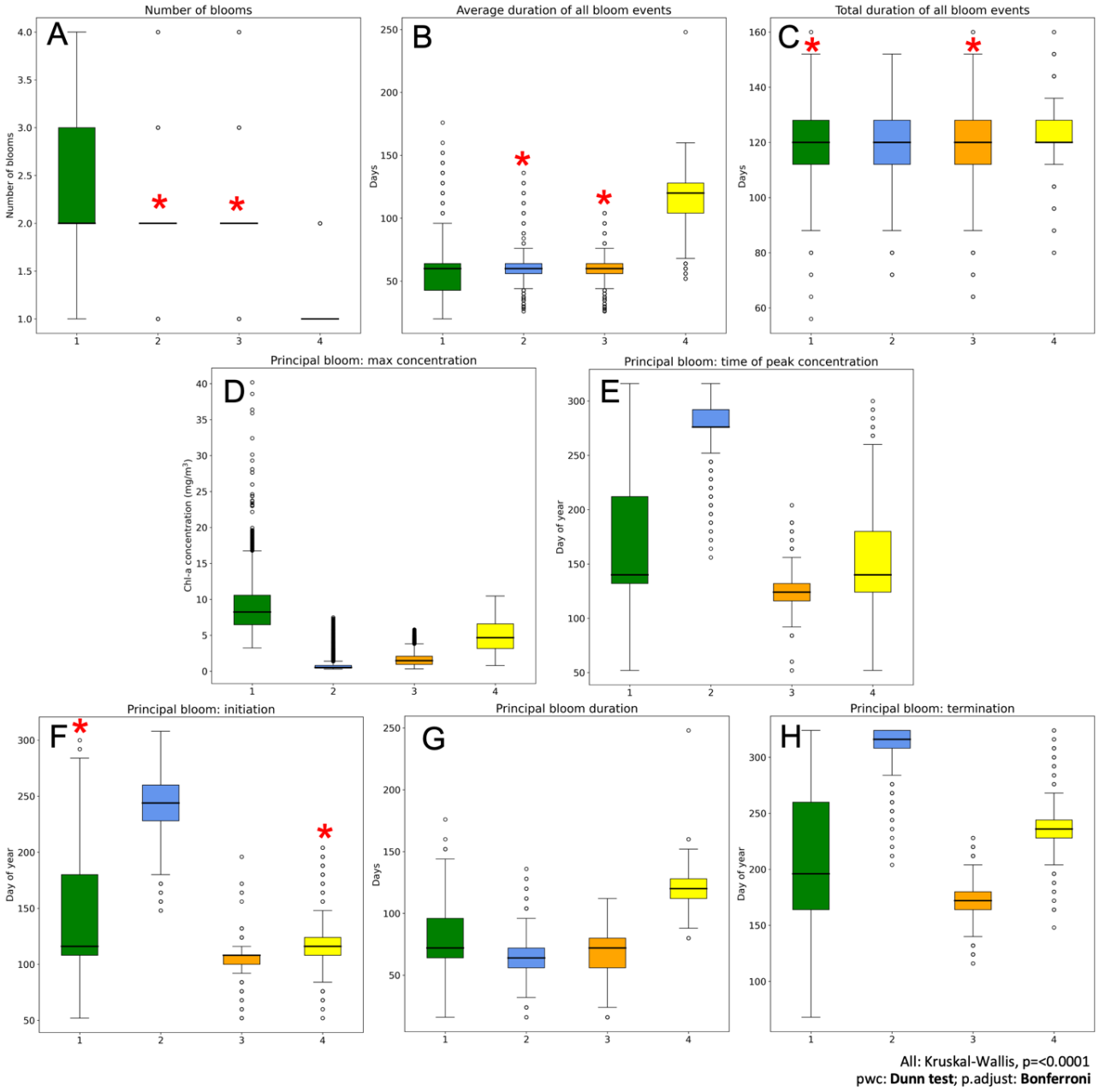

Figure 13: Phytoplankton phenology indices for the four phenological bioregions delineated off the B.C. and SE Alaska coast estimated for the Chl-a climatology averaged over a period of 23 years (February 1998 – November 2020). (A) Number of bloom events; (B) Average duration of all bloom events; (C) Total duration of all bloom events; (D) Chl-a peak value. Taking into consideration the bloom associated with the peak Chl-a value: (E) Time of Chl-a peak concentration; (F) Principal bloom initiation; (G) Duration of principal bloom; (H) Principal bloom termination. The median is represented by the black line in the middle of each box. The 25th and 75th percentiles are represented by the top and bottom limits of each box, respectively. The full range of non-outlier observations for each variable beyond the quartile range is represented by the whiskers, and the outliers are represented by the dots. The Kruskal-Wallis H test results are shown at the top or bottom of each figure (A-I), with significant results ($p < 0.05$) suggesting that at least one bioregion differs from all others. The results of the Dunn's multiple comparison test are shown by the red asterisk, indicating bioregions without statistically significant differences between the phenological indices, and no asterisk indicates significant differences between bioregions ($p < 0.05$). Refer to Figure 11 for region location and colour code.

3.4.4 Cold and warm ocean phases: Interannual variability of spring bloom initiation

The variability of the spring bloom differs between clusters and years, as shown in **Figure 14**. The variability of the timing of the spring bloom does not change much between years compared to the variability of the timing of the principal bloom (**Figure A1**). The average of the start of the spring bloom for all clusters over the 23-year period is in April, ranging from the 4th-22nd April (black line, **Figure 14**). For all clusters, the full range of interannual variability of the bloom initiation (i.e., minimum and maximum date) spans from March to May, meaning that in extreme cases the spring bloom initiation can vary between 2 months. The offshore region (Cluster 2) has the largest range of timing of bloom initiation, spanning from the 8th March-8th May (61 days), which indicates that this region has the highest variability compared to the coastal and shelf regions (Clusters 1,3,4). The spring bloom initiation for most of the years are within one standard deviation of the mean, indicating that the spring bloom does not experience much variability. However, the interannual variability that is observed in the timing of the spring bloom initiation can be related to SST anomaly and ENSO cycles.

For the warm years (positive SST anomaly), the spring bloom initiation tends to be earlier than the mean initiation (**Figure 14**). This generalization holds true for all years in the offshore region (Cluster 2; **Figure 14B**), with exception of 2010 for the coastal and shelf regions (Cluster 1, 3 and 4, **Figure 14A,C,D**), as well as 2003 in Cluster 1 (**Figure 14A**), and 2016 and 2017 for Cluster 3 (**Figure 14C**). For cold years (negative SST anomaly) the spring bloom initiation tends to be later than the mean climatology initiation, however, there tends to be more exceptions to this generalization.

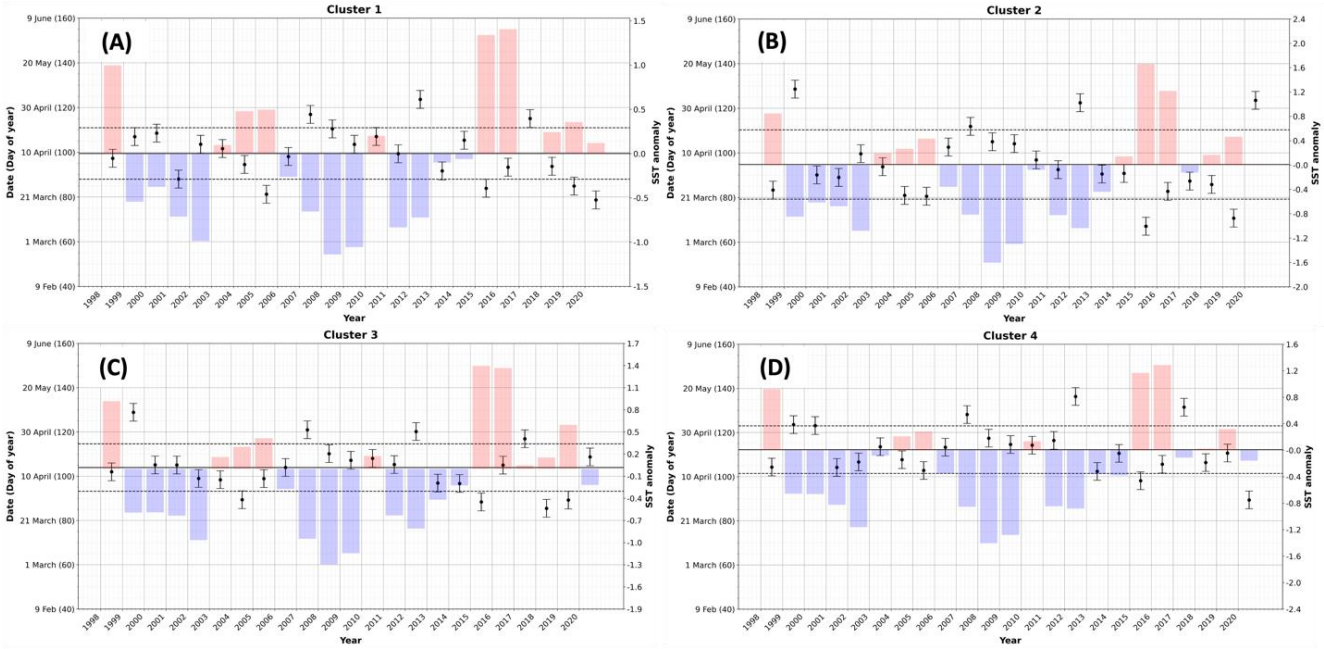

Figure 14: Interannual variability of spring bloom initiation and SST anomaly per cluster. SST anomaly was averaged over mid-February to May. Black line shows the mean spring start date over the 23-year period.

The spring bloom initiation has been shown to be generally related to SST anomaly (**Figure 14**), where warm SST tend to result in earlier spring bloom initiation. Similar analysis but considering the principal bloom initiation (**Figure A1**), did not result in such a clear relationship. SST anomaly correlates with ENSO cycles (January-May), with El Nino generally having a warmer SST, and La Nina phases having cold SST (**Figure A2**). Neutral ENSO phases have SST that lie between El Nino and La Nina phases but tend to overlap more with SST experienced during La Nina phases (**Figure A2**). Similar to the relationship between SST anomaly and spring bloom initiation, **Figure 15** shows that warm phase El Nino years generally have an earlier spring bloom initiation than the cool phase La Nina year for all clusters, with neutral phase years having the greatest range of bloom initiation dates.

Figure 16 shows the relationship between the timing of the principal bloom initiation and the timing of the spring bloom initiation. By observing the median line of the boxplot (**Figure 16**), when there is an early spring bloom (i.e., spring bloom initiation is earlier than the 23-year mean) the initiation of the principal bloom tends to be earlier, and when there is a later spring bloom (i.e., spring bloom initiation is later than the 23-year mean) the initiation of the principal bloom is later.

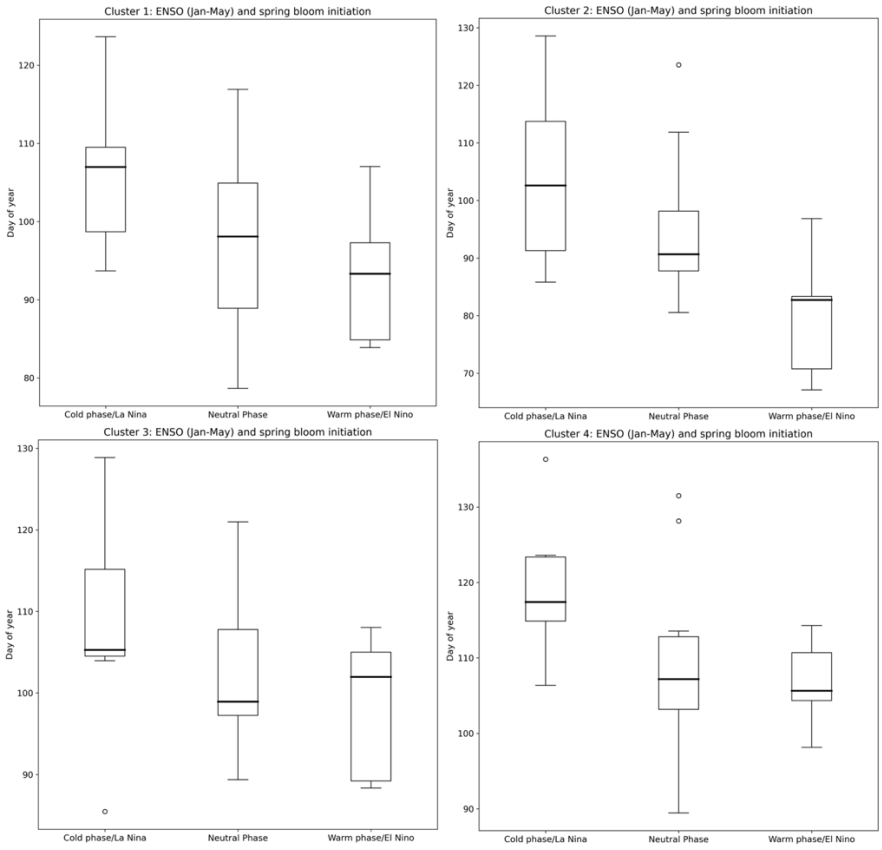

Figure 15: Boxplot of spring bloom initiation for cold phase/La Nina, neutral Phase and warm phase/El Nino per cluster. Where the ENSO index is less than -0.5 for La Nina/cold phase, between -0.5 and 0.5 for neutral phase, and greater than 0.5 for El Nino/warm phase.

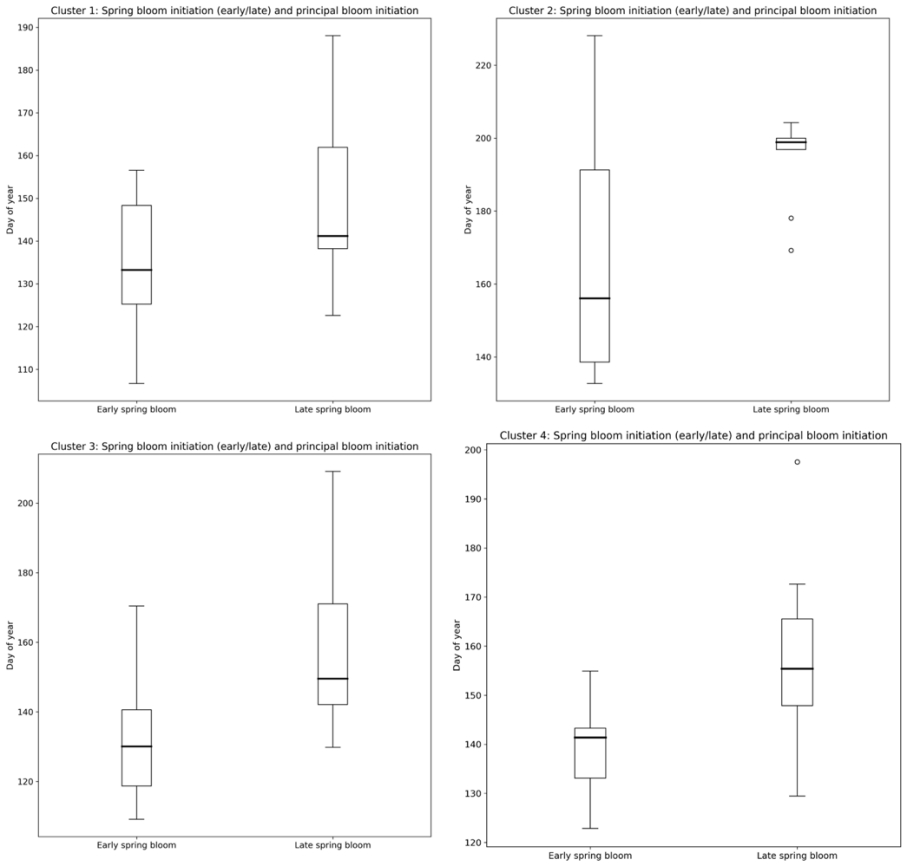

Figure 16: Boxplot of principal bloom initiation for early and late spring bloom initiation per cluster. Where the early spring bloom are the years where the spring bloom initiation is earlier than the 23-year mean, and late spring bloom initiation is later than the 23-year mean.

3.5 Discussion

This study used a 23-year (1998-2020) climatology of GlobColour interpolated Chl-a data to characterize phytoplankton phenology patterns over the British Columbia and Southeast Alaska coast. Phytoplankton phenology indices delineated the study region into four distinct bioregions, which were used as a framework to investigate phytoplankton phenology patterns over a heterogenous marine domain, and to evaluate the interannual trends of spring bloom initiation and interactions with environmental variables such as SST anomaly and the ENSO index. This study is unique in that it considers multiple bloom events by including the number of bloom

events and the total duration of all events per year. Taking into consideration multiple blooms helps to improve the understanding of processes shaping phytoplankton phenology (Krug et al., 2018; Vargas et al., 2009). Additionally, analyzing the principal bloom in this region is beneficial since it encompasses a greater variability than would be considered using the spring bloom alone. Therefore, using the principal bloom event enables the derivation of independent metrics from the cluster analysis. From the derived clusters, we can then investigate the interannual variability of the spring bloom initiation, which is of great ecological importance considering the interconnection between food webs and fisheries (Marchese et al., 2022; Platt et al., 2003; Suchy et al., 2022).

3.5.1 Seasonal and regional patterns in Chl-a

The GlobColour interpolated Chl-a product demonstrated the expected seasonal and local dynamics for this region, and average concentrations within ranges reported for satellite-derived observations (Carswell et al., 2017; Giannini et al., 2021; Gower et al., 2013; Jackson et al., 2015; Marchese et al., 2022; Suchy et al., 2019), and in situ measurements (Masson & Peña, 2009). Specifically, the monthly climatological cycle derived from the GlobColour interpolated Chl-a concentrations over the period 1998-2020 share similar trends (**Figure A3**) as shown by Marchese et al. (2022) with limited time series (2016-2021). In February, Chl-a concentrations were generally low, particularly in offshore waters, with slightly higher concentrations over the shelf. In March, the SoG, the Vancouver Island shelf and the east coast of Haida Gwaii experienced an increase in Chl-a concentrations. As expected, in April and May (spring) and sustained over June-August (summer), we observed a clear intensification of Chl-a concentration along the shelf, particularly in the vicinity of Vancouver Island waters (Carswell et al., 2017; Del

Bel Belluz et al., 2021; Giannini et al., 2021; Jackson et al., 2015; Masson & Peña, 2009; Noakes et al., 2000; Suchy et al., 2019). In contrast, the offshore waters maintained a low Chl-a concentration throughout the spring and summer, and only experienced an increase in Chl-a concentration in the fall (September-November; Marchese et al., 2022; Yoo et al., 2008; Zhang et al., 2016). By mid-November, the Chl-a values decreased throughout the entire study area (Marchese et al., 2022). The west coast of Haida Gwaii generally experiences low Chl-a concentrations due to the regions narrow (<5 km wide) continental shelf, which allows nutrient-poor offshore oceanic water to be present in close proximity to the coastline (Jackson et al., 2015).

The Chl-a peak values revealed a distinct gradient from the coastal to offshore regions, with high Chl-a concentrations being found along the coast, particularly in the Strait of Georgia in the proximity of the Fraser River, along the Vancouver Island shelf, in Queen Charlotte Strait, North Vancouver Island, Hecate Strait and the area surrounding the Dixon shelf (**Figure 10D**). Moderate Chl-a concentrations were found along the continental slope and low Chl-a concentrations were found in offshore waters (**Figure 10D**). These trends are expected, and have also been observed in Marchese et al. (2022) and Giannini et al. (2021). High productivity along the southern B.C. coast can be attributed to upwelling favourable winds in summer (April-September), which brings nutrient-rich water toward the surface (Allen & Wolfe, 2013; Jackson et al., 2015; Masson & Peña, 2009; Peña et al., 2019; Ware & Thomson, 2005). Similarly, freshwater discharge increases the stability which keeps both nutrients and phytoplankton in the euphotic zone (Jackson et al., 2015; Masson & Peña, 2009; Ware & Thomson, 2005). The northern B.C. coast to western Alaska regions are dominated by downwelling favourable winds

most of the year, though nutrients supplied by river discharge, current-induced upwelling, coastal eddies, and winter upwelling winds increase phytoplankton production (Ware & Thomson, 2005). Conversely, we observe low Chl-a concentrations in the offshore region in the subarctic North Pacific known to experience relatively low phytoplankton biomass due to iron limitation and microzooplankton grazing (Boyd et al., 2007; McNair et al., 2021; Miller et al., 1991; Strom et al., 1993).

3.5.2 Phenology indices per bioregion

The phenology-based objective partition strategy delineated four regions over the B.C. and SE Alaska coast, comprising of two coastal clusters, a shelf region, and an offshore region. We observed a distinctive spatial coherency, with noticeable coastal-offshore and latitudinal gradients. For example, the coastal cluster, Cluster 1, occupies regions in the B.C. and SE Alaska coast in the vicinity of the Fraser River mouth, the inner coastal waters, and the fjord systems, which are characterized by strong stratification influenced by freshwater runoff (Allen & Wolfe, 2013b; Collins et al., 2009; Suchy et al., 2019). These areas have glacier fed rivers flowing into inlets and out to the coast (**Figure 11A**), where the strong influence of the river runoff creates a stratified surface layer allowing phytoplankton to be better exposed to the available sunlight, resulting in a greater phytoplankton biomass (Collins et al., 2009; Del Bel Belluz et al., 2021; Dosser et al., 2021; Jarníková et al., 2022). These conditions generally lead to multiple blooms per year (Suchy et al., 2019) and compared to all the clusters it has the largest range of number of blooms, reaches the highest peak Chl-a concentrations, and has the greatest range of the timing of peak Chl-a concentration (range: 21st February – 12th November, median: 20th May) and principal bloom initiation (range: 21st February – 11th October, median: 26th April). This

region overlaps with bioregions #9 from Marchese et al. (2022), which, in contrast to our findings, did not show a clear seasonal cycle. However, Marchese et al. (2022) speculates that this region experiences estuarine circulation that is driven by river runoff which resupplies nutrients and keeps Chl-a concentrations reasonably high and stable under a sufficient light regime. Suchy et al. (2022), having a longer time series (2003-2016) than Marchese et al. (2022), observed similar patterns to ours, with the SoG having multiple peaks throughout the productive season and Chl-a concentration rarely decreasing below 2 mg m^{-3}. Harrison et al. (1983) confirms the conditions of the central SoG being diluted by freshwater, particularly from the Fraser River, creating a very stable surface layer that supports phytoplankton growth. Lastly, Collins et al. (2009) was able to successfully predict the timing of the spring bloom in the SoG using a coupled biophysical model since wind was found to control the spring bloom timing – weak wind conditions decreased the mixing-layer depth enabling phytoplankton to receive enough light to support their growth.

The offshore region, Cluster 2, lies mostly beyond the B.C. continental shelf at depths ranging from 1000-3000m (**Figure 11A**). The subarctic North Pacific open ocean waters are considered a high nitrate low chlorophyll region (HNLC), controlled by large-scale currents with minimal seasonal variability of primary productivity, and is relatively more homogenous than coastal waters (Brickley & Thomas, 2004; Childers et al., 2005). This cluster has been characterized by two bloom events, with the first occurring in spring, and the second bloom, which is the principal bloom event, occurring in the fall (**Figure 11C**). Compared to the other clusters, Cluster 2 has the lowest peak Chl-a concentrations, the shortest principal bloom duration on average, and the latest timing of principal bloom initiation and termination, and timing of peak Chl-a

concentration (**Figure 13A-H**). Having found similar results to ours, Marchese et al. (2022) reported off-shelf bioregions that showed comparatively low values of phytoplankton biomass with fall blooms that reached higher concentrations than spring blooms. These findings were also confirmed by Brickley & Thomas (2004), Yoo et al. (2008) and Zhang et al. (2016) who observed a small spring peak in Chl-a followed by an elevated Chl-a peak in fall. The absence of pronounced spring blooms can be accounted for by an iron limitation in these HNLC regions, which inhibits diatom blooms from occurring (Ribalet et al., 2010). Additionally, the Chl-a accumulation throughout summer that enables the peak Chl-a concentration to occur in late summer and fall can be explained by the consumption of microzooplankton by mesozooplankton which in turn reduces the microzooplankton grazing on phytoplankton, allowing phytoplankton biomass to flourish (Zhang et al., 2021).

The continental shelf region, Cluster 3, occupies most of the Queen Charlotte Sound area, Hecate Strait, Dixon entrance and the offshore region west of SE Alaska (**Figure 11A**), and is a region that is notable for its high productivity and abundance in iron (Jackson et al., 2015; Whitney et al., 2005). Cluster 3 is characterized by two bloom events consisting of a dominant spring bloom and a secondary fall bloom (**Figure 11D**). This region has the second lowest peak Chl-a concentrations, being second to the offshore region (**Figure 13D**). Cluster 3 has the timing of peak Chl-a concentration and principal bloom initiation occurring in spring (**Figure 13E,F**). This region is most similar to bioregion #6 from Marchese et al. (2022), who also found two bloom events, with the first occurring between April and May in spring, and the second bloom occurring in September. Similarly, the Cluster 3 region overlaps with ‘regime 1’ outlined by Jackson et al. (2015), which spans the southern coast of Alaska and northern inland waters of

B.C. and is characterized by a spring bloom that begins around mid-April and reaches peak Chl-a concentrations between April and June, with a fall bloom occurring in September. These findings were also confirmed by Waite & Mueter (2013) who identified a coast-wide "eastern Gulf of Alaska" cluster which was distinguished by a relatively intense spring bloom occurring in May, and a fall bloom in September. The patterns experienced in this region can be explained by the oceanographic conditions that are primarily resolved by coastal runoff, winds and light levels (Whitney et al., 2005). In winter dominant southeast winds cause downwelling to occur, either weakening or stopping completely in April when the winds transition to northwest winds, which enables the productive season to commence. During the summer months, from June to August, stratified surface waters are experienced due to freshwater runoff and an absence of strong winds. The winds increase in strength by the end of summer, and become progressively stronger by the end of October when the storm season begins (Thomson, 1981; Whitney et al., 2005).

The coastal cluster, Cluster 4, occupies the regions along the B.C. and SE Alaska coast consisting of the Juan de Fuca Eddy region, Haro Strait, southern Strait of Georgia, Queen Charlotte Strait, the B.C. coastline adjacent to the Hecate Strait as well as the Frederick Sound region in SE Alaska (**Figure 11A**). This region is highly dynamic, characterized by high mixing and therefore a deeper mixed layer depth (Thomson, 1994). Cluster 4 is characterized by a single bloom event (**Figure 13A**), the second highest peak Chl-a concentrations amongst all the clusters, and the timing of the peak Chl-a concentration generally occurring in spring/summer (**Figure 13D,E**). The timing of the principal bloom initiation of Cluster 4 generally occurs in spring, and it has the longest principal bloom duration compared to the other clusters (**Figure 13F,G**). This region overlaps with bioregions #8 and #10 from Marchese et al. (2022), which

were both characterized by a single bloom period that peaked in spring and experienced a prolonged production throughout the summer. Bioregion #8 from Marchese et al. (2022) extended from south to north along the inner shelf through Dixon entrance and included the area of Cook Bank, which is south of Queen Charlotte Strait. The prolonged summer productivity in this region could be caused by the steady supply of nutrients into the surface layer which could result from a continually mixed and re-stratified water column, as well as from the well-mixed and nutrient-rich waters from Queen Charlotte Strait (Borstad et al., 2011; Henson, 2007; Marchese et al., 2022; O'Neel et al., 2015; Stabeno et al., 2016; Tortell et al., 2012). Bioregion #10 from Marchese et al. (2022) included most of the Strait of Georgia and the Juan de Fuca Eddy region, which is an area that provides high nutrient concentrations that supports elevated phytoplankton productivity on the eddy margins. Other studies have also observed the seasonal trends noticed in this region, for instance, the increase of phytoplankton biomass in spring which was maintained throughout summer has been observed in the central and southern SoG (Masson & Peña, 2009; Peña et al., 2016). Numerous studies on phytoplankton productivity in the SoG have exhibited how the river runoff, light conditions, winds, tides, and nutrient and grazing dynamics determine the spatial and inter-annual variability in this region (Allen et al., 2015; Allen & Wolfe, 2013a; Collins et al., 2009; Masson & Peña, 2009; Suchy et al., 2019).

3.5.3 Spring bloom initiation, SST anomalies, ENSO

The spring bloom initiation is an important event as it dictates the beginning of food availability season for zooplankton and juvenile salmon (Li et al., 2013; Malick et al., 2015; Perry et al., 2021; Suchy et al., 2022). Additionally, we have evaluated the environmental variables such as SST anomalies and ENSO index, to potentially give an indication of the driving forces behind the interannual variability of the spring bloom initiation. And lastly, we have related the spring

bloom initiation and principal bloom initiation. Prior to these analyses, we have compared the timing of the spring bloom initiation to dates found in the literature, to ensure that our findings reflect reality.

The spring bloom has been analyzed extensively in the central SoG, which corresponds to an area within Cluster 1 (Allen & Wolfe, 2013b; Bornhold, 2000; Peña et al., 2016; Schweigert et al., 2013; Suchy et al., 2022). We have found the climatological spring bloom initiation throughout the time period (1998-2020) in the region of the central SoG to occur end of March-beginning of April (3 April ±4 days; DOY 89-96), which overlaps with the average spring bloom initiation found by Suchy et al. (2022) to be during the last week of March (DOY 85-92). Other studies have found similar bloom timings in this region, such as around the 25th March (DOY 84) by Allen & Wolfe (2013), mid-March to mid-April identified by Bornhold (2000), and 2nd-15th April observed by Peña et al. (2016), despite using different methods, comparing different years, considering different spatial regions and defining bloom initiation in different ways (see Suchy et al., 2022). In general, we find reasonable agreement between our annual spring bloom initiation dates and results from other studies. For example, out of the 14 years (2003-2016) that overlap between our study and Suchy et al. (2022), 6 of the years show similar dates (2005, 2006, 2008, 2010, 2014, 2016; Table A1) and another 6 years showed results that were within two weeks (2003, 2004, 2009, 2011, 2013, 2015; Table A1). The years 2007 and 2012 had different results to Suchy et al. (2022), however the year 2007 was in agreement with Gower et al. (2013), leaving 2012 as the only year with anomalous results (4 May ± 40 days; **Table A1**).

At a broader scale, over the entire study area, the climatological spring bloom initiation (1998-2020) seemed to replicate the patterns described in Marchese et al. (2022) derived from the climatological average (2016-2020) of Chl-a Sentinel 3A data, which is depicted in **Figure A4**. Similar to the results found by Marchese et al. (2022), the spring bloom initiation generally occurred earlier around late February to late March (DOY 64-88) south of 51°N. Later spring bloom initiation occurred on the west coast of Vancouver Island, the north tip of Vancouver island and in the Queen Charlotte Strait (Marchese et al., 2022). In the Queen Charlotte Sound, in the vicinity of Calvert Island the spring bloom initiation occurred between the middle and end of March. In the coastal areas north of 52°N, later blooms occurring from the start of April to the start of May (DOY 96-120) were experienced on the west coast of Haida Gwaii, in Hecate Strait and along Dixon Entrance. Localized zones of earlier start dates starting in March was found along the northeast coast of Haida Gwaii, and in the vicinity of Dogfish Banks. Any discrepancies found between this study and Marchese et al. (2022) could be due to the differences in time scales, since we consider a time span of 1998-2020, whereas Marchese et al. (2022) considers 2016-2020, which is a period of time that was under the influence of the Blob (anomalously warm water that dominated much of the North Pacific Ocean) more heavily.

The interannual variability of the spring bloom initiation can range from just over month (43-47 days) for the coastal and shelf regions, and to two months (61 days) for the offshore region between March and May (**Figure 14A-D**). Therefore, the offshore region has the greatest interannual variability compared to the coastal and shelf regions, and in extreme cases the spring bloom initiation can vary between 2 months. However, we have shown that warm phase El Nino years generally have an earlier spring bloom initiation than the cool phase La Nina year for all

clusters, and therefore a trend exists between the interannual variability of bloom timing in the B.C. and SE Alaska coast and environmental drivers investigated here, SST anomaly and the ENSO index. For the offshore region, early spring blooms are experienced in all years that undergo a positive SST anomaly, which in turn is associated with an El Nino phase (ENSO index > 0.5; **Figure 14 and 15**). This relationship also holds true for the coastal and shelf region, however with some exceptions (**Figure 14**). In the coast and shelf region, the influence of river runoff, winds, upwelling/downwelling conditions, light and currents may also play a role in the timing of the spring bloom initiation (Allen & Wolfe, 2013b; Suchy et al., 2019, 2022). The tendency for spring blooms to occur earlier during warmer years has been observed in many other studies (Henson et al., 2013; Hunter-Cevera et al., 2016; Sasaoka et al., 2011; Suchy et al., 2022; Zhao et al., 2013). We also observed a trend of late spring blooms events occurring during negative SST anomaly and during a La Nina phase (ENSO index < -0.5), however there are some exceptions to this generalization (**Figure 14 and 15**). This trend is also observed by Suchy et al. (2022) in the SoG, where cold years exhibited average or late blooms. Similarly, Sasaoka et al. (2011) also found that the spring bloom timing in was earlier in El Nino phase (warmer SST) and later in La Nina phase (cooler SST). Therefore, to a certain degree, the SST anomaly and ENSO phases can be used as an indicator of earlier than average timing of spring bloom initiation in this region.

In contrast to the spring bloom initiation, the principal bloom initiation does not show a clear relationship with SST anomaly (**Figure A1**), and therefore the timing of the principal bloom cannot be indicated by the SST anomaly directly. However, our results do show that a relationship exists between the timing of the spring bloom initiation and the timing of the

principal bloom (**Figure 16**). When the timing of the spring bloom occurs earlier than the 23-year mean, the timing of the principal bloom initiation tends to occur earlier than the timing of principal bloom initiation that occurs after a later spring bloom initiation (**Figure 16**). It is for this reason that we can generally assume that when there is a later spring bloom initiation we can expect a later principal bloom initiation, and vice versa.

3.6 Conclusion

A 23-year time series of satellite derived Chl-a was used to evaluate phytoplankton phenology on a per pixel basis, these phenology indices were then used directly as an input for objectively partitioning the heterogenous B.C. and SE Alaska coast, deriving the bioregions. This analysis identified four spatially coherent phenological bioregions, which consisted of two coastal clusters, a shelf region, and an offshore region with similar phenological patterns. The coastal clusters exhibited different phenological properties, potentially as a result of different physical forcings acting on these areas. The first coastal region (Cluster 1) is characterized by strong stratification influenced by freshwater runoff and conditions most conducive for phytoplankton growth, which resulted in multiple bloom events throughout the year and the highest phytoplankton biomass over the study region. The second coastal region (Cluster 4) has highly dynamic physical conditions, characterized by high mixing and therefore a deeper mixed layer depth, which resulted in a single bloom event that peaked in spring and was maintained throughout summer, yielding the second highest phytoplankton biomass over the study region. The shelf region (Cluster 3) is dominated by oceanographic conditions that are primarily resolved by winds, coastal runoff and light levels, which creates a bimodal pattern in Chl-a concentrations, with a spring peak in April-May and a second peak in September. Lastly, the

offshore region (Cluster 2) is defined as a high nitrate low chlorophyll region, which results in lowest phytoplankton biomass in the study area, and a bimodal pattern with the fall peak being more prominent than the spring peak.

The interannual trends of the spring bloom initiation and interactions with environmental variables such as SST anomaly and the ENSO index were evaluated in this study. We found that early spring blooms were associated with a positive SST anomaly and El Nino conditions. Conversely, average or late spring blooms occurred in years where there was a negative SST anomaly and La Nina conditions. Therefore, to a certain degree, the SST anomaly and ENSO phases can be used to inform the timing of spring bloom initiation in the entire region. Furthermore, the relationship between spring bloom initiation and principal bloom initiation was evaluated, and we found that when there is a later spring bloom initiation we can expect a later principal bloom initiation, and vice versa.

Overall, this study has adapted previous methods that used remotely sensed Chl-a data to create a phenology based bioregionalization (Krug et al., 2018). To our knowledge, this is the first study to perform a satellite-based 23-year phenology bioregionalization considering multiple bloom events in the British Columbia and SE Alaska coast, thus enabling this heterogenous marine domain to be simplified into coherent spatial regions from which the complex interactions with environmental drivers can be unraveled in future work. The findings of this study can help better inform fisheries management and conservation programs, by being able to indicate the timing of spring bloom initiation in relation to SST anomalies and ENSO index. The variability in spring

bloom initiation has been shown to result in a mismatch between phytoplankton and larger crustacean phenology (Suchy et al., 2022), which results in lower overall biomass available for higher trophic levels, thus highlighting the importance of being able to foresee these conditions.

4.0 Summary and Conclusions

4.1 Thesis Overview

The main goal of this research was to characterize the spatial and temporal dynamics of phytoplankton phenology in the B.C. and SE Alaska coastal oceans using 23-years (1998-2020) of merged satellite ocean colour data. We defined two research objectives to achieve this goal:

(1) In the second chapter (2.0), we evaluate the performance of merged multi-sensor ocean colour Chl-a products, from GlobColour and OC-CCI, in the B.C. and SE Alaska coastal waters via a statistical match-up analysis and a qualitative analysis to determine whether the data reflects the region's large scale seasonal and latitudinal trends.

To determine which merged multi-sensor ocean colour Chl-a product performs best in our study region, we performed a match-up analysis that compared product Chl-a data in a 3 × 3 pixel window to in situ HPLC data. This 3 × 3 pixel window is widely applied to account for the spatial variability of biogeochemical information and as a rationale for satellite sensor navigation not being accurate to the pixel. A time window of ± 3 hours from 12:00 in the Strait of Georgia, ± 5 hours for the west coast of Vancouver Island and ± 12 hours for Line P was also applied to reduce the effects of temporal variability of in situ data, particularly in more dynamic regions. An additional qualitative analysis was done to determine whether the data reflects the region's large-scale seasonal trends and latitudinal dynamics. The satellite to in situ match-up analysis in this region revealed that GlobColour CHL1 emerged as the best performer across most metrics (RMSE = 0.23, r = 0.91, MdAD = 1.35, BIAS = 0.99), followed closely by OC-CCI (RMSE = 0.27, r = 0.91, MdAD = 1.45, BIAS = 0.87). The GlobColour CHL1 dataset also reflects the expected general seasonal and latitudinal averages over the entire study region. Compared to other studies, the GlobColour statistics obtained here were comparable to, and in some cases

outperformed other validation statistics. Lastly, the GlobColour interpolated product has the highest spatial coverage since it has been 'gap-filled,' and would be appropriate for use in studies requiring a spatially and temporally complete dataset with a slight disregard for absolute Chl-a concentration, such as phytoplankton phenology studies. Our results show the importance of regional validation of merged multi-sensor satellite products in study areas that are solely Case 2, to enable product selection in optically complex waters.

> **(2)** In chapter three (3.0), we partition the study area into phenological bioregions using an objective unsupervised partition strategy based on a suite of phenological indices computed on a pixel-by-pixel basis, to evaluate the climatological region-specific phytoplankton phenology indices and describe the interannual variability of the spring bloom initiation in relation to sea-surface temperature (SST) anomaly and large-scale climate index, the El Nino Southern Oscillation (ENSO) index.

Using the interpolated GlobColour product we evaluated in chapter two (2.0), we derived a suite of phytoplankton phenology indices on a per pixel basis, which were then used as an input for objectively partitioning the heterogenous B.C. and SE Alaska coast. This analysis identified four spatially coherent phenological bioregions, consisting of two coastal clusters, a shelf region, and an offshore region. Broadly, we showed the phenological characteristics that distinguished each bioregion from one another, explored some of the driving forces that could be controlling these characteristics, and compared these results to the literature. Additionally, the interannual trends of the spring bloom initiation and interactions with environmental variables such as SST anomaly and the ENSO index were evaluated in this study. We found that early spring blooms occurred in years where there was a positive SST anomaly and El Nino conditions. Conversely, average, or late spring blooms occurred in years where there was a negative SST anomaly and La

Nina conditions. Therefore, to a certain degree, the SST anomaly and ENSO phases can be used as indicators of the timing of spring bloom initiation in this region. Furthermore, we found that later spring bloom initiation are generally associated with later principal bloom initiation, and vice versa.

4.2 Contributions of the research

The coastal waters of British Columbia (B.C.) support diverse food webs and provide habitats for various species of Pacific salmon, which are of vital importance to the regional economy and for First Nations culture and subsistence. To effectively monitor marine environmental health of these regions and any changes thereof, it is necessary to employ ecological indicators to provide objective and quantitative metrics upon which to evaluate the state of the ecosystem and their response to environmental and climatic perturbation. Phytoplankton phenology is an important ecological indicator that characterises the timing of annually occurring phytoplankton growing periods and has been typically synthesized into a set of indices encompassing the timing, duration, and magnitude of bloom events. Here we characterize the spatial and temporal patterns of phytoplankton phenology and simplify the heterogenous marine domain into four spatially coherent phenological bioregions, which consisted of two coastal clusters, a shelf region, and an offshore region with similar phenological patterns. We showed that the SST anomaly and ENSO phases can be used to inform the timing of spring bloom initiation in the entire region. The findings of this study can help better inform fisheries management and conservation programs, by being able to indicate the timing of spring bloom initiation in relation to SST anomalies and ENSO index. This work also contributes to the broader literature related to remote sensing of phytoplankton phenology dynamics in the B.C. and SE Alaska coasts. We have evaluated the

performances of the available merged multi-sensor satellite Chl-a products in this region, which can help inform researchers studying the B.C. coast on which products would be most appropriate to utilize for various purposes. Additionally, we have separated the study region into Case 1 and Case 2 waters, to investigate how these products perform differently in more optically complex waters, and therefore highlight the need for regional product validation.

4.3 Limitations and Future Research

Using satellite derived Chl-a data limits the analysis to only surface level Chl-a biomass, making it difficult to account for information on the vertical distribution of phytoplankton in the water column. Nevertheless, Suchy et al. (2019) performed a comparison of satellite data and in situ Chl-a in the Strait of Georgia and found that the surface satellite measurement reflected any deep water Chl-a maxima that occurred. Even so, it is possible for discrepancies between surface and subsurface Chl-a concentrations to occur, particularly in the presence of a deep-water Chl-a maximum (Suchy et al., 2019). Therefore, caution must be taken when interpreting results since satellite derived Chl-a is not always an optimal indicator of phytoplankton biomass despite its widespread use (Behrenfeld et al., 2016; Behrenfeld & Boss, 2014; Chittenden et al., 2010), and it may not reflect what zooplankton are actually feeding on (Friedland et al., 2015; Ji et al., 2010). Additionally, a potential source of uncertainty can be derived from satellite retrievals in optically complex Case 2 water bodies. As shown in Chapter 2, the contributions of CDOM and inorganic mineral particles can affect the optical signal, making the application of ocean colour remote sensing challenging in dynamic nearshore environments. Lastly, the bloom start dates may be associated with a certain degree of error due to several factors relating to data gaps,

different models or algorithms to retrieve Chl-a data and different methods and metrics to derive phenology indices (Ferreira et al., 2014).

This is the first study to perform a satellite-based 23-year phenology bioregionalization considering multiple bloom events in the British Columbia and SE Alaska coast, thus enabling this heterogenous marine domain to be simplified into coherent spatial regions. In future work, complex interactions with environmental drivers, such as the ocean optical variable (PAR), physical ocean variables (SST, winds, river discharge, stratification) and large-scale climate indices (PDO, NPGO, SOI), can be determined. This improved understanding of the link between phytoplankton phenology and the environmental conditions is crucial to predicting the possible responses of phytoplankton to natural variability and climate change in the future. Therefore, this research lays the groundwork for future studies examining how variations in bottom-up processes might impact the entire food web, which in turn can inform future decision making and conservation efforts.

5.0 References

ACRI-ST. (2007). *ESA DUE GlobColour Global Ocean Colour for Carbon Cycle Research Full Validation Report Reference : GC-PL-NIVA-FVR-01. 1.* https://www.globcolour.info/validation/report/GlobCOLOUR_FVR_v1.1.pdf

ACRI-ST GlobColour Team. (2020). GlobColour Product User Guide. *Ref: GC-UM-ACR-PUG-01, Version 4.2.1*. https://www.globcolour.info/CDR_Docs/GlobCOLOUR_PUG.pdf

Ajmani, A. M. (2011). *The growth and diet composition of sockeye salmon smolts in Rivers Inlet, British Columbia*. https://open.library.ubc.ca/collections/24/items/1.0053302

Allen, S. E., Latornell, D., Olson, E., & Pawlowicz, R. (2015). Timing of the spring phytoplankton bloom in the Strait of Georgia, 2015 and 2016. *State of the Physical, Biological and Selected Fishery Resources of Pacific Canadian Marine Ecosystems In*, 147–152.

Allen, S. E., & Wolfe, M. A. (2013a). Hindcast of the timing of the spring phytoplankton bloom in the Strait of Georgia, 1968--2010. *Progress in Oceanography*, *115*, 6–13.

Allen, S. E., & Wolfe, M. A. (2013b). Hindcast of the timing of the spring phytoplankton bloom in the strait of Georgia, 1968-2010. *Progress in Oceanography*, *115*, 6–13. https://doi.org/10.1016/j.pocean.2013.05.026

Alvain, S., Le Quéré, C., Bopp, L., Racault, M.-F., Beaugrand, G., Dessailly, D., & Buitenhuis, E. T. (2013). Rapid climatic driven shifts of diatoms at high latitudes. *Remote Sensing of*

Environment, *132*, 195–201.

Ardyna, M., Claustre, H., Sallée, J.-B., d'Ovidio, F., Gentili, B., van Dijken, G., d'Ortenzio, F., & Arrigo, K. R. (2017). Delineating environmental control of phytoplankton biomass and phenology in the Southern Ocean. *Geophysical Research Letters*, *44*(10), 5016–5024.

Bailey, S. W., & Werdell, P. J. (2006). A multi-sensor approach for the on-orbit validation of ocean color satellite data products. *Remote Sensing of Environment*, *102*(1–2), 12–23. https://doi.org/10.1016/j.rse.2006.01.015

Barnes, B. B., Cannizzaro, J. P., English, D. C., & Hu, C. (2019). Validation of VIIRS and MODIS reflectance data in coastal and oceanic waters: An assessment of methods. *Remote Sensing of Environment*, *220*, 110–123.

Beardall, J., Stojkovic, S., & Larsen, S. (2009). Living in a high CO2 world: Impacts of global climate change on marine phytoplankton. *Plant Ecology and Diversity*, *2*(2), 191–205. https://doi.org/10.1080/17550870903271363

Behrenfeld, M. J., & Boss, E. S. (2014). Resurrecting the ecological underpinnings of ocean plankton blooms. *Annu. Rev. Mar. Sci*, *6*(1), 167–194.

Behrenfeld, M. J., O'Malley, R. T., Boss, E. S., Westberry, T. K., Graff, J. R., Halsey, K. H., Milligan, A. J., Siegel, D. A., & Brown, M. B. (2016). Revaluating ocean warming impacts on global phytoplankton. *Nature Climate Change*, *6*(3), 323–330.

Belo Couto, A., Brotas, V., Mélin, F., Groom, S., & Sathyendranath, S. (2016). Inter-comparison of OC-CCI chlorophyll-a estimates with precursor data sets. *International Journal of Remote Sensing*, *37*(18), 4337–4355. https://doi.org/10.1080/01431161.2016.1209313

Blondeau-Patissier, D., Gower, J. F. R., Dekker, A. G., Phinn, S. R., & Brando, V. E. (2014). A review of ocean color remote sensing methods and statistical techniques for the detection, mapping and analysis of phytoplankton blooms in coastal and open oceans. *Progress in Oceanography*, *123*, 123–144. https://doi.org/10.1016/j.pocean.2013.12.008

Bojinski, S., Verstraete, M., Peterson, T. C., Richter, C., Simmons, A., & Zemp, M. (2014). The concept of essential climate variables in support of climate research, applications, and policy. *Bulletin of the American Meteorological Society*, *95*(9), 1431–1443. https://doi.org/10.1175/BAMS-D-13-00047.1

Bornhold, E. A. (2000). *Interannual and interdecadal patterns in timing and abundance of phytoplankton and zooplankton in the central straight of Georgia, BC with special reference to Neocalanus plumchrus*. University of British Columbia.

Borstad, G., Crawford, W., Hipfner, J. M., Thomson, R., & Hyatt, K. (2011). Environmental control of the breeding success of rhinoceros auklets at Triangle Island, British Columbia. *Marine Ecology Progress Series*, *424*, 285–302.

Boyce, D. G., Lewis, M. R., & Worm, B. (2010). Global phytoplankton decline over the past century. *Nature*, *466*(7306), 591–596. https://doi.org/10.1038/nature09268

Boyd, P. W., Jickells, T., Law, C. S., Blain, S., Boyle, E. A., Buesseler, K. O., Coale, K. H., Cullen, J. J., De Baar, H. J. W., Follows, M., & others. (2007). Mesoscale iron enrichment experiments 1993-2005: synthesis and future directions. *Science*, *315*(5812), 612–617.

Brickley, P. J., & Thomas, A. C. (2004). Satellite-measured seasonal and inter-annual chlorophyll variability in the Northeast Pacific and Coastal Gulf of Alaska. *Deep-Sea Research Part II: Topical Studies in Oceanography*, *51*(1–3), 229–245.

https://doi.org/10.1016/j.dsr2.2003.06.003

Brody, S. R., Lozier, M. S., & Dunne, J. P. (2013). A comparison of methods to determine phytoplankton bloom initiation. *Journal of Geophysical Research: Oceans*, *118*(5), 2345–2357. https://doi.org/10.1002/jgrc.20167

Carstensen, J., Klais, R., & Cloern, J. E. (2015). Phytoplankton blooms in estuarine and coastal waters: Seasonal patterns and key species. *Estuarine, Coastal and Shelf Science*, *162*, 98–109. https://doi.org/https://doi.org/10.1016/j.ecss.2015.05.005

Carswell, T., Costa, M., Young, E., Komick, N., Gower, J., & Sweeting, R. (2017). Evaluation of MODIS-aqua atmospheric correction and chlorophyll products of western North American coastal waters based on 13 years of data. *Remote Sensing*. https://doi.org/10.3390/rs9101063

Chandler, P. C., King, S. A., & Editors, R. I. P. (2015). *State of the Physical , Biological and Selected Fishery Resources of Pacific Canadian Marine Ecosystems in 2014 Canadian Technical Report of Fisheries and Aquatic Sciences 3131*.

Chebanova, V. V, Frenkel, S. E., & Zelenikhina, G. S. (2018). Relation of Feeding in Juvenile Chum Salmon (Oncorhynchus keta) and Pink Salmon (O. gorbuscha) to Abundance of Zooplankton in Coastal Waters of the Prostor Bay (Iturup Island). *Journal of Ichthyology*, *58*(5), 741–750. https://doi.org/10.1134/S0032945218050041

Cherkasheva, A., Bracher, A., Melsheimer, C., Köberle, C., Gerdes, R., Nöthig, E. M., Bauerfeind, E., & Boetius, A. (2014). Influence of the physical environment on polar phytoplankton blooms: A case study in the Fram Strait. *Journal of Marine Systems*, *132*, 196–207. https://doi.org/10.1016/j.jmarsys.2013.11.008

Childers, A. R., Whitledge, T. E., & Stockwell, D. A. (2005). Seasonal and interannual variability in the distribution of nutrients and chlorophyll a across the Gulf of Alaska shelf: 1998-2000. *Deep-Sea Research Part II: Topical Studies in Oceanography*, *52*(1-2 SPEC. ISS.), 193–216. https://doi.org/10.1016/j.dsr2.2004.09.018

Chittenden, C. M., Jensen, J. L. A., Ewart, D., Anderson, S., Balfry, S., Downey, E., Eaves, A., Saksida, S., Smith, B., Vincent, S., & others. (2010). Recent salmon declines: a result of lost feeding opportunities due to bad timing? *PLoS One*, *5*(8), e12423.

Clay, S., Peña, A., DeTracey, B., & Devred, E. (2019). Evaluation of satellite-based algorithms to retrieve chlorophyll-a concentration in the Canadian Atlantic and Pacific Oceans. *Remote Sensing*, *11*(22), 1–29. https://doi.org/10.3390/rs11222609

Cloern, J. E. (2005). Phytoplankton community ecology: principles applied in San Francisco Bay . *Marine Ecology Progress Series*, *285*, 11–28. https://www.int-res.com/abstracts/meps/v285/p11-28/

Cloern, J. E., Abreu, P. C., Carstensen, J., Chauvaud, L., Elmgren, R., Grall, J., Greening, H., Johansson, J. O. R., Kahru, M., Sherwood, E. T., & others. (2016). Human activities and climate variability drive fast-paced change across the world's estuarine--coastal ecosystems. *Global Change Biology*, *22*(2), 513–529.

CMEMS. (2021a). Copernicus Marine Environment Monitoring Service: Quality Information Document. *Ref: CMEMS-OC-QUID-009-30-32-33-37-81-82-83-85-86-98, Issue: 3.3*. https://catalogue.marine.copernicus.eu/documents/QUID/CMEMS-OC-QUID-009-030-032-033-037-081-082-083-085-086-098.pdf

CMEMS. (2021b). *Product User Manual*. *8.0*.

https://catalogue.marine.copernicus.eu/documents/PUM/CMEMS-OC-PUM-009-ALL.pdf

Cole, H., Henson, S., Martin, A., & Yool, A. (2012). Mind the gap: The impact of missing data on the calculation of phytoplankton phenology metrics. *Journal of Geophysical Research: Oceans*, *117*(8), 2–9. https://doi.org/10.1029/2012JC008249

Collins, A. K., Allen, S. E., & Pawlowicz, R. (2009). The role of wind in determining the timing of the spring bloom in the Strait of Georgia. *Canadian Journal of Fisheries and Aquatic Sciences*, *66*(9), 1597–1616.

Craddock, D. R., Blahm, T. H., & Parente, W. D. (1976). Occurrence and Utilization of Zooplankton by Juvenile Chinook Salmon in the Lower Columbia River. *Transactions of the American Fisheries Society*, *105*(1), 72–76. https://doi.org/https://doi.org/10.1577/1548-8659(1976)105<72:OAUOZB>2.0.CO;2

Cushing, D. H. (1959). The seasonal variation in oceanic production as a problem in population dynamics. *ICES Journal of Marine Science*. https://doi.org/10.1093/icesjms/24.3.455

Cushing, D. H. (1990). Plankton production and year-class strength in fish populations: an update of the match/mismatch hypothesis. In *Advances in marine biology* (Vol. 26, pp. 249–293). Elsevier.

d'Ortenzio, F., Antoine, D., Martinez, E., & Ribera d'Alcalà, M. (2012). Phenological changes of oceanic phytoplankton in the 1980s and 2000s as revealed by remotely sensed ocean-color observations. *Global Biogeochemical Cycles*, *26*(4).

D'Ortenzio, F., & Ribera d'Alcalà, M. (2009). On the trophic regimes of the Mediterranean Sea: a satellite analysis. *Biogeosciences*, *6*(2), 139–148. https://doi.org/10.5194/bg-6-139-2009

Del Bel Belluz, J., Peña, M. A., Jackson, J. M., & Nemcek, N. (2021). Phytoplankton Composition and Environmental Drivers in the Northern Strait of Georgia (Salish Sea), British Columbia, Canada. *Estuaries and Coasts*. https://doi.org/10.1007/s12237-020-00858-2

Di Lorenzo, E., Schneider, N., Cobb, K. M., Franks, P. J. S., Chhak, K., Miller, A. J., McWilliams, J. C., Bograd, S. J., Arango, H., Curchitser, E., Powell, T. M., & Rivière, P. (2008). North Pacific Gyre Oscillation links ocean climate and ecosystem change. *Geophysical Research Letters*, *35*(8). https://doi.org/https://doi.org/10.1029/2007GL032838

Dosser, H. V, Waterman, S., Jackson, J. M., Hannah, C. G., Evans, W., & Hunt, B. P. V. (2021). Stark Physical and Biogeochemical Differences and Implications for Ecosystem Stressors in the Northeast Pacific Coastal Ocean. *Journal of Geophysical Research: Oceans*, *126*(11), e2020JC017033.

Dowell, M., Platt, T., & others. (2009). *Partition of the Ocean into Ecological Provinces: Role of Ocean-Colour Radiometry*.

Edwards, M., & Richardson, A. J. (2004). Impact of climate change on marine pelagic phenology and trophic mismatch. *Nature*. https://doi.org/10.1038/nature02808

El Hourany, R., Abboud-Abi Saab, M., Faour, G., Aumont, O., Crépon, M., & Thiria, S. (2019). Estimation of Secondary Phytoplankton Pigments From Satellite Observations Using Self-Organizing Maps (SOMs). *Journal of Geophysical Research: Oceans*, *124*(2), 1357–1378. https://doi.org/10.1029/2018JC014450

ESA OC-CCI. (2021). ESA Ocean Colour Climate Change Initiative – Phase 3 Product Validation and Inter-comparison Report. *Plymouth Marine Laboratory*, *D4.1*(1.0

ESA/ESRIN), 1–17. https://docs.pml.space/share/s/xztLpM-NRka9rqoeSQFw5A

Fendereski, F., Vogt, M., Payne, M. R., Lachkar, Z., Gruber, N., Salmanmahiny, A., & Hosseini, S. A. (2014). Biogeographic classification of the Caspian Sea. *Biogeosciences*, *11*(22), 6451–6470. https://doi.org/10.5194/bg-11-6451-2014

Ferreira, A. S., Visser, A. W., Mackenzie, B. R., & Payne, M. R. (2014). Accuracy and precision in the calculation of phenology metrics. *Journal of Geophysical Research: Oceans*. https://doi.org/10.1002/2014JC010323

Field, C. B., Behrenfeld, M. J., Randerson, J. T., & Falkowski, P. (1998). Primary Production of the Biosphere: Integrating Terrestrial and Oceanic Components. *Science*, *281*(5374), 237–240. https://doi.org/10.1126/science.281.5374.237

Ford, D. A., Edwards, K. P., Lea, D., Barciela, R. M., Martin, M. J., & Demaria, J. (2012). Assimilating GlobColour ocean colour data into a pre-operational physical-biogeochemical model. *Ocean Science*, *8*(5), 751–771. https://doi.org/10.5194/os-8-751-2012

Foukal, N. P., & Thomas, A. C. (2014). Biogeography and phenology of satellite-measured phytoplankton seasonality in the California current. *Deep Sea Research Part I: Oceanographic Research Papers*, *92*, 11–25.

Friedland, K. D., Leaf, R. T., Kane, J., Tommasi, D., Asch, R. G., Rebuck, N., Ji, R., Large, S. I., Stock, C., & Saba, V. S. (2015). Spring bloom dynamics and zooplankton biomass response on the US Northeast Continental Shelf. *Continental Shelf Research*, *102*, 47–61.

Friedland, K. D., Mouw, C. B., Asch, R. G., Ferreira, A. S. A., Henson, S., Hyde, K. J. W., Morse, R. E., Thomas, A. C., & Brady, D. C. (2018). Phenology and time series trends of

the dominant seasonal phytoplankton bloom across global scales. *Global Ecology and Biogeography*, *27*(5), 551–569. https://doi.org/10.1111/geb.12717

Garnesson, P., Mangin, A., D'Andon, O. F., Demaria, J., & Bretagnon, M. (2019). The CMEMS GlobColour chlorophyll a product based on satellite observation: Multi-sensor merging and flagging strategies. *Ocean Science*, *15*(3), 819–830. https://doi.org/10.5194/os-15-819-2019

Gbagir, A. G., & Colpaert, A. (2020). *Assessing the Trend of the Trophic State of Lake*.

Giannini, F., Hunt, B. P. V., Jacoby, D., & Costa, M. (2021). Performance of OLCI Sentinel-3A satellite in the Northeast Pacific coastal waters. *Remote Sensing of Environment*, *256*(September 2020). https://doi.org/10.1016/j.rse.2021.112317

Gohin, F., Lampert, L., Guillaud, J.-F., Herbland, A., & Nézan, E. (2003). Satellite and in situ observations of a late winter phytoplankton bloom, in the northern Bay of Biscay. *Continental Shelf Research*, *23*(11), 1117–1141. https://doi.org/https://doi.org/10.1016/S0278-4343(03)00088-8

Gordon, H. R., & Morel, A. Y. (1983). *Remote Assessment of Ocean Color for Interpretation of Satellite Visible Imagery: A reviw*. Springer, New York, NY. https://doi.org/https://doi.org/10.1007/978-1-4684-6280-7

Gower, J., King, S., Statham, S., Fox, R., & Young, E. (2013). The Malaspina Dragon: a newly-discovered pattern of the early spring bloom in the Strait of Georgia, British Columbia, Canada. *Progress in Oceanography*, *115*, 181–188.

Gregr, E. J., & Bodtker, K. M. (2007). Adaptive classification of marine ecosystems: Identifying biologically meaningful regions in the marine environment. *Deep-Sea Research Part I:*

Oceanographic Research Papers, *54*(3), 385–402. https://doi.org/10.1016/j.dsr.2006.11.004

Groom, S. B., Sathyendranath, S., Ban, Y., Bernard, S., Brewin, B., Brotas, V., Brockmann, C., Chauhan, P., Choi, J. K., Chuprin, A., Ciavatta, S., Cipollini, P., Donlon, C., Franz, B. A., He, X., Hirata, T., Jackson, T., Kampel, M., Krasemann, H., … Wang, M. (2019). Satellite ocean colour: Current status and future perspective. *Frontiers in Marine Science*, *6*(JUL). https://doi.org/10.3389/fmars.2019.00485

Halkidi, M., Batistakis, Y., & Vazirgiannis, M. (2001). On clustering validation techniques. *Journal of Intelligent Information Systems*, *17*(2–3), 107–145. https://doi.org/10.1023/A:1012801612483

Hammond, M. L., Beaulieu, C., Sahu, S. K., & Henson, S. A. (2017). Assessing trends and uncertainties in satellite-era ocean chlorophyll using space-time modeling. *Global Biogeochemical Cycles*. https://doi.org/10.1002/2016GB005600

Harrison, P. J., Fulton, J. D., Taylor, F. J. R., & Parsons, T. R. (1983). Review of the biological oceanography of the Strait of Georgia: pelagic environment. *Canadian Journal of Fisheries and Aquatic Sciences*, *40*(7), 1064–1094.

Henson, S. A. (2007). Water column stability and spring bloom dynamics in the Gulf of Alaska. *Journal of Marine Research*, *65*(6), 715–736.

Henson, S. A., Dunne, J. P., & Sarmiento, J. L. (2009). Decadal variability in North Atlantic phytoplankton blooms. *Journal of Geophysical Research: Oceans*, *114*(4), 1–11. https://doi.org/10.1029/2008JC005139

Henson, S., Cole, H., Beaulieu, C., & Yool, A. (2013). The impact of global warming on

seasonality of ocean primary production. *Biogeosciences*, *10*(6), 4357–4369.

Hilborn, A., & Costa, M. (2018). Applications of DINEOF to satellite-derived chlorophyll-a from a productive coastal region. *Remote Sensing*. https://doi.org/10.3390/rs10091449

Hunter-Cevera, K. R., Neubert, M. G., Olson, R. J., Solow, A. R., Shalapyonok, A., & Sosik, H. M. (2016). Physiological and ecological drivers of early spring blooms of a coastal phytoplankter. *Science*, *354*(6310), 326–329.

Hussain, N. J., Wang, Z., Giannini, F., & Costa, M. (2022). Spatial Variability of In Situ Above-Water Reflectance in Coastal Dynamic Waters: Implications for Satellite Match-Up Analysis. *Frontiers in Remote Sensing*, *3*(June), 1–17. https://doi.org/10.3389/frsen.2022.876748

IOCCG. (2000). Remote sensing of ocean colour in coastal, and other optically-complex, waters, (ed. S. Sathyendranath.) Dartmouth, NS, Canada, International Ocean-Colour Coordinating Group (IOCCG), 140pp. *Reports of the International Ocean-Colour Coordinating Group, No. 3*. https://doi.org/http://dx.doi.org/10.25607/OBP-95

Jackson, J. M., Thomson, R. E., Brown, L. N., Willis, P. G., & Borstad, G. A. (2015). Satellite chlorophyll off the British Columbia Coast, 1997-2010. *Journal of Geophysical Research C: Oceans*. https://doi.org/10.1002/2014JC010496

Jackson, T. (2020). *ESA Ocean Colour Climate Change Initiative – Phase 3 Product User Guide for v5 . 0 Dataset*. 1–50.

Jarn\’\iková, T., Olson, E. M., Allen, S. E., Ianson, D., & Suchy, K. D. (2022). A clustering approach to determine biophysical provinces and physical drivers of productivity dynamics

in a complex coastal sea. *Ocean Science*, *18*(5), 1451–1475.

Ji, R., Edwards, M., MacKas, D. L., Runge, J. A., & Thomas, A. C. (2010). Marine plankton phenology and life history in a changing climate: Current research and future directions. *Journal of Plankton Research*, *32*(10), 1355–1368. https://doi.org/10.1093/plankt/fbq062

Joh, Y., & Di Lorenzo, E. (2017). Increasing Coupling Between NPGO and PDO Leads to Prolonged Marine Heatwaves in the Northeast Pacific. *Geophysical Research Letters*, *44*(22), 11,663-11,671. https://doi.org/10.1002/2017GL075930

Johnson, R., Strutton, P. G., Wright, S. W., McMinn, A., & Meiners, K. M. (2013). Three improved satellite chlorophyll algorithms for the Southern Ocean. *Journal of Geophysical Research: Oceans*, *118*(7), 3694–3703. https://doi.org/10.1002/jgrc.20270

K.B. Bishop, J., E. Calvert, S., & Soon, M. Y. S. (1999). Spatial and temporal variability of POC in the northeast subarctic Pacific. *Deep-Sea Research Part II: Topical Studies in Oceanography*, *46*(11–12), 2699–2733. https://doi.org/10.1016/S0967-0645(99)00081-8

Kahru, M., Brotas, V., Manzano-Sarabia, M., & Mitchell, B. G. (2011). Are phytoplankton blooms occurring earlier in the Arctic? *Global Change Biology*, *17*(4), 1733–1739. https://doi.org/10.1111/j.1365-2486.2010.02312.x

Karna, A., & Gibert, K. (2022). Automatic identification of the number of clusters in hierarchical clustering. *Neural Computing and Applications*, *34*(1), 119–134. https://doi.org/10.1007/s00521-021-05873-3

Kirby, R. R. (2011). *Ocean Drifters: A Secret World Beneath the Waves*. Firefly Books. https://books.google.ca/books?id=1biZKQEACAAJ

Kogeler, J., & Rey, F. (1999). Ocean colour and the spatial and seasonal distribution of phytoplankton in the Barents Sea. *International Journal of Remote Sensing*, *20*(7), 1303–1318.

Komick, N. M. (2007). Remote sensing chlorophyll-a in the Strait of Georgia. *Masters Abstracts International. Vol. 47, No. 01, 159 p. 2007.*, *47*(01), 159. http://search.proquest.com/docview/20751872?accountid=14656

Komick, N. M., Costa, M. P. F., & Gower, J. (2009). Bio-optical algorithm evaluation for MODIS for western Canada coastal waters: An exploratory approach using in situ reflectance. *Remote Sensing of Environment*, *113*(4), 794–804. https://doi.org/10.1016/j.rse.2008.12.005

Kostadinov, T. S., Cabré, A., Vedantham, H., Marinov, I., Bracher, A., Brewin, R. J. W., Bricaud, A., Hirata, T., Hirawake, T., Hardman-Mountford, N. J., Mouw, C., Roy, S., & Uitz, J. (2017). Inter-comparison of phytoplankton functional type phenology metrics derived from ocean color algorithms and Earth System Models. *Remote Sensing of Environment*, *190*, 162–177. https://doi.org/10.1016/j.rse.2016.11.014

Krug, L. A., Platt, T., Sathyendranath, S., & Barbosa, A. B. (2017). Ocean surface partitioning strategies using ocean colour remote Sensing: A review. *Progress in Oceanography*, *155*, 41–53. https://doi.org/https://doi.org/10.1016/j.pocean.2017.05.013

Krug, L. A., Platt, T., Sathyendranath, S., & Barbosa, A. B. (2018). Patterns and drivers of phytoplankton phenology off SW Iberia: A phenoregion based perspective. *Progress in Oceanography*, *165*(March), 233–256. https://doi.org/10.1016/j.pocean.2018.06.010

Laiolo, L., Matear, R., Soja-Woźniak, M., Suggett, D. J., Hughes, D. J., Baird, M. E., & Doblin,

M. A. (2021). Modelling the impact of phytoplankton cell size and abundance on inherent optical properties (IOPs) and a remotely sensed chlorophyll-a product. *Journal of Marine Systems*, *213*(August 2020). https://doi.org/10.1016/j.jmarsys.2020.103460

Land, P. E., Shutler, J. D., Platt, T., & Racault, M. F. (2014). A novel method to retrieve oceanic phytoplankton phenology from satellite data in the presence of data gaps. *Ecological Indicators*, *37*(PART A), 67–80. https://doi.org/10.1016/j.ecolind.2013.10.008

Lavigne, H., d'Ortenzio, F., Migon, C., Claustre, H., Testor, P., d'Alcalã, M. R., Lavezza, R., Houpert, L., & Prieur, L. (2013). Enhancing the comprehension of mixed layer depth control on the Mediterranean phytoplankton phenology. *Journal of Geophysical Research: Oceans*, *118*(7), 3416–3430.

Li, L., Mackas, D., Hunt, B., Schweigert, J., Pakhomov, E., Perry, R. I., Galbraith, M., & Pitcher, T. J. (2013). Zooplankton communities in the Strait of Georgia, British Columbia, track large-scale climate forcing over the Pacific Ocean. *Progress in Oceanography*, *115*, 90–102.

Lieth, H. (1974). Purposes of a phenology book. In *Phenology and seasonality modeling* (pp. 3–19). Springer.

Longhurst, A. R. (2010). *Ecological geography of the sea*. Elsevier.

Loos, E. A., & Costa, M. (2010). Inherent optical properties and optical mass classification of the waters of the Strait of Georgia, British Columbia, Canada. *Progress in Oceanography*, *87*(1–4), 144–156. https://doi.org/10.1016/j.pocean.2010.09.004

Loos, E., Costa, M., & Johannessen, S. (2017). Underwater optical environment in the coastal

waters of British Columbia, Canada. *Facets*, *2*(2), 872–891. https://doi.org/10.1139/facets-2017-0074

Malick, M. J., Cox, S. P., Mueter, F. J., & Peterman, R. M. (2015). Linking phytoplankton phenology to salmon productivity along a north-south gradient in the Northeast Pacific Ocean. *Canadian Journal of Fisheries and Aquatic Sciences*, *72*(5), 697–708. https://doi.org/10.1139/cjfas-2014-0298

Mantua, N. J., & Hare, S. R. (2002). The Pacific Decadal Oscillation. *Journal of Oceanography*, *58*(1), 35–44. https://doi.org/10.1023/A:1015820616384

Mantua, N. J., Hare, S. R., Zhang, Y., Wallace, J. M., & Francis, R. C. (1997). A Pacific interdecadal climate oscillation with impacts on salmon production. *Bulletin of the American Meteorological Society*, *78*(6), 1069–1080.

Marchese, C., Castro de la Guardia, L., Myers, P. G., & Bélanger, S. (2019). Regional differences and inter-annual variability in the timing of surface phytoplankton blooms in the Labrador Sea. *Ecological Indicators*, *96*(June 2018), 81–90. https://doi.org/10.1016/j.ecolind.2018.08.053

Marchese, C., Hunt, B. P. V, Giannini, F., Ehrler, M., & Costa, M. (2022). Bioregionalization of the coastal and open oceans of British Columbia and Southeast Alaska based on Sentinel-3A satellite-derived phytoplankton seasonality. *Frontiers in Marine Science*, *9*. https://doi.org/10.3389/fmars.2022.968470

Martinez, E., Raapoto, H., Maes, C., & Maamaatuaihutapu, K. (2018). Influence of tropical instability waves on phytoplankton biomass near the Marquesas islands. *Remote Sensing*, *10*(4), 1–12. https://doi.org/10.3390/rs10040640

Masson, D., & Peña, A. (2009). Chlorophyll distribution in a temperate estuary: The Strait of Georgia and Juan de Fuca Strait. *Estuarine, Coastal and Shelf Science*, *82*(1), 19–28. https://doi.org/10.1016/j.ecss.2008.12.022

Matsushita, B., Yang, W., Chang, P., Yang, F., & Fukushima, T. (2012). A simple method for distinguishing global Case-1 and Case-2 waters using SeaWiFS measurements. *ISPRS Journal of Photogrammetry and Remote Sensing*, *69*, 74–87. https://doi.org/10.1016/j.isprsjprs.2012.02.008

Mayot, N, Matrai, P. A., Arjona, A., Bélanger, S., Marchese, C., Jaegler, T., Ardyna, M., & Steele, M. (2020). Springtime export of Arctic sea ice influences phytoplankton production in the Greenland Sea. *Journal of Geophysical Research: Oceans*, *125*(3), e2019JC015799.

Mayot, Nicolas, d'Ortenzio, F., Ribera d'Alcalà, M., Lavigne, H., & Claustre, H. (2016). Interannual variability of the Mediterranean trophic regimes from ocean color satellites. *Biogeosciences*, *13*(6), 1901–1917.

McNair, H. M., Morison, F., Graff, J. R., Rynearson, T. A., & Menden-Deuer, S. (2021). Microzooplankton grazing constrains pathways of carbon export in the subarctic North Pacific. *Limnology and Oceanography*, *66*(7), 2697–2711.

McNicol, G., Bulmer, C., D'Amore, D., Sanborn, P., Saunders, S., Giesbrecht, I., Arriola, S. G., Bidlack, A., Butman, D., & Buma, B. (2019). Large, climate-sensitive soil carbon stocks mapped with pedology-informed machine learning in the North Pacific coastal temperate rainforest. *Environmental Research Letters*, *14*(1). https://doi.org/10.1088/1748-9326/aaed52

Mélin, F., Vantrepotte, V., Chuprin, A., Grant, M., Jackson, T., & Sathyendranath, S. (2017).

Assessing the fitness-for-purpose of satellite multi-mission ocean color climate data records: A protocol applied to OC-CCI chlorophyll-a data. *Remote Sensing of Environment*, *203*, 139–151. https://doi.org/10.1016/j.rse.2017.03.039

Miller, C. B., Frost, B. W., Wheeler, P. A., Landry, M. R., Welschmeyer, N., & Powell, T. M. (1991). Ecological dynamics in the subarctic Pacific, a possibly iron-limited ecosystem. *Limnology and Oceanography*, *36*(8), 1600–1615.

Moradi, M. (2021). Evaluation of merged multi-sensor ocean-color chlorophyll products in the Northern Persian Gulf. *Continental Shelf Research*, *221*(April), 104415. https://doi.org/10.1016/j.csr.2021.104415

Muller-Karger, F. E., Hestir, E., Ade, C., Turpie, K., Roberts, D. A., Siegel, D., Miller, R. J., Humm, D., Izenberg, N., Keller, M., Morgan, F., Frouin, R., Dekker, A. G., Gardner, R., Goodman, J., Schaeffer, B., Franz, B. A., Pahlevan, N., Mannino, A. G., … Jetz, W. (2018). Satellite sensor requirements for monitoring essential biodiversity variables of coastal ecosystems. *Ecological Applications*, *28*(3), 749–760. https://doi.org/10.1002/eap.1682

Navarro, G., Caballero, I., Prieto, L., Vázquez, A., Flecha, S., Huertas, I. E., & Ruiz, J. (2012). Seasonal-to-interannual variability of chlorophyll-a bloom timing associated with physical forcing in the Gulf of Cádiz. *Advances in Space Research*, *50*(8), 1164–1172. https://doi.org/10.1016/j.asr.2011.11.034

Nemcek, N., & Pena, M. A. (2014). Institute of Ocean Sciences protocols for phytoplankton pigment analysis by HPLC. In *Canadian technical report of fisheries and aquatic sciences 3117*. http://ezproxy.library.ubc.ca/login?url=http://search.proquest.com/docview/1668253275?ac

countid=14656%0Ahttp://gw2jh3xr2c.search.serialssolution.com?ctx_ver=Z39.88-2004&ctx_enc=info:ofi/enc:UTF-8&rfr_id=info:sid/Aquatic+Science+%26+Fisheries+Abstracts+%28

Noakes, D. J., Beamish, R. J., & Kent, M. L. (2000). On the decline of Pacific salmon and speculative links to salmon farming in British Columbia. In *Aquaculture*. https://doi.org/10.1016/S0044-8486(99)00294-X

O'Neel, S., Hood, E., Bidlack, A. L., Fleming, S. W., Arimitsu, M. L., Arendt, A., Burgess, E., Sergeant, C. J., Beaudreau, A. H., Timm, K., Hayward, G. D., Reynolds, J. H., & Pyare, S. (2015). Icefield-to-ocean linkages across the northern pacific coastal temperate rainforest ecosystem. *BioScience*, *65*(5), 499–512. https://doi.org/10.1093/biosci/biv027

Oliver, A. A., Tank, S. E., Giesbrecht, I., Korver, M. C., Floyd, W. C., Sanborn, P., Bulmer, C., & Lertzman, K. P. (2017). A global hotspot for dissolved organic carbon in hypermaritime watersheds of coastal British Columbia. *Biogeosciences*, *14*(15), 3743–3762. https://doi.org/10.5194/bg-14-3743-2017

Pahlevan, N., Sarkar, S., & Franz, B. A. (2016). Uncertainties in coastal ocean color products: Impacts of spatial sampling. *Remote Sensing of Environment*, *181*, 14–26.

Patt, F. S. (2002). *Navigation algorithms for the SeaWiFS mission*. NASA Center for AeroSpace Information.

Peña, M. A., Fine, I., & Callendar, W. (2019). Interannual variability in primary production and shelf-offshore transport of nutrients along the northeast Pacific Ocean margin. *Deep Sea Research Part II: Topical Studies in Oceanography*, *169–170*, 104637. https://doi.org/https://doi.org/10.1016/j.dsr2.2019.104637

Peña, M. A., Masson, D., & Callendar, W. (2016). Annual plankton dynamics in a coupled physical--biological model of the Strait of Georgia, British Columbia. *Progress in Oceanography*, *146*, 58–74.

Perry, R. I., Young, K., Galbraith, M., Chandler, P., Velez-Espino, A., & Baillie, S. (2021). Zooplankton variability in the Strait of Georgia, Canada, and relationships with the marine survivals of Chinook and Coho salmon. *Plos One*, *16*(1), e0245941.

Philander, S. G. H. (1983). El Niño Southern Oscillation phenomena. *Nature*, *302*(5906), 295–301. https://doi.org/10.1038/302295a0

Phillips, S. R., & Costa, M. (2017a). Spatial-temporal bio-optical classification of dynamic semi-estuarine waters in western North America. *Estuarine, Coastal and Shelf Science*. https://doi.org/10.1016/j.ecss.2017.09.029

Phillips, S. R., & Costa, M. (2017b). Spatial-temporal bio-optical classification of dynamic semi-estuarine waters in western North America. *Estuarine, Coastal and Shelf Science*, *199*, 35–48. https://doi.org/10.1016/j.ecss.2017.09.029

Pitarch, J., Volpe, G., Colella, S., Krasemann, H., & Santoleri, R. (2016). Remote sensing of chlorophyll in the Baltic Sea at basin scale from 1997 to 2012 using merged multi-sensor data. *Ocean Science*, *12*(2), 379–389. https://doi.org/10.5194/os-12-379-2016

Platt, T., Fuentes-Yaco, C., & Frank, K. T. (2003). Spring algal bloom and larval fish survival. *Nature*, *423*(6938), 398–399.

Platt, T., & Sathyendranath, S. (2008). Ecological indicators for the pelagic zone of the ocean from remote sensing. *Remote Sensing of Environment*, *112*(8), 3426–3436.

https://doi.org/10.1016/j.rse.2007.10.016

Platt, T., Sathyendranath, S., White, G. N., Fuentes-Yaco, C., Zhai, L., Devred, E., & Tang, C. (2010). Diagnostic properties of phytoplankton time series from remote sensing. *Estuaries and Coasts*, *33*(2), 428–439. https://doi.org/10.1007/s12237-009-9161-0

Platt, T., White, G. N., Zhai, L., Sathyendranath, S., & Roy, S. (2009). The phenology of phytoplankton blooms: Ecosystem indicators from remote sensing. *Ecological Modelling*, *220*(21), 3057–3069. https://doi.org/10.1016/j.ecolmodel.2008.11.022

Racault, M. F., Le Quéré, C., Buitenhuis, E., Sathyendranath, S., & Platt, T. (2012). Phytoplankton phenology in the global ocean. *Ecological Indicators*, *14*(1), 152–163. https://doi.org/10.1016/j.ecolind.2011.07.010

Racault, M. F., Platt, T., Sathyendranath, S., Ağirbaş, E., Martinez Vicente, V., & Brewin, R. (2014). Plankton indicators and ocean observing systems: Support to the marine ecosystem state assessment. *Journal of Plankton Research*, *36*(3), 621–629. https://doi.org/10.1093/plankt/fbu016

Racault, M. F., Raitsos, D. E., Berumen, M. L., Brewin, R. J. W., Platt, T., Sathyendranath, S., & Hoteit, I. (2015). Phytoplankton phenology indices in coral reef ecosystems: Application to ocean-color observations in the Red Sea. *Remote Sensing of Environment*, *160*, 222–234. https://doi.org/10.1016/j.rse.2015.01.019

Racault, M. F., Sathyendranath, S., & Platt, T. (2014). Impact of missing data on the estimation of ecological indicators from satellite ocean-colour time-series. *Remote Sensing of Environment*, *152*, 15–28. https://doi.org/10.1016/j.rse.2014.05.016

Reygondeau, G., & Dunn, D. (2019). Pelagic biogeography. *Encyclopedia of Ocean Sciences*, 588–598.

Reynolds, R. W. (1988). A real-time global sea surface temperature analysis. *Journal of Climate*, *1*(1), 75–87.

Reynolds, R. W., & Marsico, D. C. (1993). An improved real-time global sea surface temperature analysis. *Journal of Climate*, *6*(1), 114–119.

Ribalet, F., Marchetti, A., Hubbard, K. A., Brown, K., Durkin, C. A., Morales, R., Robert, M., Swalwell, J. E., Tortell, P. D., & Armbrust, E. V. (2010). Unveiling a phytoplankton hotspot at a narrow boundary between coastal and offshore waters. *Proceedings of the National Academy of Sciences of the United States of America*, *107*(38), 16571–16576. https://doi.org/10.1073/pnas.1005638107

Richardson, K. (1997). Harmful or exceptional phytoplankton blooms in the marine ecosystem. *Advances in Marine Biology*. https://doi.org/10.1016/s0065-2881(08)60225-4

Sá, C., D'Alimonte, D., Brito, A. C., Kajiyama, T., Mendes, C. R., Vitorino, J., Oliveira, P. B., da Silva, J. C. B., & Brotas, V. (2015). Validation of standard and alternative satellite ocean-color chlorophyll products off Western Iberia. *Remote Sensing of Environment*, *168*, 403–419. https://doi.org/10.1016/j.rse.2015.07.018

Salgado-Hernanz, P. M., Racault, M. F., Font-Muñoz, J. S., & Basterretxea, G. (2019). Trends in phytoplankton phenology in the Mediterranean Sea based on ocean-colour remote sensing. *Remote Sensing of Environment*, *221*(October 2018), 50–64. https://doi.org/10.1016/j.rse.2018.10.036

Santoleri, R., Banzon, V., Marullo, S., Napolitano, E., d'Ortenzio, F., & Evans, R. (2003). Year-to-year variability of the phytoplankton bloom in the southern Adriatic Sea (1998--2000): Sea-viewing Wide Field-of-view Sensor observations and modeling study. *Journal of Geophysical Research: Oceans*, *108*(C9).

Sapiano, M. R. P., Brown, C. W., Schollaert Uz, S., & Vargas, M. (2012). Establishing a global climatology of marine phytoplankton phenological characteristics. *Journal of Geophysical Research: Oceans*, *117*(C8).

Sasaoka, K., Chiba, S., & Saino, T. (2011). Climatic forcing and phytoplankton phenology over the subarctic North Pacific from 1998 to 2006, as observed from ocean color data. *Geophysical Research Letters*, *38*(15), 1–6. https://doi.org/10.1029/2011GL048299

Sathyendranath, S., Brewin, R. J. W., Brockmann, C., Brotas, V., Calton, B., Chuprin, A., Cipollini, P., Couto, A. B., Dingle, J., Doerffer, R., Donlon, C., Dowell, M., Farman, A., Grant, M., Groom, S., Horseman, A., Jackson, T., Krasemann, H., Lavender, S., … Platt, T. (2019). An ocean-colour time series for use in climate studies: The experience of the ocean-colour climate change initiative (OC-CCI). *Sensors (Switzerland)*, *19*(19). https://doi.org/10.3390/s19194285

Saulquin, B., Gohin, F., & Fanton d'Andon, O. (2019). Interpolated fields of satellite-derived multi-algorithm chlorophyll-a estimates at global and European scales in the frame of the European Copernicus-Marine Environment Monitoring Service. *Journal of Operational Oceanography*, *12*(1), 47–57. https://doi.org/10.1080/1755876X.2018.1552358

Schweigert, J. F., Thompson, M., Fort, C., Hay, D. E., Therriault, T. W., & Brown, L. N. (2013). Factors linking Pacific herring (Clupea pallasi) productivity and the spring plankton bloom

in the Strait of Georgia, British Columbia, Canada. *Progress in Oceanography*, *115*, 103–110.

Seegers, B. N., Stumpf, R. P., Schaeffer, B. A., Loftin, K. A., & Werdell, P. J. (2018). Performance metrics for the assessment of satellite data products: an ocean color case study. *Optics Express*, *26*(6), 7404. https://doi.org/10.1364/oe.26.007404

Siegel, D. A., Doney, S. C., & Yoder, J. A. (2002). The North Atlantic spring phytoplankton bloom and Sverdrup's critical depth hypothesis. *Science*, *296*(5568), 730–733. https://doi.org/10.1126/science.1069174

Siegel, H., Gerth, M., Neumann, T., & Doerffer, R. (1999). Case studies on phytoplankton blooms in coastal and open waters of the Baltic Sea using Coastal Zone Color Scanner data. *International Journal of Remote Sensing*, *20*(7), 1249–1264.

Sim, J., & Wright, C. C. (n.d.). The Kappa Statistic in Reliability Studies: Use, Interpretation, and Sample Size Requirements. *Physical Therapy.*, *85*(3).

St. Pierre, K. A., Oliver, A. A., Tank, S. E., Hunt, B. P. V., Giesbrecht, I., Kellogg, C. T. E., Jackson, J. M., Lertzman, K. P., Floyd, W. C., & Korver, M. C. (2020). Terrestrial exports of dissolved and particulate organic carbon affect nearshore ecosystems of the Pacific coastal temperate rainforest. *Limnology and Oceanography*, *65*(11), 2657–2675. https://doi.org/10.1002/lno.11538

Stabeno, P. J., Bond, N. A., Kachel, N. B., Ladd, C., Mordy, C. W., & Strom, S. L. (2016). Southeast Alaskan shelf from southern tip of Baranof Island to Kayak Island: currents, mixing and chlorophyll-a. *Deep Sea Research Part II: Topical Studies in Oceanography*, *132*, 6–23.

Stock, A., Subramaniam, A., Van Dijken, G. L., Wedding, L. M., Arrigo, K. R., Mills, M. M., Cameron, M. A., & Micheli, F. (2020). Comparison of cloud-filling algorithms for marine satellite data. *Remote Sensing*, *12*(20), 1–25. https://doi.org/10.3390/rs12203313

Straile, D. (2002). North Atlantic Oscillation synchronizes food-web interactions in central European lakes. *Proceedings of the Royal Society B: Biological Sciences*. https://doi.org/10.1098/rspb.2001.1907

Strom, S. L., Postel, J. R., & Booth, B. C. (1993). Abundance, variability, and potential grazing impact of planktonic ciliates in the open subaratic Pacific Ocean. *Progress in Oceanography*, *32*(1–4), 185–203.

Suchy, K. D., Le Baron, N., Hilborn, A., Perry, R. I., & Costa, M. (2019). Influence of environmental drivers on spatio-temporal dynamics of satellite-derived chlorophyll a in the Strait of Georgia. *Progress in Oceanography*. https://doi.org/10.1016/j.pocean.2019.102134

Suchy, K. D., Young, K., Galbraith, M., Perry, R. I., & Costa, M. (2022). Match/Mismatch Between Phytoplankton and Crustacean Zooplankton Phenology in the Strait of Georgia, Canada. *Frontiers in Marine Science*, *9*(May), 1–22. https://doi.org/10.3389/fmars.2022.832684

Swart, S., Thomalla, S. J., Monteiro, P. M. S., & Ansorge, I. J. (2012). Mesoscale features and phytoplankton biomass at the GoodHope line in the Southern Ocean during austral summer. *African Journal of Marine Science*, *34*(4), 511–524. https://doi.org/10.2989/1814232X.2012.749811

Thackeray, S. J., Sparks, T. H., Frederiksen, M., Burthe, S., Bacon, P. J., Bell, J. R., Botham, M. S., Brereton, T. M., Bright, P. W., Carvalho, L., & others. (2010). Trophic level asynchrony

in rates of phenological change for marine, freshwater and terrestrial environments. *Global Change Biology*, *16*(12), 3304–3313.

Thomas, A. C., Townsend, D. W., & Weatherbee, R. (2003). Satellite-measured phytoplankton variability in the Gulf of Maine. *Continental Shelf Research*, *23*(10), 971–989.

Thomson, R E. (1994). Physical oceanography of the strait of Georgia-Puget Sound-Juan de Fuca strait system. *Review of the Marine Environment and Biota of Strait of Georgia, Puget Sound and Juan de Fuca Strait*, 13–14.

Thomson, Richard E. (1981). Oceanography of the British Columbia Coast. In *Canadian special publications of fisheries and aquatic sciences* (Vol. 56). http://www.dfo-mpo.gc.ca/Library/487.pdf

Tommasi, D. A. G., Routledge, R. D., Hunt, B. P. V., & Pakhomov, E. A. (2013). The seasonal development of the zooplankton community in a British Columbia (Canada) fjord during two years with different spring bloom timing. *Marine Biology Research*, *9*(2), 129–144. https://doi.org/10.1080/17451000.2012.708044

Tortell, P. D., Merzouk, A., Ianson, D., Pawlowicz, R., & Yelland, D. R. (2012). Influence of regional climate forcing on surface water pCO2, $Δ$O2/Ar and dimethylsulfide (DMS) along the southern British Columbia coast. *Continental Shelf Research*, *47*, 119–132.

Vargas, M., Brown, C. W., & Sapiano, M. R. P. (2009). Phenology of marine phytoplankton from satellite ocean color measurements. *Geophysical Research Letters*, *36*(1), 2–6. https://doi.org/10.1029/2008GL036006

Waite, J. N., & Mueter, F. J. (2013). Spatial and temporal variability of chlorophyll-a

concentrations in the coastal Gulf of Alaska, 1998--2011, using cloud-free reconstructions of SeaWiFS and MODIS-Aqua data. *Progress in Oceanography*, *116*, 179–192.

Ware, D. M., & Thomson, R. E. (2005). Bottom-Up Ecosystem Trophic Dynamics Determine Fish Production in the Northeast Pacific. *Science*, *308*(5726), 1280 LP – 1284. https://doi.org/10.1126/science.1109049

Welch, H., Brodie, S., Jacox, M. G., Robinson, D., Wilson, C., Bograd, S. J., Oliver, M. J., & Hazen, E. L. (2020). Considerations for transferring an operational dynamic ocean management tool between ocean color products. *Remote Sensing of Environment*, *242*(March), 111753. https://doi.org/10.1016/j.rse.2020.111753

Whitney, F. A., Crawford, W. R., & Harrison, P. J. (2005). Physical processes that enhance nutrient transport and primary productivity in the coastal and open ocean of the subarctic NE Pacific. *Deep Sea Research Part II: Topical Studies in Oceanography*, *52*(5–6), 681–706.

Wilks, D. S. (2011). *Statistical methods in the atmospheric sciences* (Vol. 100). Academic press.

Winder, M., & Sommer, U. (2012). Phytoplankton response to a changing climate. *Hydrobiologia*, *698*(1), 5–16. https://doi.org/10.1007/s10750-012-1149-2

Wolfe, A. M., Allen, S. E., Hodal, M., Pawlowicz, R., Hunt, B. P. V, & Tommasi, D. (2016). Impact of advection loss due to wind and estuarine circulation on the timing of the spring phytoplankton bloom in a fjord. *ICES Journal of Marine Science*, *73*(6), 1589–1609. https://doi.org/10.1093/icesjms/fsv151

Xu, Y., Ishizaka, J., Yamaguchi, H., Siswanto, E., & Wang, S. (2013). Relationships of

interannual variability in SST and phytoplankton blooms with giantjellyfish (Nemopilema nomurai) outbreaks in the Yellow Sea and East China Sea. *Journal of Oceanography*, *69*(5), 511–526. https://doi.org/10.1007/s10872-013-0189-1

Yoo, S., Batchelder, H. P., Peterson, W. T., & Sydeman, W. J. (2008). Seasonal, interannual and event scale variation in North Pacific ecosystems. *Progress in Oceanography*, *77*(2–3), 155–181.

Zebiak, S. E., & Cane, M. A. (1987). A Model El Ni&ntilde–Southern Oscillation. *Monthly Weather Review*, *115*(10), 2262–2278. https://doi.org/10.1175/1520-0493(1987)115<2262:AMENO>2.0.CO;2

Zhai, L., Platt, T., Tang, C., Sathyendranath, S., & Walne, A. (2013). The response of phytoplankton to climate variability associated with the North Atlantic Oscillation. *Deep Sea Research Part II: Topical Studies in Oceanography*, *93*, 159–168. https://doi.org/https://doi.org/10.1016/j.dsr2.2013.04.009

Zhang, H.-R., Wang, Y., Xiu, P., & Chai, F. (2021). Modeling the seasonal variability of phytoplankton in the subarctic northeast Pacific Ocean. *Marine Ecology Progress Series*, *680*, 33–50.

Zhang, M., Zhang, Y., Qiao, F., Deng, J., & Wang, G. (2016). Shifting trends in bimodal phytoplankton blooms in the North Pacific and North Atlantic Oceans from Space with the holo-hilbert spectral analysis. *IEEE Journal of Selected Topics in Applied Earth Observations and Remote Sensing*, *10*(1), 57–64.

Zhao, H., Han, G., & Wang, D. (2013). Timing and magnitude of spring bloom and effects of physical environments over the Grand Banks of Newfoundland. *Journal of Geophysical*

Research: Biogeosciences, *118*(4), 1385–1396.

6.0 Appendix

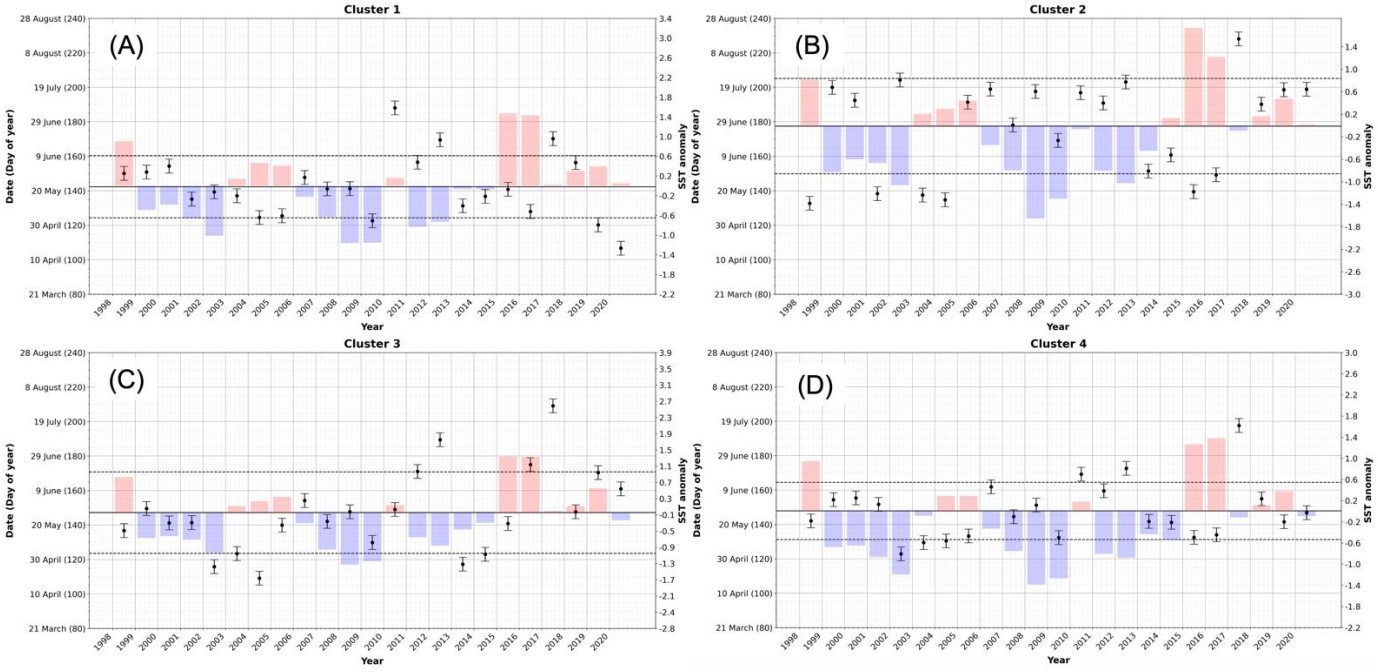

Figure A1: Interannual variability of principal bloom initiation and SST anomaly per cluster.

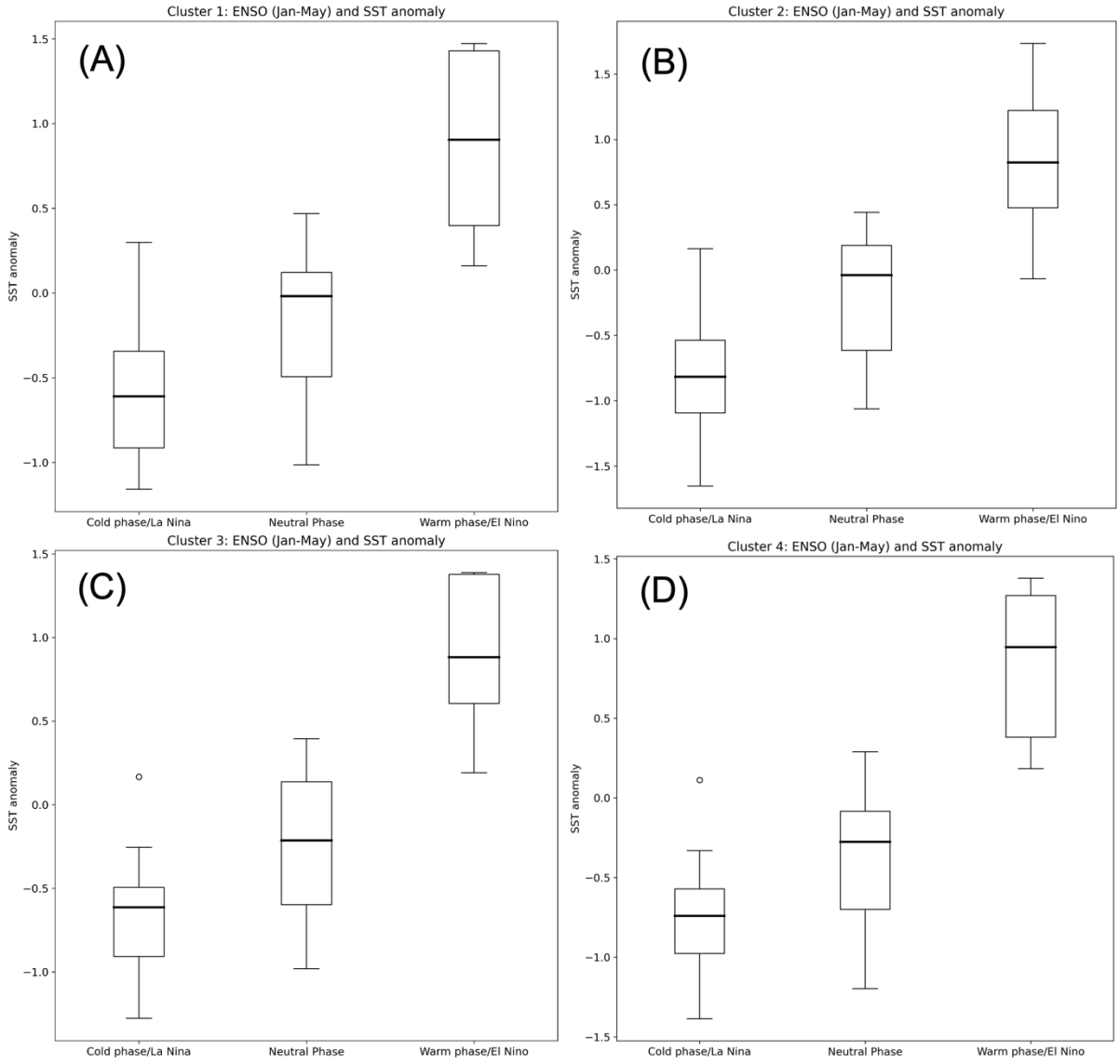

Figure A2: Boxplot of SST for La Nina, neutral and El Nino phases per cluster. Where the ENSO index is less than -0.5 for La Nina phase, between -0.5 and 0.5 for neutral phase, and greater than 0.5 for El Nino phase.

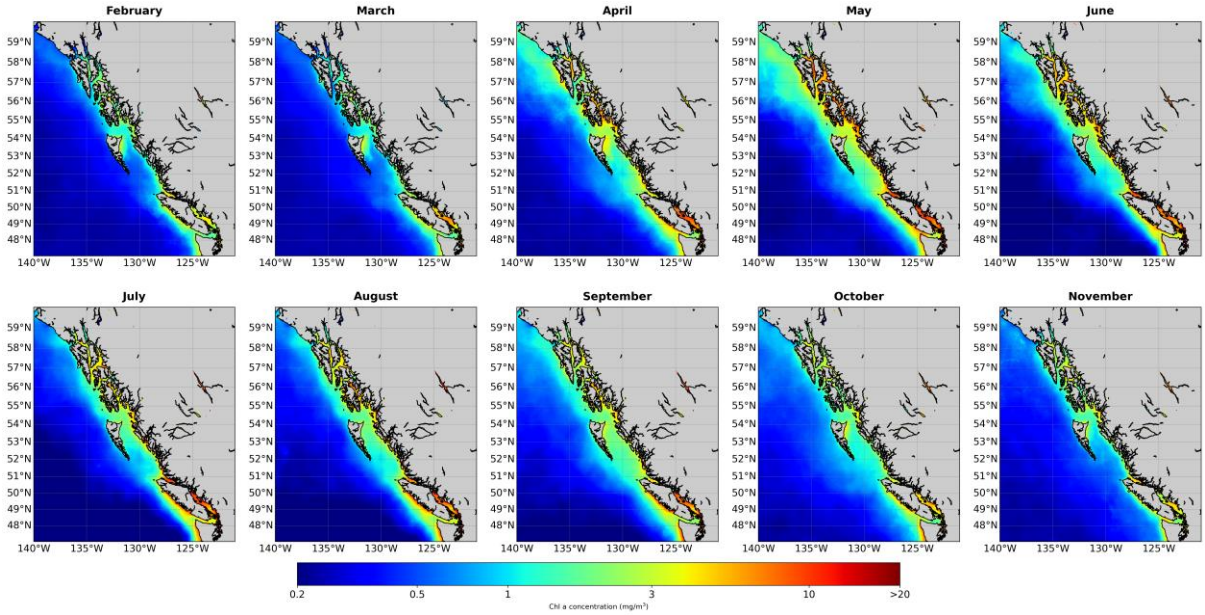

Figure A3: GlobColour interpolated monthly climatology

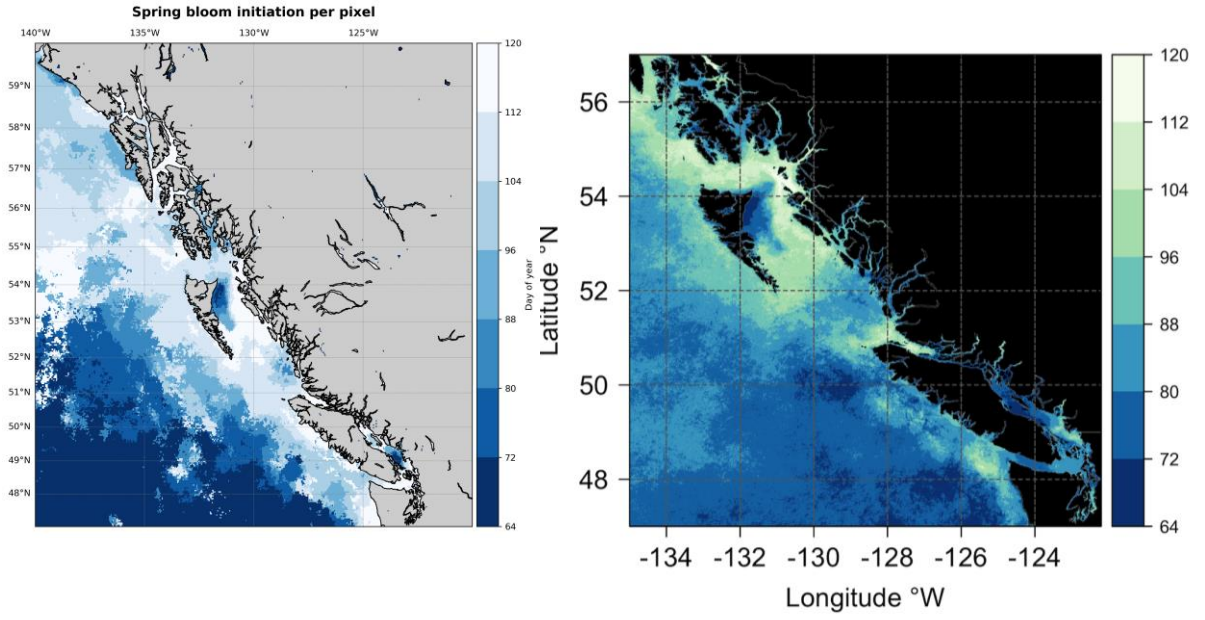

Figure A4: (A) The climatological (1998-2020) spring bloom initiation over the study area compared to (B) Marchese et al. (2022) Figure 12A showing the climatological (2016-2020) bloom onset dates.

Table A1: Comparing the spring bloom initiation found in the central Strait of Georgia to dates found in Suchy et al. (2022)

	DOY			Date		Conclusion
	DOY	Suchy et al. (2022) DOY	Difference	Date	Suchy et al. (2022) Date	13/14 Agreement
2003	109	101	8	19-Apr	11-Apr	Similar
2004	85	69	16	25-Mar	9-March	Similar
2005	53	53	0	22-Feb	22-Feb	Agreement
2006	85	85	0	26-Mar	26-Mar	Agreement
2007	69	117	-48	10-Mar	27-April	Agreement with Gower 2013
2008	117	117	0	26-Apr	26-April	Agreement
2009	93	101	-8	03-Apr	11-April	Similar
2010	101	101	0	11-Apr	11-April	Agreement
2011	101	93	8	11-Apr	3-April	Similar
2012	125	85	40	04-May	25-March	Different
2013	77	93	-16	18-Mar	3-April	Similar
2014	93	93	0	03-Apr	3-April	Agreement
2015	61	53	8	02-Mar	22-Feb	Similar
2016	77	77	0	17-Mar	17-March	Agreement